IMPACT OF FUEL OXYGENATION ON NO_x FORMATION IN BIODIESEL FLAMES

JOSEPHAT KIPYEGON TANUI

MASTER OF SCIENCE

(Mechanical Engineering)

JOMO KENYATTA UNIVERSITY OF AGRICULTURE AND TECHNOLOGY

2013

Impact of Fuel Oxygenation on NO_x Formation in Biodiesel Flames

Josephat Kipyegon Tanui

A thesis submitted in partial fulfillment for the degree of Master of Science in Mechanical Engineering in the Jomo Kenyatta University of Agriculture and Technology

2013

DECLARATION

This thesis is my original work and has not been presented for a degree award in any other University.

Sign..... Date.....

Josephat Kipyegon Tanui

This thesis has been submitted for examination with our approval as University Supervisors.

Sign..... Date.....

Prof. P. N. Kioni

DeKUT, Kenya

Sign..... Date.....

Mr. A. Gitahi

JKUAT, Kenya

DEDICATION

This research work is dedicated to Catherine, my mother, and my lovely wife Fancy, for their continuous encouragement and support.

ACKNOWLEDGEMENT

The success of this research work is greatly owed to my supervisor, Prof. P. N. Kioni. He provided a deep insight, great support and invaluable guidance throughout the work. He also dedicated his time and provided valuable materials for this work. For all these, I am very grateful to him. I am also greatly indebted to my second supervisor, Mr. Anthony Gitahi for not only guiding and supporting me throughout the work but also introducing me to Combustion Simulation Laboratory Software package (COSILAB) and giving me the instruction manuals.

My gratitude are also to many people who have contributed to the success of this work in one way or the other. I can only mention but a few; to all others, my most sincere gratitude. I would like to particularly mention Dr. Hiram Ndiritu whose advice was valuable in this work. I would also mention my colleagues: F.M. Madaraka, J. N. Mburu and S. K. Musau for their companionship and moral support.

I would also be very grateful for the financial support of Kimathi University College of Technology. This enabled me to procure the software (COSILAB) required for this work.

Finally, I fully appreciate the moral and spiritual support of my wife Fancy and my entire family throughout this period.

TABLE OF CONTENTS

LIST OF TABLES

LIST OF FIGURES

LIST OF APPENDICES

ABBREVIATIONS

COSILAB	Combustion Simulation Laboratory software
ppm	parts per million

NOMENCLATURE

a	Strain rate, [s^{-1}]
A	Spatially variable cross sectional area, [m^2]
A_k	Pre-exponential factor in rate constant K_k, [s^{-1} (mol/m^3)]
A_s	Local wetted surface area per unit void volume, [m^{-1}]
c_p	Mixture's frozen specific heat capacity at constant pressure, [J kg^{-1} K^{-1}]
c_{pi}	Specific heat capacity at constant pressure for species i, [J kg^{-1} K^{-1}]
c_{vi}	Specific heat capacity at constant volume for species i, [J kg^{-1} K^{-1}]
D_{ij}	Binary diffusion coefficient for species i and j, [m^2 s^{-1}]
$D_{T,i}$	Thermal diffusion coefficient for species i, [kg m^{-1} s^{-1}]
E_k	Activation energy in rate constant K_k, [J mol^{-1}]
$\mathbf{f}_i$	External force per unit mass on species i, [N/kg]
h_i	Specific enthalpy of species i, [J kg^{-1}]
h_s	Heat transfer coefficient, [W m^{-2} K^{-1}]
k	Bulk viscosity coefficient, [Ns m^{-2}]
K_k	Rate constant of the k^{th} reaction, [s^{-1} (mol/m^3)]
L	Lewis number, [-]
N	Total number of chemical species present
p	Hydrostatic pressure, [Pa]
$\mathbf{P}$	Stress tensor, [Pa]
Pr	Prandtl number, [-]
R	Universal gas constant, [J mol^{-1} K^{-1}]
s	Specific entropy, [J kg^{-1} K^{-1}]
t	Time, [s]
T	Temperature, [K]

u	Internal energy per unit mass for the gas mixture, [J kg^{-1}]
$\mathbf{U}$	Unit tensor, [-]
U_i	Diffusion velocity of species i in x direction, [m s^{-1}]
V	Reactor volume, [m^3]
v', v'', v	Stoichiometric coefficient, [-]
V_i	Diffusion velocity of species i in y direction, [m s^{-1}]
V_x	Velocity component in x direction, [m s^{-1}]
V_y	Velocity component in y direction, [m s^{-1}]
w_i	Rate of production of species i by chemical reactions, [kg m^{-3} s^{-1}]
W	Molecular weight of species of the mixture, [kg mol^{-1}]
W_i	Molecular weight of species i, [kg mol^{-1}]
x	Spatial coordinate, [m]
X	Mole fraction, [-]
y	Spatial coordinate, [m]
Y	Mass fraction, [-]
λ	Thermal conductivity, [W m^{-1} K^{-1}]
μ	Coefficient of dynamic viscosity, [Ns m^{-2}]
γ	Specific heat capacity ratio, [-]
ρ	Mass density, [kg m^{-3}]
$\mathbf{q}$	Heat flux vector, [W m^{-1}]
$\mathbf{q}_R$	Radiant heat flux vector, [W m^{-1}]
$\mathbf{v}$	Velocity vector, [m s^{-1}]
R	Relating to Radiant heat
T	Relating to Thermal diffusion
m	Conditions at time level m

∇	Spatial gradient operator, [m^{-1}]

ABSTRACT

The increasing demand for energy and the need for reduction of greenhouse gases has necessitated the development of renewable sources such as biodiesel fuel. Methyl ester fuel burns more efficiently and has lower emissions of particulate matter, unburned hydrocarbon and carbon monoxide than fossil fuels. However, combustion of a methyl ester fuel results in increased nitrogen oxides (NO_x) emissions relative to fossil fuels. This study is concerned with the formation of NO_x in combustion of methyl formate, the simplest methyl ester molecule, under different flame conditions. Homogeneous ignition, freely propagating and diffusion flames of methane, methanol and methyl formate have been numerically simulated. To this end, recently developed chemical kinetic mechanism for methyl formate (Dooley 2009) has been identified and further developed to capture the production processes of pollutants. This is particularly important given that kinetics of combustion of methyl esters have not received much attention in existing literature. NO_x concentration profiles for methyl formate in all configurations studied have been compared to those of methane/air and methanol/air flames which are well understood.

It has been established that, the thermal NO in the three fuels are produced in nearly the same amount (within the same order of magnitude), while the prompt NO production in methane is observed to have a significant difference (one order of magnitude higher) compared to those of methanol and methyl formate flames. For thermal NO, the rate-limiting step: $N_2 + O \longrightarrow NO + N$, which has a high activation energy is the decisive reaction. N_2 and O are readily available in all the three fuels, hence the thermal NO production is nearly the same. In prompt NO, reaction: $CH + N_2 \longrightarrow HCN + N$ is the determining step. A small amount of CH and subsequently N atoms in CH_3OH and CH_3OCHO explain the low values of NO concentration as compared to that for methane. In addition, NO concentration showed a high sensitivity to reaction: $NNH + O \longrightarrow NH$

+ NO in oxygenated fuels (CH_3OH and CH_3OCHO) as opposed to high sensitivity of reaction: $CH + N_2 \longrightarrow HCN + N$ seen in CH_4 flames. The low concentration of N atoms in oxygenated fuels makes the contribution through the reaction path that results in NNH being significant.

The NO formation in freely propagating and diffusion flames is mostly through prompt NO since the maximum flame temperatures attained are relatively low (approximately $\leq$2000 K). While the NO formation in a homogeneous system is mostly through thermal NO mechanism (Zel'dovich mechanism) since they attained high flame temperatures (approximately between 2800 and 3200 K) due to high initial temperatures. It is observed that, NO concentration in a homogeneous system is significantly higher (by three orders of magnitude) than those in freely propagating and diffusion flames.

CHAPTER ONE

1.0 INTRODUCTION

1.1 Background and Literature Review

The increasing demand for energy and the need for reduction of greenhouse gases has necessitated the development of renewable sources such as biodiesel fuel. Both pure and diesel-blended methyl ester fuels burn more efficiently, due to the presence of oxygen atom in their structure, than pure fossil fuels. For instance, it has been shown that diesel blended with the croton megalocarpus methyl ester yields higher thermal efficiency [1]. Furthermore, several research works [2–4] have shown that combustion of methyl ester fuels in diesel engine result in lower emissions of particulate matter, unburned hydrocarbons and carbon monoxide. However, combustion of methyl esters result in increased NO_x emissions as compared to fossil fuels [3–5].

A typical biodiesel fuel has C14-C18 fatty acid methyl esters: methyl palmitate, methyl stearate, methyl oleate, methyl linoleate and methyl linolenate in different compositions. The chemical kinetics of these large carbon chain esters are complex. Their combustion processes contain hundreds of intermediate compounds thus making computation difficult. To tackle this problem, researchers have been using surrogate fuels (both single and multi-component) to represent a real fuel. Surrogate fuels are used to represent or approximate the combustion processes in biodiesel fuels. However, amongst suitable candidates for surrogate fuels are the esters. They, however, are of unknown chemical kinetics. Methyl formate has the simplest molecular structure (see Fig.1.1) of all the methyl esters. Even though methyl formate does not have as high a molecular weight as a real biodiesel fuel, it has the essential chemical structural features of an ester. Hence it can be used to study

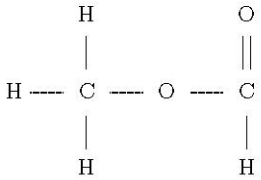

Figure 1.1: Molecular structure of methyl formate

the combustion behaviour of a biodiesel fuel.

The formation of NO_x in the combustion of methyl formate has been investigated under different flame conditions. An understanding of the chemical reaction pathways of NO_x formation during fuel oxidation is very important in determining the reduction techniques to be employed in a combustion system. In a combustion system, NO is formed in four different ways; thermal NO at high temperature flame zone or post-flame zone, prompt NO at low temperature flame zone, NO formed from the N_2O mechanism, and fuel NO produced by nitrogen portions in the fuel. The primary mechanism for thermal NO formation in a flame is attributed to extended Zel'dovich mechanism [6];

$$O + N_2 \rightleftharpoons NO + N, \tag{1.1}$$

$$N + O_2 \rightleftharpoons NO + O, \tag{1.2}$$

$$N + OH \rightleftharpoons NO + H. \tag{1.3}$$

In this mechanism, reaction in Eq. (1.1) is the rate determining step for NO formation. Prompt NO formation in the flame zone is associated with the presence of CH radical which react with nitrogen. N atom from this reaction then forms NO through reactions in Eqs (1.2) and (1.3). HCN, the other product, reacts following various paths to form NCO and NH which subsequently form N atom responsible for NO formation. Fuel NO does

not play a role in engine combustion, because fuels for internal combustion engines contain negligible amounts of nitrogen.

The aim of this study is to investigate the chemical reaction pathways for the formation of NO_x in methyl formate flames. The results are compared to those of methane and methanol flames. NO_x formation in methane has been well understood, ranging from the development of mechanisms to the influence of flame types. Several mechanisms for NO_x formation have been developed; Li and William mechanism [7], Leeds mechanism [8], GRI 3.0 mechanism [9], GDF-Kin®3.0-NCN mechanism [10] and Konnov (version 0.6) [11]. The earlier versions of these mechanisms [7–9] use the reaction $CH + N_2 \rightleftharpoons HCN + N$ and the subsequent reactions. In the current versions [10, 11], the reaction has been replaced with $CH + N_2 \rightleftharpoons NCN + H$ and the subsequent reactions. Mechanisms with NCN route have been proven to have satisfying prediction of NO mole fraction profiles [12] in flames. The work of Li and Williams [7] showed that NO_x formation in a two-stage methane-air flame strongly depend on the flame structure, the premixing equivalence ratio, and the mass fraction of water and carbon dioxide added in the air stream. Guo *et al.* [13] reported on NO_x formation in counterflow methane-air triple flames. They observed that a triple flame produces more NO and NO_2 than the corresponding premixed flames due to the appearance of the diffusion flame branch where NO is mainly produced by the thermal mechanism. Naha *et al.* [14] investigated the effect of using different fuels on NO_x formation in a counterflow partially premixed flame. They observed a significantly higher formation of CH radicals in n-heptane flame than that in methane flame which was responsible for the difference in NO_x characteristics of the two fuels. The most recent studies of NO_x formation in methane flames [11, 12] have been geared toward understanding the role of NCN radical in prompt-NO formation. Few studies [15] on NO_x formation in methanol flames have been reported. The chemical kinetics of methyl formate have recently been

studied by Dooley *et al.* [16, 17]. The mechanism developed [16] has been validated in a wide range of conditions; a variable pressure flow reactor, shock tube facility and outwardly propagating flames. In a later investigation [17], Dooley *et al.* studied a series of burner stabilized flames at pressures of 22-30 Torr and equivalence ratios from 1.0 to 1.8 for flame conditions of 25-35% fuel to further validate their chemical kinetic reaction mechanism. To our knowledge, NO_x formation pathways for methyl formate flames have never been reported. With the earlier reports [3, 5] that NO_x formation in biodiesel fuel are higher than those of fossil fuel, it is important to understand how the NO_x formation is affected by oxygenation in the fuel. Motivated by this consideration, the present study focuses on the analysis of dominant reactions responsible for NO_x formation in methyl formate/air flame and the subsequent comparison to methane/air and methanol/air flames. Chemical kinetic analysis of the dominant pathways, concentration profiles and rate of production of key radical species will be used to explain the differences in NO_x formation in the three flames.

1.2 Problem Statement

When a methyl ester fuel is used in a diesel engine, there is a high level of exhaust NO_x emissions. Therefore, the aim is to determine the mechanism that leads to formation of NO_x in methyl formate fuel in different reactants flow configurations.

1.3 Objectives

The main objective of the study is to investigate the effects of oxygenation on NO_x formation in fuels. The specific objectives include:

1. To establish and build suitable chemical kinetic mechanism for NO_x formation in methyl formate.

2. To establish the key reaction pathways for NO_x formation in methyl formate flames.

3. To determine the influence of flow configuration on NO_x formation; homogeneous mixtures and non-homogeneous mixtures (premixed and diffusion flames).

4. To verify the validity of the results by performing sensitivity analysis for NO_x formation in methyl formate flames.

1.4 Thesis Overview

This study deals with the numerical simulations of methane/air, methanol/air, and methyl formate/air under different flow configurations; homogeneous system, freely propagating flame, and diffusion flame. These simulations have been done with an aim of establishing the influence of fuel oxidation on generation of nitrogen oxides (NO_x).

In this thesis, a detailed literature review has been done in chapter 2. Different types of fuels are first reviewed, in which the complexity of computing a real fuel is emphasized. Thus, the importance of using a surrogate fuel, which is relatively simpler and easier to compute, is highlighted. The chemical kinetics of NO_x formation is then reviewed. The various ways in which NO_x forms in a combustion system are discussed in detail. Then, it is followed by a review on the combustion processes in various flow configurations, which have been considered in this study. Lastly, reviews on the detailed chemical kinetic mechanisms for the oxidation of methane, methanol and methyl formate fuels, as well as the thermodynamic and transport properties of species are presented. The mechanisms

that have reactions involving nitrogen compounds have also been discussed. This section is supplemented by Appendix A to C.

A chapter on the governing equations for chemically reactive flows, chapter 3, follows the literature review. The general conservation equations governing multi-component, chemically reacting, ideal gas mixtures are first presented. Then followed by the recast of these equations for the specific flow configurations; homogeneous system, freely propagating flame, and diffusion flame. The last section of the chapter presents the boundary conditions for each of the flow configuration.

The numerical solution method for the laminar, chemically reactive flow is presented in chapter 4. The finite difference schemes adopted for the discretization of the governing equations are discussed. In a reactive flow, the heat release associated with combustion processes results in steep gradients and strong curvature for the dependent variables profiles. Therefore, in order to reduce the temporal and spatial discretization errors, adaptive gridding method is required. The adaptive gridding method is thus discussed. Then the two methods; Modified Newton method and Euler method, used for solving the system of non-linear equations resulting from discretization is presented. Finally, the convergence criterion for the solutions is highlighted.

Presented in the next three chapters (chapter 5 to chapter 7) are the results and discussions for the different flow configurations. For each configuration, a comparison of NO concentration profiles and other radicals that are dominant in its formation is made. In addition, a plot of major and minor species concentration profiles, and temperature profiles is shown. Finally, the sensitivity of CH and NO concentrations to the reactions in the mechanism is presented.

Presented in chapter 8 is a summary of the main findings of this study while the recom-

mendations arising out of the study are given in chapter 9.

CHAPTER TWO

2.0 LITERATURE REVIEW

2.1 Fuel Types

Organic fuels are made up of a mixture of different hydrocarbons of various group ($C_\alpha H_\beta O_\varepsilon$). Petroleum fuels - gasoline, diesel, jet fuel, kerosene - are pure hydrocarbon fuels. They contain carbon and hydrogen atoms which are combined in many ways to form different molecular compounds such as n-alkanes, branched alkanes, cycloalkanes, aromatics and others. The amounts of these molecular compounds in a given fuel differ greatly depending on the source of crude oil [18].

On the other hand, oxygenated hydrocarbon fuels such as alcohol, ketone, ether, aldehydes and esters contain oxygen atom(s) in their chemical structure. The presence of oxygen atoms in these fuels affects their combustion processes. Excess oxygen could result to a higher oxidation of nitrogen available and hence more NO_x emissions.

A real fuel consists of several species which makes computation of its reaction difficult. For instance, a typical biodiesel fuel has several long chain fatty acid methyl esters, normally between long-chain carbon (C14) and (C18) which vary in compositions depending on the source. The chemical kinetics of these large carbon chain esters are complex. Therefore, a surrogate fuel is used to correctly predict the combustion properties of a fuel.

2.1.1 Surrogate Fuel

Surrogate fuels are used to represent or approximate the combustion behaviour of a fuel. A surrogate fuel should have properties which are similar to those of the real fuel to

be emulated. In order to formulate a surrogate fuel, physical and chemical properties of the components are closely matched to those of the real fuel. The selection of fuel surrogate components and compositions does not follow a particular algorithm. However, the components chosen are constrained by their physical and chemical properties.

A surrogate fuel can be classified either as single-component or multi-component. In a single-component formulation, a chemical component which has properties such as molecular structure, cetane number, viscosity, density, etc, similar to that of the real fuel is used. Studies such as those by Dooley *et al.* [16,17] have used this approach. On the other hand, a multi-component surrogate fuel consists of different components whose compositions are constrained by their physical and chemical properties to match those of the real fuel. Generally, there are no clear ways of defining the surrogate components and compositions. However, methodologies based on matching fuel's properties; molecular structure, molecular weight, cetane number, hydrogen/carbon ratio, threshold soot index, viscosity, etc are generally accepted. In this study methyl formate (CH_3OCHO) is used to represent a biodiesel fuel. It has a simple structure with two C atoms. Even though methyl formate does not have a high molecular weight as a real biodiesel fuel, it has the essential chemical structural features of an ester.

2.2 Combustion of Methyl Esters

A methyl ester is an oxygenated fuel formed by the reaction of an alcohol (methanol) and vegetable or animal fat (triglyceride). A typical biodiesel fuel has over 90% of its composition being five unique long-chain carbon (C16) and (C18) saturated and unsaturated methyl esters [19]: methyl palmitate, methyl stearate, methyl oleate, methyl linoleate and methyl linolenate. An ester can generally be represented as R-C(=O)O-CH_3, where R is

a saturated or unsaturated hydrocarbon. The presence of the ester moiety (the oxygen atoms attached to the carbon atom) make this fuel to have different combustion properties in relation to pure hydrocarbon fuel.

Over the last decade, the research on the combustion characteristics of methyl esters as well as biodiesel fuels have been intensified. Several kinetics models for both small-chain and long-chain methyl esters have been developed. These include: detailed chemical kinetic mechanism for methyl formate [20–22], methyl butanoate [21], methyl hexanoate and methyl heptanoate [23], methyl-5-decenoate and methyl-9-decenoate [24], methyl stearate and methyl oleate [25]. Recently, Westbrook *et al.* [26] developed a mechanism for the five major components of soy biodiesel and rapeseed biodiesel fuel. These mechanisms usually have numerous chemical species taking part in enormous reactions, for instance, Naik *et al.* [25] chemical reaction mechanism has 3500 species taking part in 17,000 chemical reactions. These detailed mechanisms can only be used to model fuels in zero dimensional homogenous transient system. It is impractical to implement them in one and two dimensional flame codes due to computational limitation. However, a skeletal (reduced) mechanism can be derived from the detailed mechanism, such as those used by Sarathy *et al.* [27] and Valeri *et al.* [28].

The kinetics models described in the preceding paragraph have been used to study several aspects of methyl esters combustion: intermediate species production; ignition and extinction; the effects of saturation; and the effects of molecular structure. The intermediate species produced during the combustion of esters have been identified by several researchers [17, 27, 29]. These intermediates are mostly low molecular weight oxygenated compounds such as, methanol, formaldehyde, ketones, ethyl formate, etc. The studies also reveal that unsaturated methyl esters are important intermediate species in the combustion of saturated fatty acid methyl esters. Seshadri *et al.* [30] used a skeletal mechanism

to study the ignition and extinction of methyl decanoate. The reduced mechanism showed that low temperature chemistry is of little importance under counter flow conditions. The effects of the presence and position of the double bond on combustion characteristics have been investigated [24,31,32]. Bax *et al.* [31] studied the oxidation of a blend containing n-decane and a large unsaturated esters (methyl oleate) in a jet stirred reactor. The results were compared to those of oxidation of a blend of n-decane and methyl palmitate performed under similar conditions. They established that unsaturated ester (methyl oleate) is slightly less reactive than saturated ester (methyl palmitate) in the low temperature region whereas the opposite trend is observed in the negative temperature coefficient (NTC) region. Wang *et al.* [32] investigated three model biodiesel fuels: methyl butanoate, methyl crotonate and methyl decanoate in a laminar premixed and non-premixed flames. They compared the results with those of n-alkanes of similar carbon number in order to assess the effect of saturation, the length of carbon-chain and the presence of the ester group. They established that the presence of the ester group has a retarding effect on the overall mixture reactivity.

Exhaust emissions of methyl esters combustion in an engine have been studied experimentally. Several research works [2–4] have shown that combustion of methyl ester fuels in diesel engine result in lower emissions of particulate matter, unburned hydrocarbons and carbon monoxide. However, combustion of methyl esters result in increased NO_x emissions as compared to fossil fuels [3–5]. Kinetics models for NO_x formation in esters do not exist in literature.

2.3 Chemical Kinetics of NO_x Formation

In a combustion system, there are four mechanisms for NO_x formation; thermal NO, prompt NO, NO formed from the N_2O mechanism, and fuel NO produced by nitrogen portions in the fuel. These mechanisms are mainly controlled by flame temperature, oxidant concentration and the length of the residence time in the high temperature flame region.

Thermal NO formation occurs at high temperature flame zones or post-flame zones. Extended Zel'dovich mechanism [6], given by reactions shown in Eqs. (1.1)-(1.3), governs the thermal NO formation.

Prompt NO formation occurs at low temperature flame zones. It is normally associated with the presence of CH radical which could react either as [33];

$$CH + N_2 \rightleftharpoons HCN + N \tag{2.1}$$

or

$$CH + N_2 \rightleftharpoons NCN + H \tag{2.2}$$

The N atom resulting from the reaction shown in Eq. (2.1) forms NO through reactions 1.2 and 1.3. HCN reacts through various paths to form NCO and NH which subsequently forms N atom responsible for NO formation. NCN in reaction shown in Eq. (2.2) can react with different species, forming HCH, CN, NCO and NO.

NO formed from N_2O mechanism occurs at lean air-fuel mixtures, low temperatures (below 1500 K) and at high pressures (above 10 atm) [6, 33]. The main reaction for this NO formation is the oxidation of N_2O;

$$N_2O + O \rightleftharpoons NO + NO \tag{2.3}$$

Fuel NO does not play a role in engine combustion, because fuels for internal combustion engines contain negligible amounts of nitrogen.

2.4 Laminar Premixed Flames

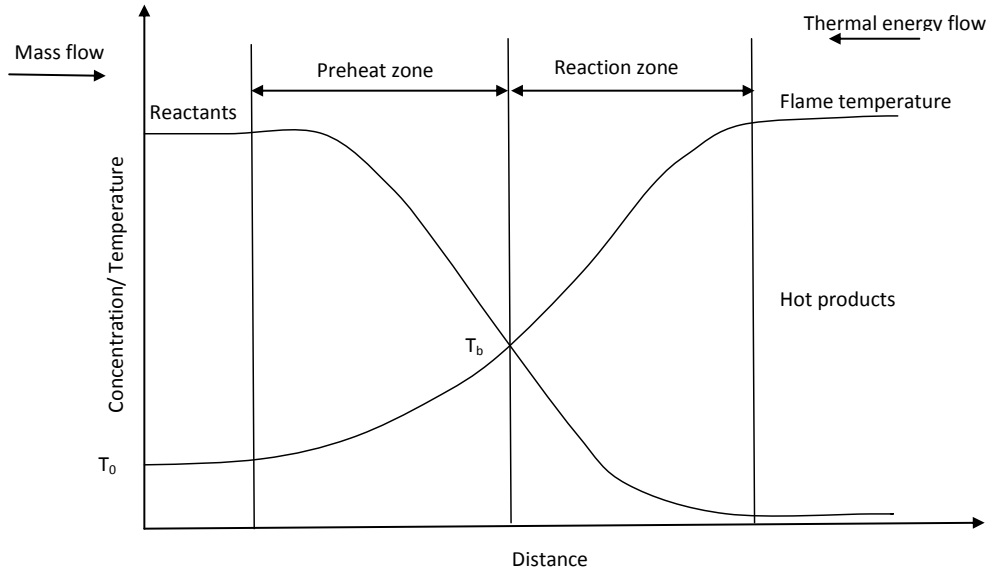

Figure 2.1: A typical structure of a premixed flame

A typical flame structure of a premixed flame is given on Fig. 6.2 [34]. Temperature increases from initial temperature of the unburnt gases, T_0, to the ignition temperature, T_b (onset of chemical reactions) and then to a maximum temperature where its gradient become zero. The maximum temperature attained is the flame temperature. Temperature profile is an important parameter in flame characterization into three regions: Preheat zone, reaction zone and product zone. Preheat zone is a diffusion dominated zone. Temperature gradient and species concentration gradient result in diffusion of heat and radical species

from the reaction zone to the preheat zone. As a result, temperature rise from T_0 to T_b is always maintained and the flame becomes self sustaining. The reaction zone is characterized by a thin region of very fast chemistry followed by a much wider region of slow chemistry. It is in this region that prompt NO formation occurs because of the presence of the radicals. The temperature is a maximum at the product zone and thermal NO plays a significant role in NO_x formation. It is expected that there is maximum NO_x formation in this region because of high flame temperature [14].

2.5 Laminar Diffusion Flames

In a non-premixed flame, there is no prior mixture of fuel and air before combustion. There is a continuous variation of the mixture fraction (equivalence ratio, ϕ), from fuel side at $\phi \longrightarrow \infty$ to pure air at $\phi = 0$. The most common configurations are parallel flow jets of the unmixed reactants and opposed flows. A typical opposed flow configuration is shown in Fig. 2.2 [35].

A diffusion flame can be established between the two nozzles, and normally located where the mixture fraction is stoichiometric. Combustion products spread to both sides of the flame while fuel and oxygen have to diffuse against those streams in order to mix and react. Fig. 2.2a shows a flame located at the air side of stagnation plane. In this case, the stoichiometric condition requires more air than fuel. On the other hand, a flame would be located at the fuel side of stagnation flame, if the stoichiometric condition require more fuel than air [35]. The temperature peaks at the position of the flame (at the stoichiometric value of fuel/air mixture). It is in this region of maximum temperature that the NO_x formation is expected to be high.

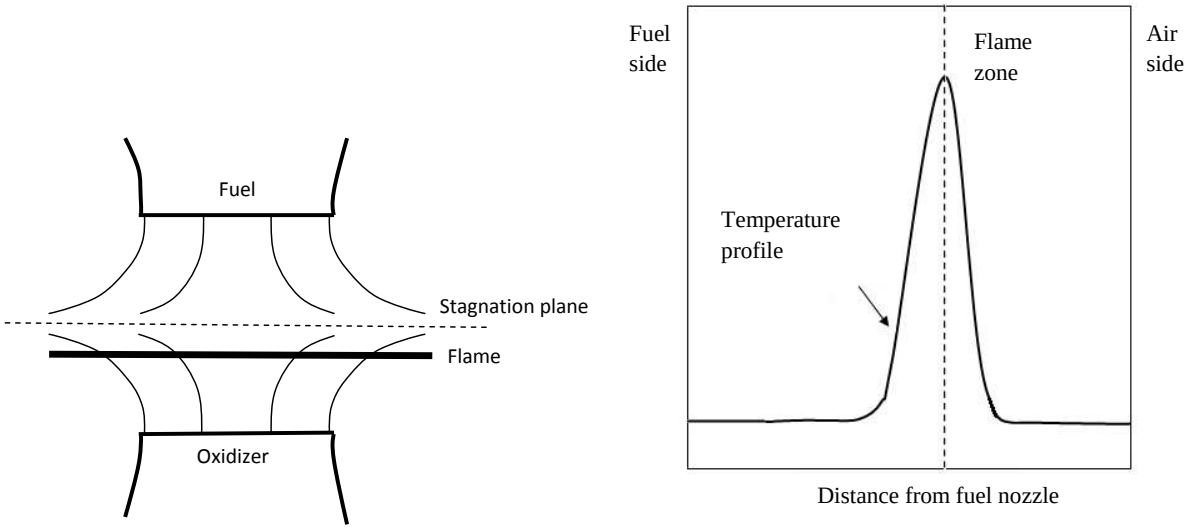

(a) Flow configuration

(b) Temperature profile

Figure 2.2: Counterflow diffusion flame

2.6 Ignition

Ignition in a combustible mixture can be achieved either through spontaneous ignition or by an external energy. In this study, spontaneous ignition in which a fuel is brought into a state which can ignite by rise in temperature and pressure, is considered. In a laboratory environment, ignition is studied using a shock tube apparatus, which is illustrated in the next section.

2.6.1 Shock Tube Apparatus

A typical shock tube equipment is illustrated in Fig. 2.3 [36]. The high pressure tube is filled with helium gas at an arbitrary high pressure (say 2-3 MPa), while the low pressure tube is filled with dry air at an arbitrary low pressure (say 30-40 kPa).

On breaking the polyester film between both tubes with a cutter, a shock wave with a high Mach number propagate through the low pressure air. Behind the shock wave reflected from

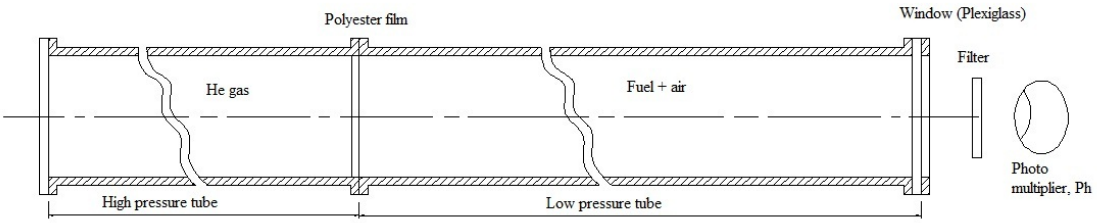

Figure 2.3: Shock tube equipment

the tube end, the air is compressed to high pressures and heated to high temperatures. The propagating velocity of the incident shock is measured by observing the passage instants of the shock front at several piezoelectric pressure transducers set at different positions on the low pressure tube.

Every time the incident shock is reflected from the end of the low pressure tube, the liquid fuel is injected into the air behind the reflected shock waves through an injection nozzle mounted at the end of the shock tube. The induction period of hot ignition in the mixture is measured by observing the ignition with a photomultiplier set on the tube axis outside the end of the shock tube through a filter. The induction period is taken as the period from the arrival and reflection of the incident shock at the tube end (plexiglass window) to the detection of light emission of ignition by the photomultiplier.

2.6.2 Ignition Delay Time

Ignition delay time is the period between the completion of reactants mixing and the instant at which thermal runaway occurs. Ignition processes in a homogenous mixture can be explained using two theories; thermal explosion theory and chain-branching kinetic theory. In thermal explosion theory, ignition occurs when heat production exceeds the heat losses on the combustion chamber walls. In case of chain-branching kinetics, there

is a delay with constant temperature. Chain reaction involves initiation, propagation, branching and termination reactions. Ignition occurs when enough radicals (such as O, H, OH, HO_2, and CH_3) [37, 38] have been produced which release enough heat to cause a temperature rise. Ignition delay time depends on the number and kind of existing carbon-hydrogen compounds hence it differs from one fuel to another. In a diesel engine, it affects the amount of fuel/air mixture formed before ignition and hence rate of heat release. Rate of heat release in turn determines the peak combustion temperature which has a direct relation with NO_x formation.

2.7 Detailed Reaction Mechanisms

A chemical kinetic reaction mechanism of a fuel is a collection of several elementary reactions necessary to describe an overall reaction process. It involves reactions of both reactants, reactive intermediate species and products. The rate parameters for each elementary reaction is presented in the reaction mechanism. The rate parameters is as defined by Arrhenius equation (see Appendix A). These include pre-exponential factor, exponent and activation energy in the specific rate constant for a reaction.

To compute the combustion characteristics of a fuel, its kinetic model is required. This can either be a detailed or reduced kinetic reaction mechanism. Several kinetic models for methyl esters combustion have been discussed in section 2.2.

2.8 Thermodynamic Properties

The thermodynamic properties required for the simulations of homogeneous system, laminar, freely propagating and laminar diffusion flames are the frozen specific heat capacities

at constant pressure of the pure species i, c_{pi}, the frozen specific heat capacity at constant pressure of the gas mixture, c_p, and the enthalpy, h_i, for pure species i.

The polynomial curve fits of NASA type are use to calculate the thermodynamic properties [39, 40]. Specifically, the properties are given as follows:

- Molar heat capacity at constant pressure, C_{pi}:

$$\frac{C_{pi}}{R_0} = a_1 + a_2 T + a_3 T^2 + a_4 T^3 + a_5 T^4. \tag{2.4}$$

- Molar enthalpy, H_i:

$$\frac{H_i}{R_0} = a_6 + a_1 T + \frac{a_2}{2} T^2 + \frac{a_3}{3} T^3 + \frac{a_4}{4} T^4 + \frac{a_5}{5} T^5. \tag{2.5}$$

- Molar entropy, S_i:

$$\frac{S_i}{R_0} = a_7 + a_1 \ln T + a_2 T + \frac{a_3}{2} T^2 + \frac{a_4}{3} T^3 + \frac{a_5}{4} T^4. \tag{2.6}$$

Here $a_1 - a_7$ are polynomial coefficients. The thermodynamic database has two set of polynomial coefficients; the first set is for the high temperature range (1000-6000 K), and the second set for the low temperature range of (300-1000 K). The molar quantities C_{pi}, H_i and S_{pi} are related to the respective mass-based quantities through $C_{pi} = c_{pi} W_i$, $H_i = h_i W_i$ and $S_i = s_i W_i$. The mass-based mixture frozen specific heat capacity, enthalpy and entropy are given by

$$c_p = \sum_{i=1}^{N} Y_i c_{pi}, \quad h = \sum_{i=1}^{N} Y_i h_i, \quad s = \sum_{i=1}^{N} Y_i s_i. \tag{2.7}$$

2.9 Transport Properties

The transport properties required for the simulations of laminar, freely propagating and laminar diffusion flames are the dynamic viscosity, μ, of the gas mixture, the thermal conductivity, λ, of the gas mixture, and the ordinary mixture-averaged and thermal diffusion coefficients for species i, D_i, and D_{Ti}, respectively.

If a global overall one-step or two-step reactions are taken to represent the combustion chemistry, then simple relationships between μ, λ and the D_i can be derived [39] by assuming constant Lewis numbers, L_i, for all species,

$$L_i = \frac{\lambda}{\rho c_p D_i} = \text{constant}_i, \quad i = 1, ..., N, \tag{2.8}$$

and a constant Prandtl number,

$$Pr = \frac{\mu c_p}{\lambda} = \text{constant}. \tag{2.9}$$

However, when a detailed chemical kinetic mechanism is used to represent the combustion chemistry (as in the case in this thesis), then a more detailed formulation of transport properties is required. A detailed modeling of molecular transport data as presented in [39] can be summarized as follows:

- Dynamic viscosity of species i, μ_i:

$$\mu_i = \frac{5}{16} \frac{\sqrt{\pi m_i K_B T}}{\pi \sigma_i^2 \Omega^{(2,2)\star}}, \tag{2.10}$$

  where σ is the Lennard-Jones collision diameter, m_i is the mass of the molecule, K_B is the Boltzmann constant, $\Omega^{(2,2)\star}$ is collision integral, which is a function of the

reduced temperature, $T^\star$, and dipole moment, $\delta^\star$. The quantities $T^\star$ and $\delta^\star$ are given as; $T^\star = T_i^\star \equiv (K_B T/\epsilon_i)$ and $\delta^\star = \delta_i^\star \equiv (1/2)(d_i^2/\epsilon_i \sigma_i^3)$, here d_i is the dipole moment of species i, ϵ_i is its Lennard-Jones potential well depth.

- Dynamic viscosity of the mixture, μ:

$$\mu = \frac{1}{2}\left(\sum_{i=1}^{N} X_i \mu_i + \frac{1}{\sum_{i=1}^{N}(X_i/\mu_i)}\right). \tag{2.11}$$

- Thermal conductivity of species i, λ_i:

$$\lambda_i = \frac{\mu_i}{W_i}\left(f_{trans} C_{v,trans} + f_{rot} C_{v,rot} + f_{vib} C_{v,vib}\right), \tag{2.12}$$

where f_{trans}, f_{rot} and f_{vib} are the species' translational, rotational and vibrational degrees of freedom, respectively, and $C_{v,trans}$, $C_{v,rot}$, $C_{v,vib}$ are the respective contribution to the molar heat capacity at constant volume, C_v, of species i.

- Thermal conductivity of the mixture, λ:

$$\lambda = \frac{1}{2}\left(\sum_{i=1}^{N} X_i \lambda_i + \frac{1}{\sum_{i=1}^{N}(X_i/\lambda_i)}\right). \tag{2.13}$$

- Binary diffusion coefficient, D_{ij}:

$$D_{ij} = \frac{3}{16}\frac{\sqrt{2\pi K_B^3 T^3/W_{ij}}}{p\pi\sigma_{ij}^2 \Omega^{(1,1)\star}}, \tag{2.14}$$

Besides the quantities defined before, $W_{ij} = 2W_i W_j/(W_i + W_j)$ is the reduced molar mass for the pair of species (i, j), and σ_{ij} is the average collision diameter. The

mixture average diffusion coefficient, D_i is given as

$$D_i = \frac{1 - Y_i}{\sum_{\substack{j=1 \\ j \neq i}}^{N} (X_i / D_{ij})}. \tag{2.15}$$

- Thermal diffusion coefficient of species i, D_{Ti}:

$$D_{Ti} = \frac{\Theta_i D_i}{X_i}, \tag{2.16}$$

where Θ_i is the thermal diffusion ratio of species i.

The thermodynamic and transport properties for the species, which are in CHEMKIN format are obtained from Princeton University kinetic model databases [41] and GRI-Mech 3.0 databases [9].

2.10 Conclusion

The development of combustion chemistry for methyl esters as well as biodiesel fuels have been advanced in the last decade. Several kinetics models for both small-chain and long-chain methyl esters have been developed. These kinetics models have been used to study several aspects of methyl esters combustion: intermediate species production; ignition and extinction; the effects of saturation; and the effects of molecular structure. Exhaust emissions of methyl esters combustion in an engine have been studied experimentally. However, no kinetic models have been developed for the studies of NO_x formation in esters.

CHAPTER THREE

3.0 GOVERNING EQUATIONS

3.1 Introduction

The governing equations for the system are the conservation of mass, species, momentum and energy for a multi-component reacting flow. This chapter presents the general conservation equations for such a system. Subsequently, conservation equations for particular configurations investigated in this study; one dimensional (1D) laminar premixed flame, 1D laminar diffusion flame, and homogeneous reactor, are presented.

3.2 Governing Equations

3.2.1 General Governing Equations

The conservation equations governing multi-component, chemically reacting, ideal gas mixtures have been derived and are available in literature [35, 42, 43]. They are summarized below:

- Mass conservation equation:

$$\frac{\partial \rho}{\partial t} + \nabla.(\rho \mathbf{v}) = 0. \tag{3.1}$$

- Momentum conservation equation:

$$\frac{\partial \mathbf{v}}{\partial t} + \mathbf{v}.\nabla \mathbf{v} = -(\nabla.\mathbf{P})/\rho + \sum_{i=1}^{N} Y_i \mathbf{f}_i, \tag{3.2}$$

where $\mathbf{P}$ is stress tensor given as;

$$\mathbf{P} = \left[p + \left(\frac{2}{3}\mu - \mathrm{k}\right)(\nabla.\mathbf{v})\right]\mathbf{U} - \mu\left[(\nabla\mathbf{v}) + (\nabla\mathbf{v})^{\mathbf{T}}\right]. \tag{3.3}$$

- Species conservation equation for a species i:

$$\frac{\partial(\rho Y_i)}{\partial t} + \nabla.[\rho Y_i(v_0 + \bar{V_i})] = w_i \quad i = 1, ..., N. \tag{3.4}$$

- Energy conservation equation:

$$\rho\frac{\partial u}{\partial t} + \rho\mathbf{v}.\nabla u = -\nabla.\mathbf{q} - \mathbf{P} : (\nabla\mathbf{v}) + \rho\sum_{i=1}^{N} Y_i\mathbf{f}_i \cdot V_i. \tag{3.5}$$

where $\mathbf{P}$ is stress tensor 3.3 and heat flux vector, $\mathbf{q}$ is

$$\mathbf{q} = -\lambda\nabla T + \rho\sum_{i=1}^{N} h_i Y_i V_i + RT\sum_{i=1}^{N}\sum_{j=1}^{N}\left(\frac{X_i D_{T,i}}{W_i D_{ij}}\right)(V_i - V_j) + \mathbf{q}_R. \tag{3.6}$$

In Eqs (3.1)-(3.6), t is time, D_{ij} is binary diffusion coefficient for species i and j, $\mathbf{f}_i$ is external force per unit mass on species i, k is bulk viscosity coefficient, N is total number of chemical species, p is hydrostatic pressure, $\mathbf{q_R}$ is radiant heat flux vector, R is universal gas constant, T is temperature, u is internal energy per unit mass for the gas mixture, $\mathbf{U}$ is unit tensor, $\mathbf{v}$ is velocity vector, $\mathbf{v_0}$ is flow velocity (mass weighted average velocity), λ is thermal conductivity, $\mathbf{q}_R$ is the radiant heat flux, μ is coefficient of dynamic viscosity, the superscript $\mathbf{T}$ denotes the transpose of the tensor, ρ is mass density and $D_{T,i}$, h_i, V_i, w_i, W_i, X_i and Y_i are thermal diffusion coefficient, specific enthalpy, diffusion velocity, rate of production by chemical reactions, molecular weight, mole fraction and mass fraction of species i respectively.

Equations (3.1)- (3.2) and (3.5) comprise N+5 equations in the N+5 unknowns, Y_i, ρ, u and $\mathbf{v_0}$. The functions $\mathbf{f}_i$, $\mathbf{P}$, $\mathbf{q}$, $\bar{V}_i$ and w_i must be related to the other dependent and independent variables for the system to form a closed set of equations.

3.2.2 Governing Equations for Laminar, One-Dimensional, Premixed, and Freely Propagating Flames

Assumptions

1. One dimensional freely propagating flame.
2. Low Mach number (deflagration) flame.
3. Thermodynamic part of the pressure is taken as spatially uniform.
4. The effect of viscous dissipation is neglected.
5. Body forces are neglected.
6. Dufour and Soret effects are neglected.

In view of assumptions 1-6, Eqs (3.1)-(3.6) can be recast [35], thus

- Mass conservation equation:

$$\frac{\partial \rho}{\partial t} + \frac{1}{A}\frac{\partial}{\partial x}(\rho V_x A) = 0. \tag{3.7}$$

- Species conservation equation for a species i:

$$\rho\left(\frac{\partial Y_i}{\partial t} + V_x\frac{\partial Y_i}{\partial x}\right) = -\frac{1}{A}\frac{\partial}{\partial x}(\rho Y_i V_i A) + w_i \quad i = 1, ..., N. \tag{3.8}$$

- Energy conservation equation:

$$\rho c_p \left(\frac{\partial T}{\partial t} + V_x \frac{\partial T}{\partial x} \right) = \frac{1}{A} \frac{\partial}{\partial x} \left(\lambda A \frac{\partial T}{\partial x} \right) - \frac{\partial T}{\partial x} \sum_{i=1}^{N} c_{pi} \rho Y_i V_i - \sum_{i=1}^{N} h_i w_i + \frac{dp}{dt} - \frac{1}{A} \frac{\partial}{\partial x} (\mathbf{q}_R A) + A_s h_s (T - T_s). \tag{3.9}$$

- Equation of sate:

$$p = \rho R T \sum_{i=1}^{N} (Y_i / W_i). \tag{3.10}$$

Besides the quantities defined before, in Eqs (3.7)-(3.10) x is the spatial coordinate, A is the spatially varying cross sectional area, V_x is the velocity in the x directions, p is the thermodynamic pressure, $\rho Y_i V_i$ is the diffusion flux, c_{pi} denote the mass-based constant pressure specific heat capacity for species i, c_p is the mixture's frozen specific heat capacity at constant pressure, h_s is the heat transfer coefficient between gas and solid phase, A_s is the local wetted surface area per unit void volume.

Equations (3.7)-(3.10) represent a system of $N + 3$ equations for $N + 3$ unknowns; ρ, V_x, T, $Y_1, ..., Y_N$, hence it is closed and can be solved.

The fluid mechanical part of pressure, p', is considered an additional unknown. It is governed by the momentum equation;

$$\rho \left(\frac{\partial V_x}{\partial t} + V_x \frac{\partial V_x}{\partial x} \right) = -\frac{\partial p'}{\partial x} + \frac{4}{A} \frac{\partial}{\partial x} \left(A \mu \frac{\partial V_x}{\partial x} \right). \tag{3.11}$$

Equation (3.11) is solved once a solution has been obtained for Eqs (3.7)-(3.10). However, the $N + 4$ equations are solved simultaneously.

3.2.2.1 Boundary Conditions

The cold boundary (unburnt mixture) is located infinitely far upstream, while the hot boundary (burnt mixture) is located infinitely far downstream. For a computational domain $[y_u, y_b]$ (where y_u and $y_b > y_u$ is the location of the cold and hot boundary respectively) and a given $p(t)$, then the computational boundary can be given as

$$T = T_u, \quad Y_i = Y_{iu} \quad \text{for} \quad i = 1, ..., N \quad \text{at} \quad y = y_u, \tag{3.12}$$

$$\frac{\partial T}{\partial y} = \frac{\partial Y_i}{\partial y} = 0 \quad \text{for} \quad i = 1, ..., N \quad \text{at} \quad y = y_b, \tag{3.13}$$

and

$$T = T_0 \quad \text{at} \quad y = y_0, \tag{3.14}$$

where Eq. (3.14) fixes the flame at $y = y_0$ (a frame of reference that moves with the flame speed, S_L) and y_0 is approximated as

$$y_0 = y_u + (y_b - y_u)/3. \tag{3.15}$$

3.2.3 Governing Equations for Laminar, Counterflow, Diffusion Flames

Assumptions

1. Two dimensional planar configuration.

2. Low Mach number (deflagration) flame.

3. Thermodynamic part of the pressure is taken as spatially uniform.

4. The effect of viscous dissipation is neglected.

5. Body forces are neglected.

6. Dufour and Soret effects are neglected.

7. The flame is embedded in a thin boundary-layer.

In view of assumptions 1-6, Eqs (3.1)-(3.6) can be recast [35], thus

- Mass conservation equation:

$$\frac{\partial \rho}{\partial t} + \frac{\partial}{\partial x}(\rho V_x) + \frac{\partial}{\partial y}(\rho V_y) = 0. \tag{3.16}$$

- Momentum conservation equations:

$$\rho\left(\frac{\partial V_x}{\partial t} + V_x\frac{\partial V_x}{\partial x} + V_y\frac{\partial V_x}{\partial y}\right) = -\frac{\partial p}{\partial x} + \left[\frac{\partial}{\partial x}(\tau_{xx}) + \frac{\partial}{\partial y}(\tau_{xy})\right], \tag{3.17}$$

$$\rho\left(\frac{\partial V_y}{\partial t} + V_x\frac{\partial V_y}{\partial x} + V_y\frac{\partial V_y}{\partial y}\right) = -\frac{\partial p}{\partial y} + \left[\frac{\partial}{\partial x}(\tau_{xy}) + \frac{\partial}{\partial y}(\tau_{yy})\right], \tag{3.18}$$

where Eqs (3.17) and (3.18) represent conservation of momentum in the x and y directions respectively. The components of the viscous part of the stress tensor is given by

$$\begin{aligned} \tau_{xx} &= \mu\left(2\frac{\partial V_x}{\partial x}\right) - (\frac{2}{3}\mu - \mathrm{k})(\nabla.\mathbf{v}), \qquad \tau_{xy} = \mu\left(\frac{\partial V_x}{\partial y} + \frac{\partial V_y}{\partial x}\right), \\ \tau_{yy} &= \mu\left(2\frac{\partial V_y}{\partial y}\right) - (\frac{2}{3}\mu - \mathrm{k})(\nabla.\mathbf{v}), \qquad \nabla.\mathbf{v} = \frac{\partial V_x}{\partial x} + \frac{\partial V_y}{\partial y}. \end{aligned} \tag{3.19}$$

- Energy conservation equation:

$$\rho c_p \left(\frac{\partial T}{\partial t} + V_x \frac{\partial T}{\partial x} + V_y \frac{\partial T}{\partial y} \right) = \frac{\partial}{\partial x} \left(\lambda \frac{\partial T}{\partial x} \right) + \frac{\partial}{\partial y} \left(\lambda \frac{\partial T}{\partial y} \right) - \frac{\partial T}{\partial x} \sum_{i=1}^{N} c_{pi} \rho Y_i U_i - \frac{\partial T}{\partial y} \sum_{i=1}^{N} c_{pi} \rho Y_i V_i - \sum_{i=1}^{N} h_i w_i + \frac{dp}{dt} - \nabla . q_R. \tag{3.20}$$

- Species conservation equation for a species i:

$$\rho \left(\frac{\partial Y_i}{\partial t} + V_x \frac{\partial Y_i}{\partial x} + V_y \frac{\partial Y_i}{\partial y} \right) = -\frac{\partial}{\partial x}(\rho Y_i U_i) - \frac{\partial}{\partial y}(\rho Y_i V_i) + w_i \quad i = 1, ..., N. \tag{3.21}$$

- Equation of state:

$$p = \rho R T \sum_{i=1}^{N} (Y_i / W_i). \tag{3.22}$$

Besides the quantities defined before, in Eqs (3.16)-(3.22), y denotes the longitudinal coordinate and x denotes the traverse (parallel to the stagnation plane) coordinate, V_x and V_y denote the velocity component in the x and y directions respectively, and U_i and V_i denote the diffusion velocity component for species i in the x and y directions respectively.

Assumption 7 requires the use of the boundary layer theory approximations. The principle here is that the temperature and species composition are assumed to depend on only one independent variable; i.e, the coordinate perpendicular to the stagnation plane (y coordinate). In addition, the velocity component in y direction, V_y is also assumed to be dependent on only y coordinate. Similarity equations are derived [44] by defining a stream function,

$$\psi(x, y, t) = xG(y, t),$$

so that the accumulative-convective operator, L_1, is given by

$$L_1(\phi) = \frac{\partial(\rho\phi)}{\partial t} + \frac{\partial(\rho V_y \phi)}{\partial y} + \rho G\phi, \tag{3.23}$$

where the function $G(y,t) = V_x/x$ is a scaled velocity.

In terms of accumulative-convective operator, L_1, similarity equations for mass, momentum, energy and species (Eqs (3.16), (3.17), (3.20) and (3.21)) can be written as

$$\begin{aligned}
L_1(1) &= 0, && (3.24)\\
L_1(G) &= \frac{\partial}{\partial y}\left(\mu\frac{\partial G}{\partial y}\right) - \rho G^2 + P'(t), && (3.25)\\
c_p L_1(T) &= \frac{\partial}{\partial y}\left(\lambda\frac{\partial T}{\partial y}\right) - \frac{\partial T}{\partial y}\sum_{i=1}^{N} c_{pi}\rho Y_i V_i - \sum_{i=1}^{N} h_i w_i + \frac{dp}{dt} - \frac{\partial q_R}{\partial y}, && (3.26)\\
L_1(Y_i) &= -\frac{\partial}{\partial y}(\rho Y_i V_i) + w_i \quad i = 1, ..., N. && (3.27)
\end{aligned}$$

The term in P' appearing in the momentum equation (3.25) represents a temporal forcing term defined by

$$P'(t) \equiv \rho_\infty \left(\frac{da}{dt} + a(t^2)\right),$$

where a is the strain rate which is prescribed.

3.2.3.1 Boundary Conditions

The assumptions for fully infinite formulation are

1. The flame is thin compared to the dimensions of stagnating-flow region between two opposed nozzles.

2. The flame is located within the thin viscous boundary layer which is embedded in

the outer, non-viscous and vorticity-free stagnating flow.

The boundary conditions are to be applied at the edges of the boundary layer (infinitely far away from the stagnation plane). At the right edge (air stream), the boundary conditions are

$$G - a(t) = T - T_{\infty} = Y_i - Y_{i,\infty} = 0 \quad \text{as} \quad y \longrightarrow \infty. \tag{3.28}$$

At the left boundary (fuel stream), the boundary conditions are

$$G - a(t)\left(\frac{\rho_{+\infty}}{\rho_{-\infty}}\right) = T - T_{-\infty} = Y_i - Y_{i,-\infty} = 0 \quad \text{as} \quad y \longrightarrow -\infty. \tag{3.29}$$

Here, the subscripts $-\infty$ and ∞ are used to identify conditions or quantities in the fuel and air streams respectively.

At the stagnation plane, $y = 0$,

$$V_y = 0. \tag{3.30}$$

It has been assumed that the stagnation point is located at $y = 0$.

3.2.4 Governing Equations for Ignition in a Homogeneous Reactor

Homogeneous ignition delay is governed by single point transient (zero-dimensional time dependent) equations. When the reactor volume, V, is given as a constant or as a function of time, the following equations apply;

- Species conservation equation:

$$\rho \frac{\partial Y_i}{\partial t} = w_i. \tag{3.31}$$

- Energy conservation equation:

$$\rho c_v \frac{\partial T}{\partial t} + \frac{p}{V}\frac{dV}{dt} = -\sum_{i=1}^{N} u_i w_i + \frac{Q}{V}. \tag{3.32}$$

- Equation of state:

$$p = \rho R T \sum_{i=1}^{N} (Y_i/W_i), \tag{3.33}$$

where $c_v = \sum_{i=1}^{N} Y_i c_{vi}$ (specific heat at constant volume), V is the reactor volume and Q is rate at which heat is transferred across the reactor. Pressure p is a function of time and has to be determined as part of the solution. An ordinary differential equation for $p(t)$, is derived from the equation of state (3.33). Differentiating Eq. (3.33) with respect to time gives

$$\frac{dp}{dt} = \rho R \left(\frac{dT}{dt} \sum_{i=1}^{N} \left(\frac{Y_i}{W_i} \right) + T \sum_{i=1}^{N} \frac{1}{W_i} \frac{dY_i}{dt} \right). \tag{3.34}$$

Substituting for $\rho R = p/T \sum_{i=1}^{N} (Y_i/W_i)$ in Eq. (3.34) results in

$$\frac{1}{p}\frac{dp}{dt} = \frac{1}{T}\frac{dT}{dt} + \sum_{i=1}^{N} \frac{W}{W_i}\frac{dY_i}{dt}, \tag{3.35}$$

where

$$W = 1/\sum_{i=1}^{N} (Y_i/W_i). \tag{3.36}$$

Using Eq. (3.32) for $(1/T)(dT/dt)$ in Eq. (3.35) gives

$$\frac{1}{p}\frac{dp}{dt} = -\frac{p}{\rho c_v T V}\frac{dV}{dt} - \sum_{i=1}^{N} \frac{u_i w_i}{\rho c_v T} + \frac{Q}{\rho c_v T V} + \sum_{i=1}^{N} \frac{W}{W_i}\frac{dY_i}{dt}. \tag{3.37}$$

Since $C_p - C_v = R$ and $C_p/C_v = \gamma$, Eq. (3.37) can be recast, thus

$$\frac{1}{p}\frac{dp}{dt} + \frac{\gamma - 1}{V}\frac{dV}{dt} = \sum_{i=1}^{N} \frac{w_i}{\rho}\left(\frac{W}{W_i} - \frac{u_i}{c_v T}\right) + \frac{Q}{\rho c_v T V}. \tag{3.38}$$

For a constant volume case, the terms that have dV/dt become zero. Species equation (3.31), energy equation (3.32) and pressure equation (3.38) are solved numerically for given initial values of $Y_1, ..., Y_N$, T, p and constant volume V.

3.2.4.1 Initial Conditions

The initial values of $Y_1, ..., Y_N$, T, p and constant volume V are to be prescribed. Initial values of mass and specific volume are computed by the code through the relations $m = \rho_0 V$ and $v_0 = 1/\rho_0$.

CHAPTER FOUR

4.0 NUMERICAL SOLUTION METHOD

4.1 Introduction

The governing equations (3.7)-(3.10), (3.24)-(3.27) and (3.31)-(3.33) in chapter three consist of first and second order partial differential equations, solution of which requires application of numerical methods. In this regard, the unknown dependent variables, viz, temperature, velocity, species mass fraction, density, and species mole fraction, are determined at selected grid points in the computational domain. Presented in this chapter are: discretization of partial differential equations; finite difference schemes adopted; and the solution method for discretized equations. The order of accuracy and truncation errors, which result from the finite difference scheme adopted are also discussed.

4.2 Discretization of the Governing Equations

The governing equations for freely propagating flame (3.7)-(3.10), laminar counterflow flame (3.24)-(3.27) and homogeneous system (3.31)-(3.33) have been discretized using finite difference scheme, as adopted in COSILAB [45]. The computational domain have been divided into a non-uniform mesh as shown in Fig. 4.1. The distance between two consecutive grid points in the same direction changes. The generation of a non-uniform mesh is discussed in the section on adaptive selection of grid points.

The PDEs are approximated by finite difference method, consecutively yielding a system of algebraic equations, which are solved for all unknown dependent variables at discrete grid points. In the next section, the finite difference scheme adopted in this thesis is discussed.

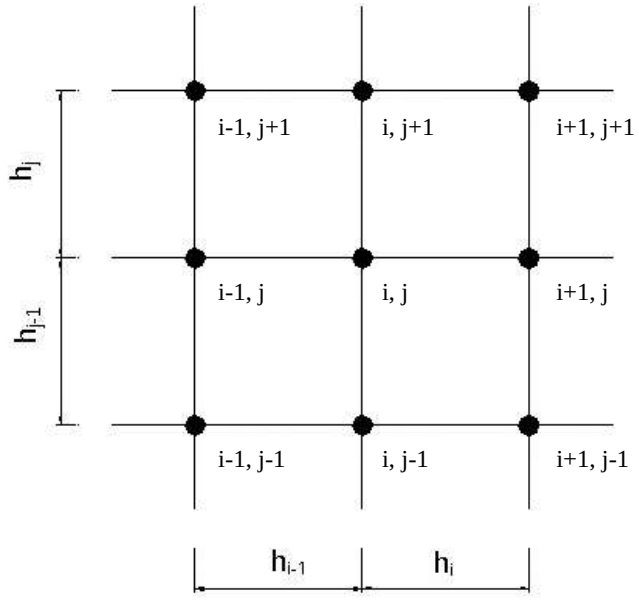

Figure 4.1: Non-uniform mesh

4.2.1 Finite Difference Schemes

In this thesis various terms in the governing equations have been approximated using different finite difference schemes.

The first-order spatial derivatives in freely propagating and diffusion flames are approximated using a hybrid scheme [44]. The hybrid differencing scheme combines both the central and the one-sided differencing (upwind) schemes. For a dependent variable, say T, at grid point j, the second-order accurate central-difference scheme is

$$\left(\frac{\partial T}{\partial x}\right)_j = \frac{h_{j-1}}{h_j(h_j+h_{j-1})}T_{j+1} + \frac{h_j - h_{j-1}}{h_j h_{j-1}}T_j - \frac{h_j}{h_{j-1}(h_j+h_{j-1})}T_{j-1} - \underbrace{\frac{h_j h_{j-1}}{6}\left(\frac{\partial^3 T}{\partial x^3}\right)_j + HOT}_{\text{Error term}}, \tag{4.1}$$

where HOT is an abbreviation for high-order terms. The leading truncation error term is second-order. The truncation error is reduced when the number of grid points is increased.

The first-order accurate one-sided differencing scheme are

- Forward difference:

$$\left(\frac{\partial T}{\partial x}\right)_j = \frac{T_{j+1} - T_j}{h_j} + 0(h_j). \tag{4.2}$$

- Backward difference:

$$\left(\frac{\partial T}{\partial x}\right)_j = \frac{T_j - T_{j-1}}{h_{j-1}} + 0(h_{j-1}). \tag{4.3}$$

If one-sided scheme is employed, then upwinding is achieved. In both expressions, the leading term in the local truncation error is first-order.

The second-order spatial derivatives in freely propagating and diffusion flames are approximated by second-order accurate central differences scheme;

$$\begin{aligned}\frac{\partial}{\partial x}\left(\lambda\frac{\partial T}{\partial x}\right)_j &= \frac{2}{h_j + h_{j-1}}\left[\frac{\lambda_{j+1/2}(T_{j+1} - T_j)}{h_j} - \frac{\lambda_{j-1/2}(T_j - T_{j-1})}{h_{j-1}}\right] - \\ &\underbrace{\frac{h_j - h_{j-1}}{3}\left(\frac{\partial^3 T}{\partial x^3}\right)_j + HOT}_{\text{Error term}},\end{aligned} \tag{4.4}$$

where λ=$\lambda(x, t, \mathbf{u})$ is given by

$$\lambda_{j-1/2} = \lambda\left(\frac{x_{j-1} + x_j}{2}, t, \frac{\mathbf{u}_{j-1} + \mathbf{u}_j}{2}\right) \quad j = 1, ..., N, \tag{4.5}$$

and $\mathbf{u}$ denotes a vector of unknown dependent variables. The leading truncation error term is first-order but vanishes when the spacing between the grid points is uniform, making it a second-order accurate. The expression shows that the truncation error is reduced by either refining the grid or having the grid points approximately equally spaced.

The time derivatives in the governing equations for all flames considered in this thesis are

discretized using backward-Euler finite difference approximation:

$$\frac{\partial T}{\partial t} = \frac{T_j^m - T_j^{m-1}}{\Delta t} + 0(\Delta t), \quad m = 1, 2, ... \tag{4.6}$$

A time marching technique is used to solve the governing equations for all flames. The time dependent version of the governing equations are first integrated with respect to time in steps starting with initial specified profiles, which should satisfy the equations at time level m=*0* with t=t^0≡*0*. The solutions to the governing equations are then sought at the subsequent time levels $(m = 1; t = t^1)$, $(m = 2; t = t^2)$,..., with $0 = t^0 < t^1 < t^2 < ... < t^m < ...$, where the superscript m is used to identify quantities at time level m. The integration is complete when either a specified time level m_{max} or time t_{max} is reached.

4.3 Adaptive Selection of Grid points

The computation of engineering problems, and more so reactive flows, requires the use of adaptive selection of grid points. This method of grid points selection assigns them automatically to where they are most needed in the computational domain. In a reactive flow, the heat release associated with combustion processes results in steep gradients and strong curvature for the dependent variables profiles. Therefore, in order to reduce the temporal and spatial discretization errors, adaptive gridding method is required.

The procedures for the adaptive computation of steady reactive-flow problems is outlined in [46]. At any fixed time level m, the mesh $\mathbf{M}^m$ is distributed equally on the interval $[x_1^m, x_B^m]$ with respect to a non-negative weight function W^m and a constant C^m. W^m is selected such that

$$\int_{x_j^m}^{x_{j+1}^m} W^m dx = C^m \quad j = 1, ..., B^m - 1, \tag{4.7}$$

or in discrete form,

$$\Delta x_j^m W^m = C^m \quad j = 1, ..., B^m - 1, \tag{4.8}$$

where $\Delta x_j^m = x_{j+1}^m - x_j^m$, and B is the number of grid points.

This condition makes the grid interval to be small where the weight function is large, and vice versa. The weight function is chosen as a measure of the solution gradient $\partial \mathbf{U}/\partial x$ and/or $\partial^2 \mathbf{U}/\partial x^2$. Thus the grid points will be closely spaced in the region of steep gradient, and widely spaced in region of low gradient. A weight function that is based on first derivative of the solution, $\partial \mathbf{U}/\partial x$, treats the regions near extrema, i.e., where $\partial \mathbf{U}/\partial x = 0$, to be similar to low gradient regions. To avoid this problem, second derivative of the solution, $\partial^2 \mathbf{U}/\partial x^2$, is incorporated into the weight function. This approach concentrate grid points even in regions of high curvature of the solution curve.

The size of adjacent mesh interval is controlled from varying rapidly by locally bounding the mesh at any time level m through;

$$R^{-1} \leq h_b/h_{b-1} \leq R, \quad b = 2, ..., B - 1, \tag{4.9}$$

where R is a constant greater than one.

4.4 Solution of Discretized Equations

The governing equations (PDEs) are discretized into a system of differential algebraic equations in the form:

$$A(\mathbf{U})\frac{d\mathbf{U}}{dt} = F(\mathbf{U}), \tag{4.10}$$

where $\mathbf{U}$ is the overall vector for the unknown dependent variables, given by;

$$\mathbf{U} = (\mathbf{u}_1, ..., \mathbf{u}_b)^T, \tag{4.11}$$

$\mathbf{u}_b$ is the vector of dependent variables at each grid point b, $b = 1, ..., B$, and $\mathbf{F}$ is the overall vector function whose components represent the governing equations in residual form with the exclusion of terms involving time-derivatives of the dependent variables. $\mathbf{F}$ is given as

$$\mathbf{F} = (\mathbf{f}_1, ..., \mathbf{f}_b)^T, \tag{4.12}$$

$\mathbf{f}_b$ is the local vector function at each grid point b, $b = 1, ..., B$.

The differential algebraic system of equation (4.10) is solved by either Modified Newton method or Euler method.

Modified Newton method can be applied to steady and time-dependent problems. When applied to unsteady problems, it has been found [47] to be very robust and, relatively, weakly sensitive towards the initial profiles. For steady-state problems with sufficiently good initial guesses, this method has been found to converge fast. The weakness of the method is its crude first-order differencing of the time derivatives, and the availability of only a limited time-step size control.

Euler method is applied to unsteady problems. This method is suitable for the solution of stiff differential algebraic system.

4.5 Accuracy of the Results

The accuracy of the results computed is dictated by the magnitude of the errors introduced during the computation process. The first error is introduced through the approximation of the PDEs into algebraic equation (discretization/truncation errors). The truncation error depends on the grid spacing and derivatives of the variable. For the case of upwind scheme and the backward Euler technique applied to first-order derivatives, a first-order accuracy is achieved. When central difference scheme is applied to a second-order derivative in a uniform mesh, approximation which are second-order, $0(h_j^2)$ accurate are obtained. However, if a non-uniform grid is used (as in the case in this thesis), one order of accuracy is lost. A systematic refinement of non-uniform grids gives a rate of reduction of truncation error that has the same order as for a uniform grid. Numerical accuracy is enhanced by having many grid points in the region of high gradient and having the grid points which are approximately equally spaced. This is achieved by applying adaptive selection of grid points technique.

Another error is introduced through the numerical method adopted. This error is normally specified to allow the convergence of the solution. A solution is considered to have converged when a steady state has been reached. When the dependent variables do not change from one time step to another, then steady state has been achieved. A commonly used convergence criterion, which represents the time rate of change of the variable considered is given by

$$\varepsilon = \frac{U_{k+1} - U_k}{\Delta t} \tag{4.13}$$

where ε is the convergence criterion for variable U.

4.6 Computation Code (COSILAB)

The computation of various flames governed by equations (3.7)-(3.10), (3.24)-(3.27) and (3.31)-(3.33) is implemented in the RUN1DL code in the software package COSILAB [45]. In order to solve a particular flame type using COSILAB, a detailed or reduced chemical kinetic model of the fuel is required. In addition, a thermodynamic and transport properties data for all species appearing in the chemical kinetic model are required. A homogenous system is zero dimension and does not require transport properties. The chemical kinetic models and properties data for different fuels are available in literature. COSILAB accepts reaction mechanisms, transport and thermodynamic data compatible to the international standard format originally put forward by Sandia National Laboratory. It has the following components: A graphical user interface, in which a flame can be set up and computed; a graph-digitizer for the generation of initial flame structures; reaction-pathway analysis option; sensitivity analysis option; and graphing, editing and export facilities for the computed results, including data saving in Excel and Matlab.

CHAPTER FIVE

5.0 HOMOGENEOUS SYSTEM

5.1 Introduction

In this chapter, we present and discuss results for ignition delay times, species concentration and temperature profiles for methane/air, methanol/air, and methyl formate/air mixtures modeled in an adiabatic homogeneous reactor. In combustion systems, a homogeneous transient system is used to study the chemical kinetics and combustion properties of the mixtures. Generally, homogeneous transient systems are classified into two: A constant pressure reaction model; and a constant volume reaction model. We have considered a constant volume case, which represent conditions of mixtures in a shock tube apparatus use for experimenting ignition delay times in fuels.

5.2 Ignition in a Shock Tube

In a laboratory environment, ignition can be studied using either a shock tube or rapid compression machine. The later is a single piston stroke apparatus, which compress the mixture in the combustion chamber to pressure and temperature similar to those at post compression condition in an engine. A shock tube apparatus is used to study the combustion kinetics; measure individual elementary reaction rates, ignition delay times, and other combustion properties at high temperatures. The operating principle of a shock tube is described above in section 2.6.1.

5.2.1 Modeling Details for Ignition in a Shock Tube

The experimental conditions behind a reflected shock in a shock tube can be modeled as adiabatic homogeneous mixture with constant internal energy and constant volume. In this numerical computation, methane/air, methanol/air, and methyl formate/air stoichiometric mixtures have been studied at constant volume of 200 cm^3, low pressure of 2.7 atm, and temperature ranging from 1000 K to 1950 K. The numerical simulations of these fuels have been done using the RUN1DL code in the software package COSILAB [45].

For this configuration and the subsequent (freely propagating and diffusion flames), methane and methanol flames are computed using GRI-Mech 3.0 reaction mechanism [9] (see Appendix C), while methyl formate flame is computed by combining the Dooley *et al.* [16] oxidation mechanism (see Appendix A) with the Leeds NOx oxidation mechanism [8] (see Appendix B). GRI-Mech 3.0 reaction mechanism has been validated and tested in previous investigations [14, 48]. Dooley *et al.* oxidation mechanism has also been validated in a wide range of conditions; a variable pressure flow reactor, shock tube facility, outwardly propagating flames and burner stabilized flames [16, 17]. Similarly, Leeds NOx oxidation mechanism has been validated in flow reactors, perfectly stirred reactors and low pressure laminar flames by Hughes *et al.* [49].

5.3 Results and Discussions

A comparison of ignition delay time in methane/air, methanol/air, and methyl formate/air stoichiometric mixtures at pressure of 2.7 atm and temperature range 1000 K to 1950 K is shown in Fig. 5.1. For lack of the exact experimental conditions from the other researchers, our model's ignition delay times are compared to those which are closely related. For

instance, for a stoichiometric homogeneous mixture of methane at an initial temperature of 1667 K, Seery and Bowman [50] obtained an ignition delay time of 160 μs for a pressure of 2.04 atm, while we have obtained 110 μs for a pressure of 2.70 atm. Ignition delay time reduces with increase in initial pressure [51], therefore, our ignition delay time value is consistent. Similarly, for a homogeneous mixture of methanol at an equivalence ratio of 0.75 and an initial temperature of 1667 K, Seiser *et al.* [52] obtained an ignition delay time of 70 μs for a pressure of 1.74 atm, while we have obtained 25 μs for a pressure of 2.70 atm. For a stoichiometric homogeneous mixture of methyl formate at an initial temperature of 1667 K, our ignition delay time (10 μs) agrees well with that of Dooley *et al.* [16] (10 μs from the model and 15 μs from the experiment).

Under all the conditions tested, methane have higher ignition delay times as compared to methanol and methyl formate. This reveals a trend of reduction of ignition delay time with increase in fuel oxygenation.

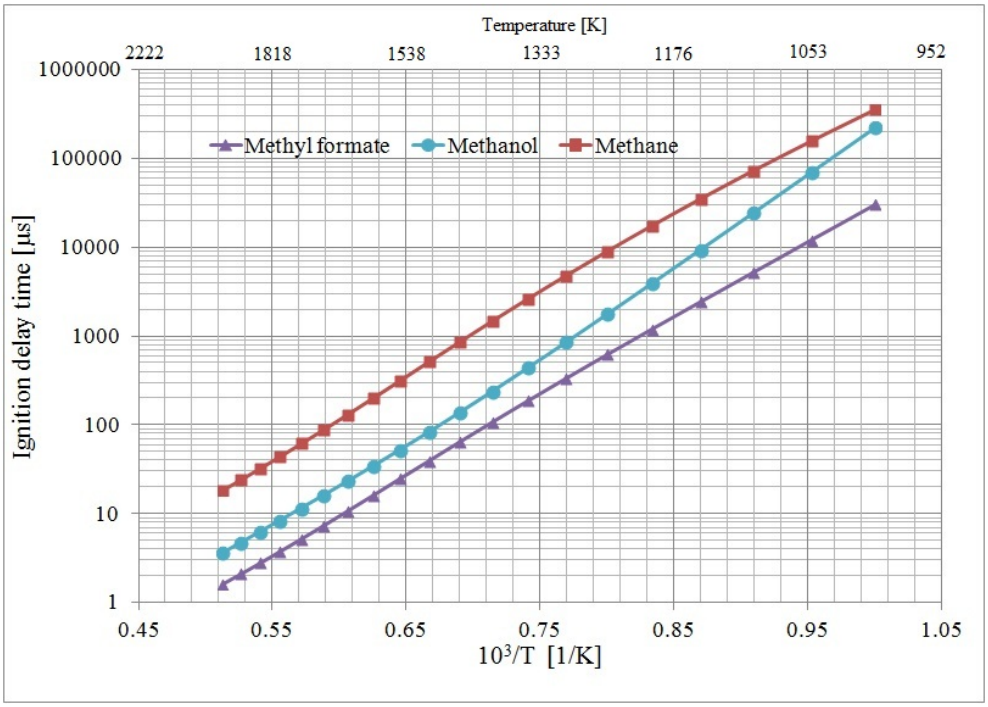

Figure 5.1: Ignition delay times for methane/air, methanol/air and methyl formate/air mixtures at pressure of 2.7 atm

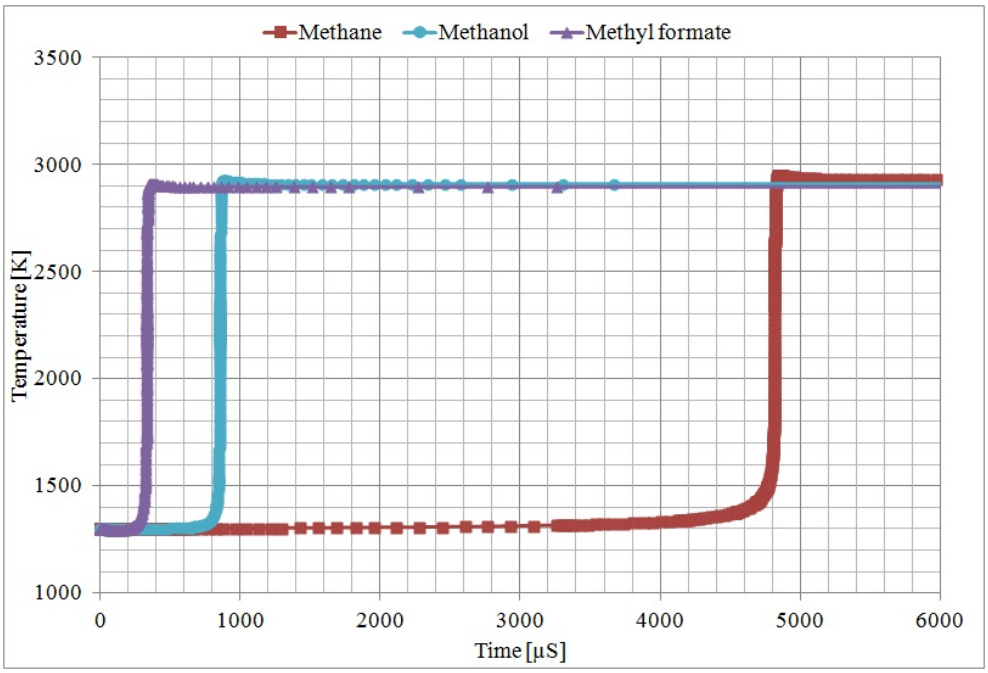

Figure 5.2: Temperature profiles for the three mixtures at the initial temperature of 1300 K and pressure of 2.7 atm

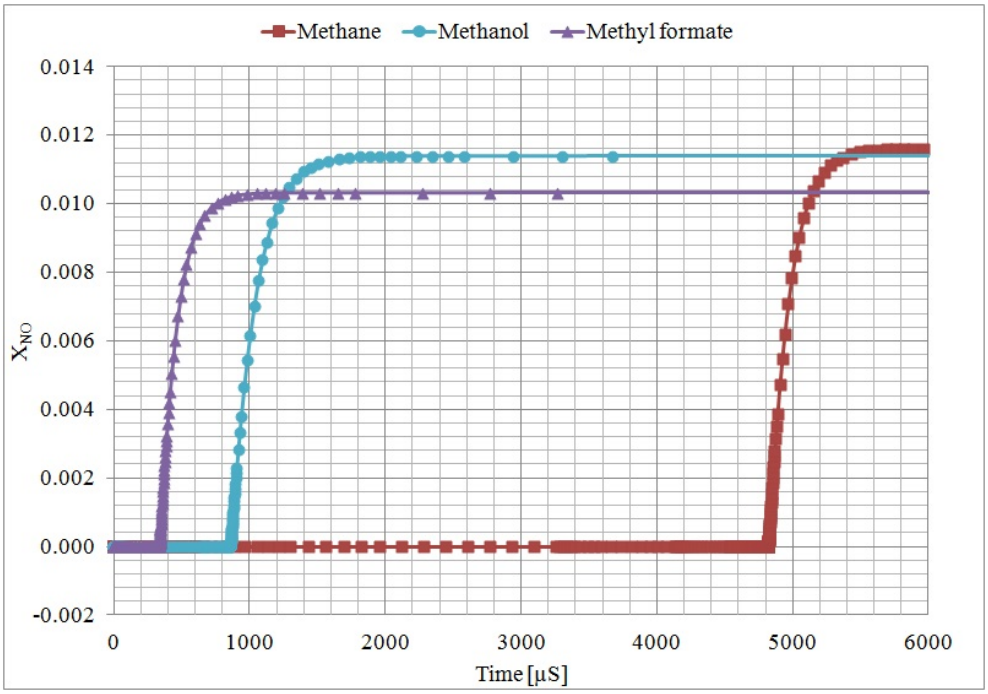

Figure 5.3: NO concentration profiles for the three mixtures at the initial temperature of 1300 K and pressure of 2.7 atm

Shown in Figs. 5.3-5.6 are the species concentration profiles for NO and other minor species related to its formation. Methane/air mixture has a significantly higher concentration of

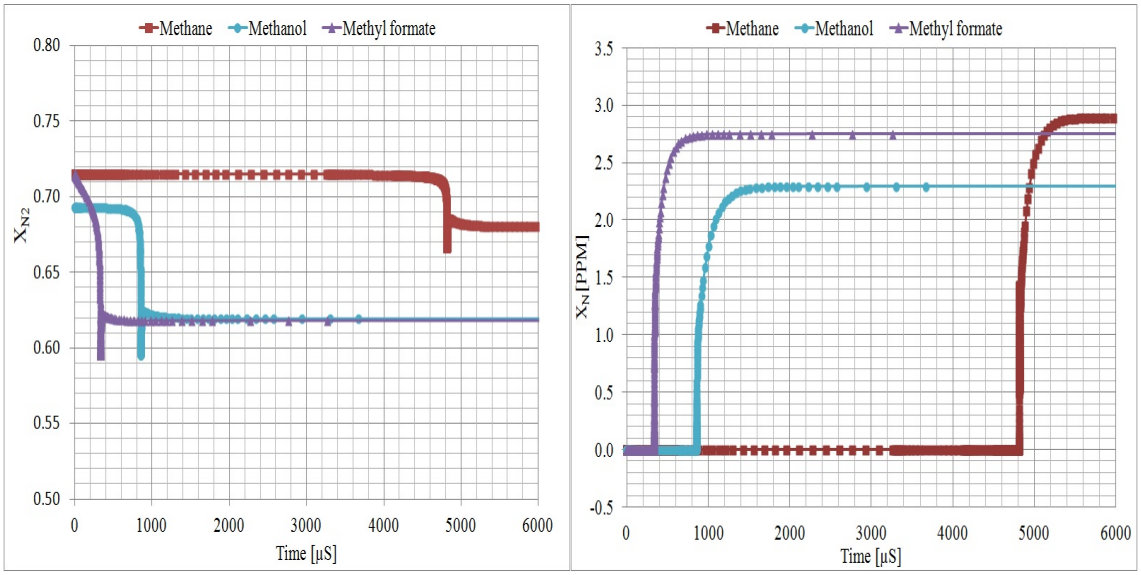

(a) N_2 mole fraction (b) N mole fraction

Figure 5.4: N_2 and N concentration profiles for the three mixtures at the initial temperature of 1300 K and pressure of 2.7 atm

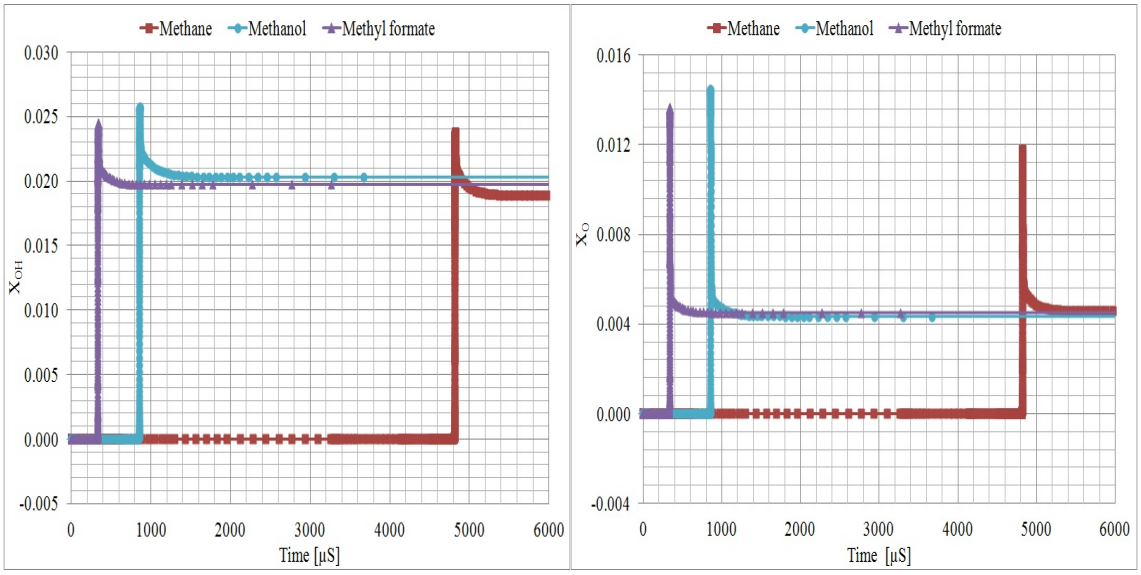

(a) OH mole fraction (b) O mole fraction

Figure 5.5: OH and O concentration profiles for the three mixtures at the initial temperature of 1300 K and pressure of 2.7 atm

profiles of immediate precursor species - CH and HCN- for prompt NO formation. Then, we would expect a significantly higher NO forming in methane than the oxygenated fuels, however, this is not the case. A slight difference is seen in the NO concentration profiles

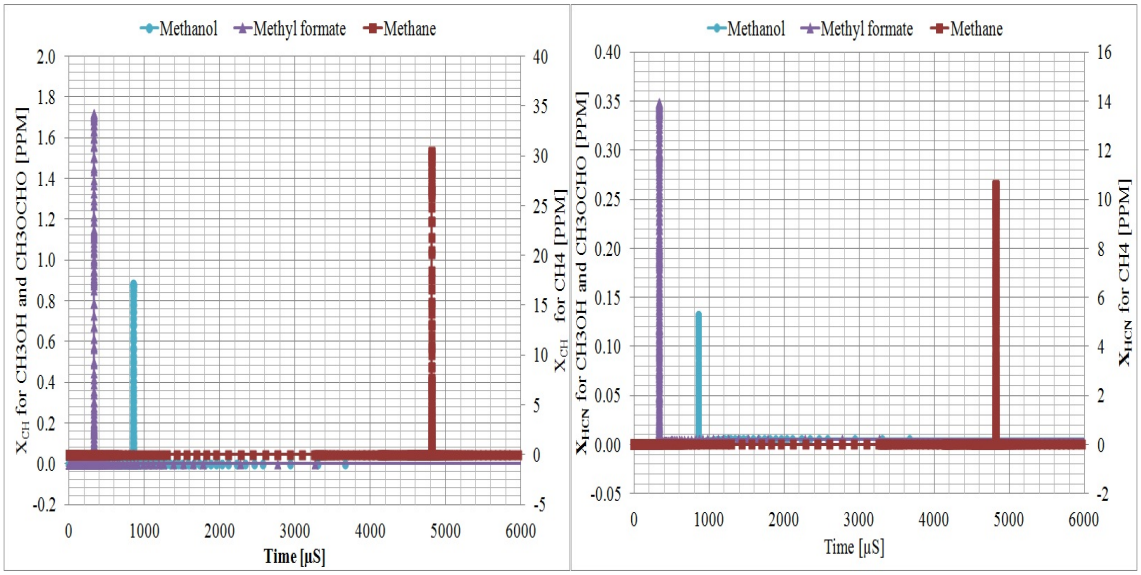

(a) CH mole fraction (b) HCN mole fraction

Figure 5.6: CH and HCN concentration profiles for the three mixtures at the initial temperature of 1300 K and pressure of 2.7 atm

for the three flames. This means that under these conditions the NO is formed mostly through the high temperature thermal NO reactions, since the temperatures are quite high (up to a maximum of approximately 2900 K as shown in Fig 5.2). The reaction between nitrogen molecule and oxygen atom in Zel'dovich mechanism: $N_2 + O \longrightarrow NO + N$ has a high activation energy, for instance a value of 318.4 KJ/mol in Leeds NOx oxidation mechanism (see Appendix B). Therefore, the reaction proceeds sufficiently fast at high temperatures and hence it is the rate-limiting step for NO formation. Other reactions with high activation energy which involve nitrogen molecule and other radicals are $CH_2 + N_2 \longrightarrow HCN + NH$ (309.69 KJ/mol) and $N_2 + C \longrightarrow CN + N$ (187.90 KJ/mol). At low temperatures, N formation route is initiated through the reaction: $CH + N_2 \longrightarrow HCN + N$, while at high temperatures N is formed through both this reaction and the high activation energy reactions mentioned before.

The plots of NO concentration profiles for the three fuels mixtures at different temperatures, Fig. 5.7, reveal a similar trend. The rate of increase of NO concentration with temperature

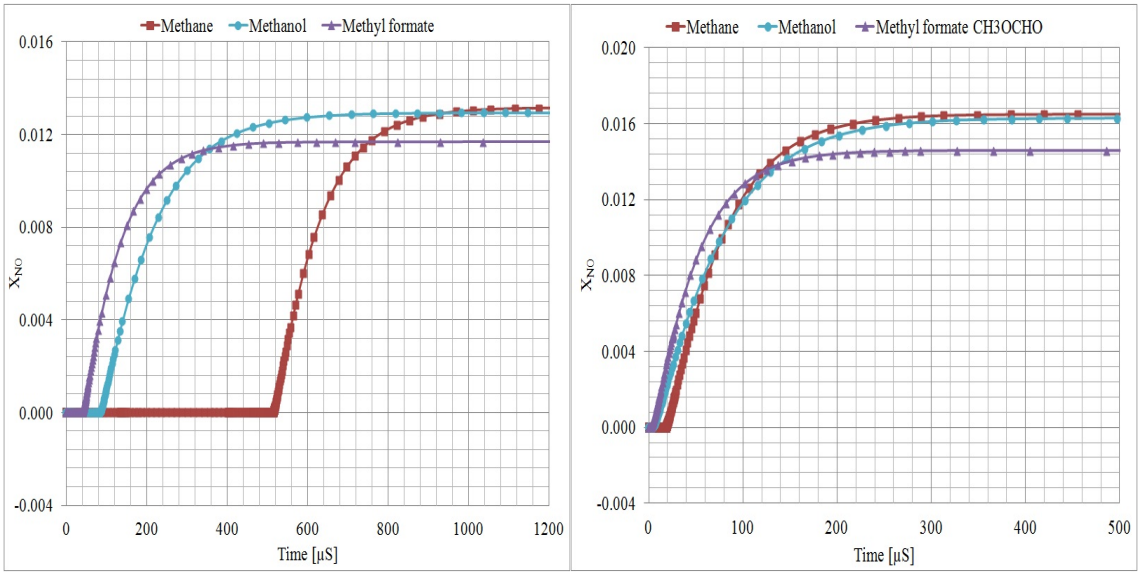

(a) At initial temperature of 1500 K (b) At initial temperature of 1950 K

Figure 5.7: NO concentration profiles for the three mixtures at pressure of 2.7 atm

is proportional in the three fuels. This trend is expected because as initial temperature is increased, the final temperature attained by mixture is also increased.

N_2O and NO_2 are produced in relatively small amounts in all the three fuels (see Fig. 5.8). Equilibrium concentration for N_2O is the same in CH_3OH and CH_3OCHO flames. However, it is attained at different points in time in each flame (due to difference in ignition delay time). A slightly higher equilibrium concentration for N_2O is observed in CH_4. N_2O is formed through reaction: $N_2 + O + M \longrightarrow N_2O + M$ and consumed through reactions: $N_2O + O \longrightarrow NO + NO$, $N_2O + H \longrightarrow N_2 + OH$ and $N_2O + OH \longrightarrow N_2 + HO_2$ [49]. These reactions are sensitive to temperature and they have significant impact at high temperatures.

A comparison of NO_2 concentration profiles is shown in Fig. 5.8b. A slightly higher equilibrium concentration for NO_2 is observed in CH_3OH flame, while CH_4 and CH_3OCHO attained the same equilibrium concentrations. NO_2 is mainly formed from the consumption of NO at low temperature through reaction: $HO_2 + NO \longrightarrow NO_2 + OH$, while at high

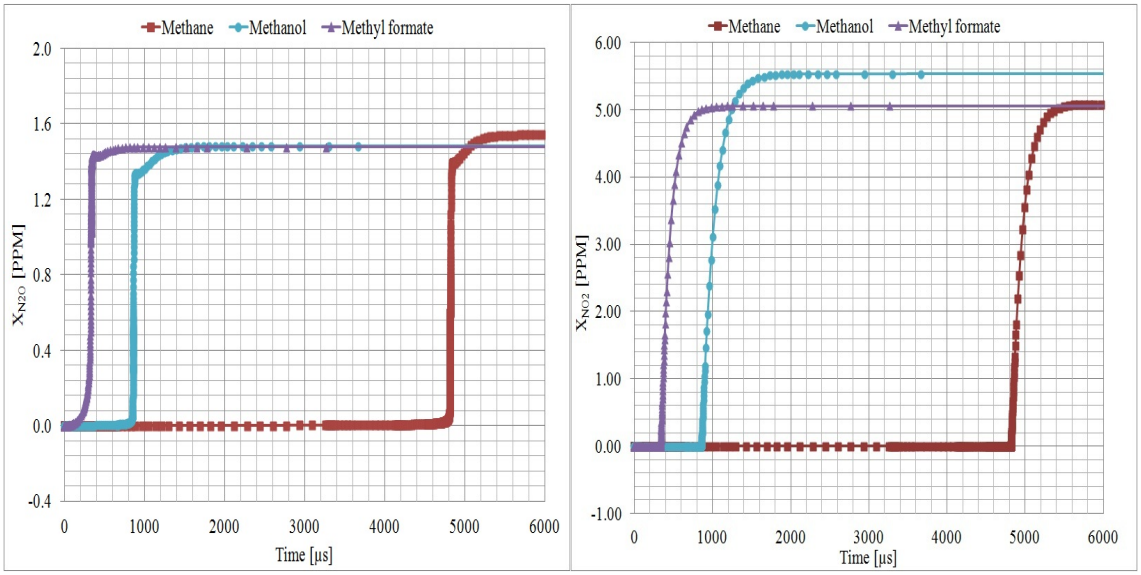

(a) N_2O mole fraction (b) NO_2 mole fraction

Figure 5.8: N_2O and NO_2 concentration profiles for the three mixtures at pressure of 2.7 atm

temperature it is formed through reaction: OH + NO $\longrightarrow$ NO_2 + H [33]. The flames' temperatures attained are high, hence the reaction involving the attack of OH on NO atom is relevant. The comparison of OH concentration profiles, Fig. 5.5a, show a similar behavior with the observed NO_2 concentration profiles.

5.4 Conclusions

NO formations in methane/air, methanol/air, and methyl formate/air stoichiometric mixtures in a homogeneous system have been discussed in this chapter. The NO concentration profiles for the three mixtures exhibit small differences in terms of magnitude. It has been established that NO formation in high temperatures is mostly through thermal NO reactions by Zel'dovich mechanism. The rate-limiting step in the Zel'dovich mechanism: N_2 + O $\longrightarrow$ NO + N is the decisive reaction for NO formation at high temperature. The availability of the O atoms and nitrogen molecules in all three fuels considered result in a

similar amount of NO formed. The small difference in the production of NO is attributed to the different maximum temperatures attained by these mixtures and the prompt NO formation. It has also been established that at high temperatures, N formation route is different from that at low temperatures. At high temperatures the rate-limiting steps: $N_2 + O \longrightarrow NO + N$ (KJ/mol), $CH_2 + N_2 \longrightarrow HCN + NH$ (309.69 KJ/mol) and $N_2 + C \longrightarrow CN + N$ (187.9 KJ/mol), involving high activation energy, dictate its formation. Hence, a small difference (within the same order of magnitude) is observed in the N concentration profiles in these mixtures as compared to that for freely propagating and diffusion flames which attained relatively low temperatures.

CHAPTER SIX

6.0 FREELY PROPAGATING FLAMES

6.1 Introduction

Flames considered in this chapter are laminar, one-dimensional premixed, freely propagating. They are free from external disturbances which may be imposed by the presence of near-by walls and flame-anchoring devices such as burner-nozzles and rods. These flames are valuable research tools for investigating flame properties of a fuel. These flames can be realized in tubes and channels with sufficiently large radius and width, respectively, in spherical and tubular geometries with sufficiently large flame radius, and in burner-stabilized geometries with sufficiently large flame stand-off distance. Major species concentrations, minor species concentrations, temperature profiles, as well as NO concentration profiles for CH_4/air, CH_3OH/air, and CH_3OCHO/air stoichiometric, freely propagating flames are presented in this chapter. Also presented, are the sensitivity analysis of the CH and NO concentrations for the fuels' oxidation.

6.2 Flow Configuration

We consider a flame front which propagates from right to left as shown in Fig. 6.1. The cold fuel-air mixture enters the computational domain through the left boundary, and hot combustion products exit the domain through the right boundary.

The flame is fixed inside the computational domain at some point y_0 so that the flame is steady in a frame of reference that moves with the flame speed. The computational domain, $[y_l, y_r]$, where y_l and y_r are the y-locations of the left and right boundaries, respectively, is

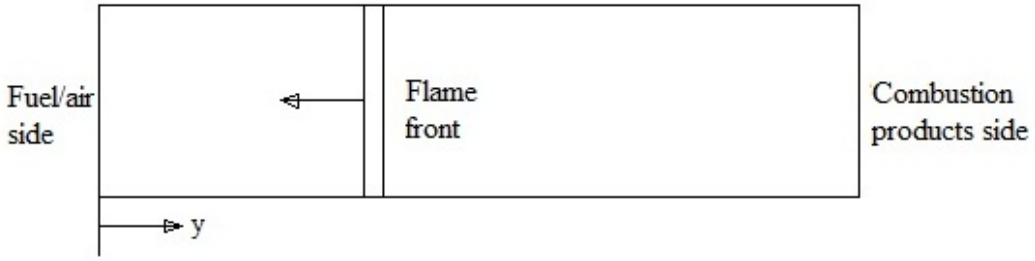

Figure 6.1: Flow configuration for a freely propagating flame

chosen as [-0.2, 1.2]. All the three flames have a constant pressure of 1 bar, a cold boundary temperature of 300 K, and zero temperature and species concentration profiles at the right boundary. The flames are fixed at $y_0 = 0.147554$ mm with the fixed temperature, T_0, being $T_0 = 400$ K. Fuel-air mixtures for the different fuels at the left boundary are stoichiometric (ϕ=1). The numerical simulations of these flames have been done using the RUN1DL code in the software package COSILAB [45].

6.3 Results and Discussions

6.3.1 Flame Structures

Major species concentration and temperature profiles for methane/air, methanol/air and methyl formate/air freely propagating flames are presented in Figs. 6.2, 6.3 and 6.4, respectively. For the flames fixed at the same reference point ($y_0 = 0.147554$ mm and T_0= 400 K), CH_3OH has a steeper temperature gradient as compared to CH_4 and CH_3OCHO temperature profiles. However, CH_4 flame attained a higher maximum temperature of 1980 K and flame speed of 38.29 cm/s with CH_3OH flame attaining 1961 K, a flame speed of 40.86 cm/s and CH_3OCHO flame attains 1935 K and a flame speed of 34.39 cm/s. The mole fraction of inert gas N_2 decreases from the onset of the flame throughout to the

product zone for all flames. The reduction is more intense in CH_3OCHO flame. This is probably explained by the total number of moles of the products present in a complete combustion for the three flames and the attack of N_2 molecule by O_2 molecule at high temperature.

$$CH_4 + 2\,O_2 + 7\cdot52\,N_2 \rightarrow CO_2 + 2\,H_2O + 7\cdot52\,N_2 \tag{6.1}$$

$$CH_3OH + 1\cdot5\,O_2 + 5\cdot64\,N_2 \rightarrow CO_2 + 2\,H_2O + 5\cdot64\,N_2 \tag{6.2}$$

$$CH_3OCHO + 2\,O_2 + 7\cdot52\,N_2 \rightarrow 2\,CO_2 + 2\,H_2O + 7\cdot52\,N_2 \tag{6.3}$$

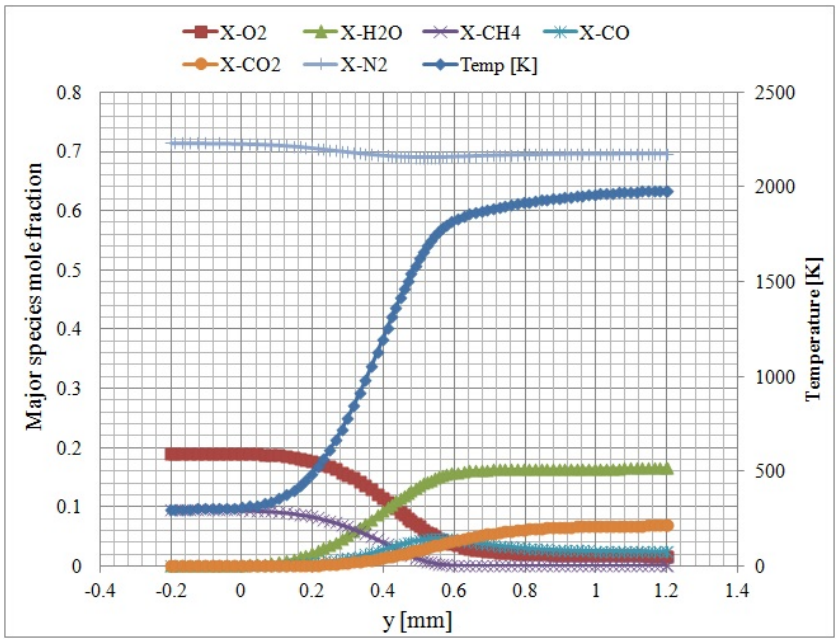

Figure 6.2: Methane/air freely propagating flame structure, $\phi = 1$

The total number of moles for reactants and products in CH_4 stoichiometric combustion as shown in Eq. (6.1), is the same, 10.52 moles. Hence, the mole fraction of N_2 gas remained the same in the reaction and product zones. For methane flame the mole fraction, X_{N2}, in the product side is expected to be 0.7148, same as for the fuel side. However, a lower figure has been obtained. The reduction of mole fraction of N_2 in methane flame in the

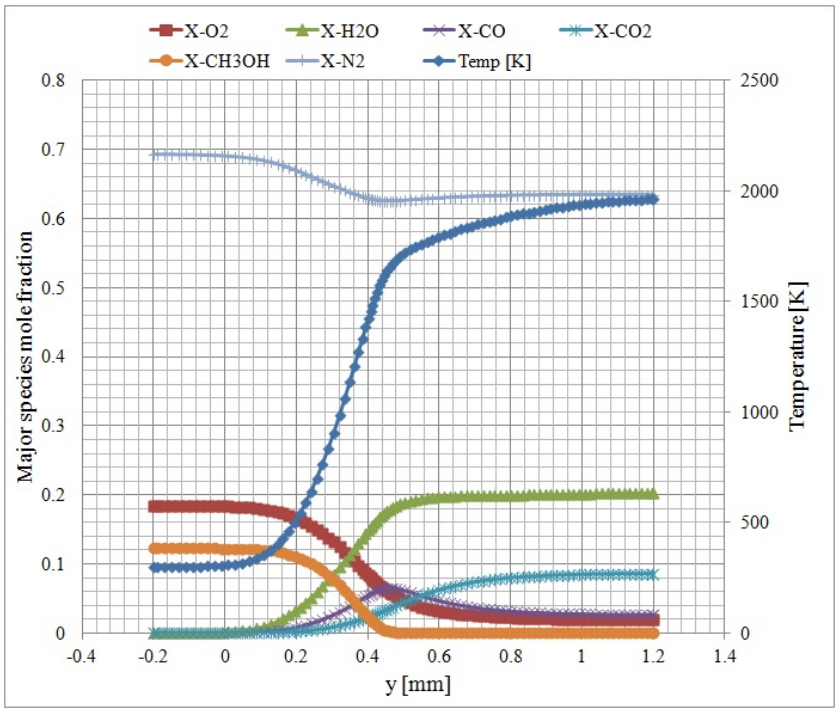

Figure 6.3: Methanol/air freely propagating flame structure, $\phi = 1$

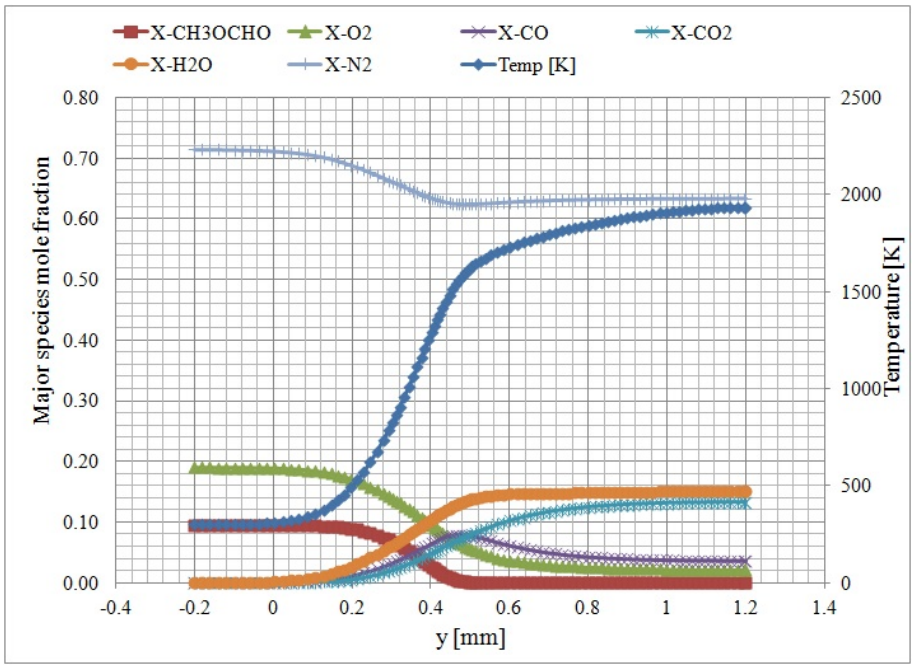

Figure 6.4: Methyl formate/air freely propagating flame structure, $\phi = 1$

product side is only explained by consumption through attack by oxygen and other radicals at high temperature. While for CH_3OH stoichiometric combustion as shown in Eq. (6.2),

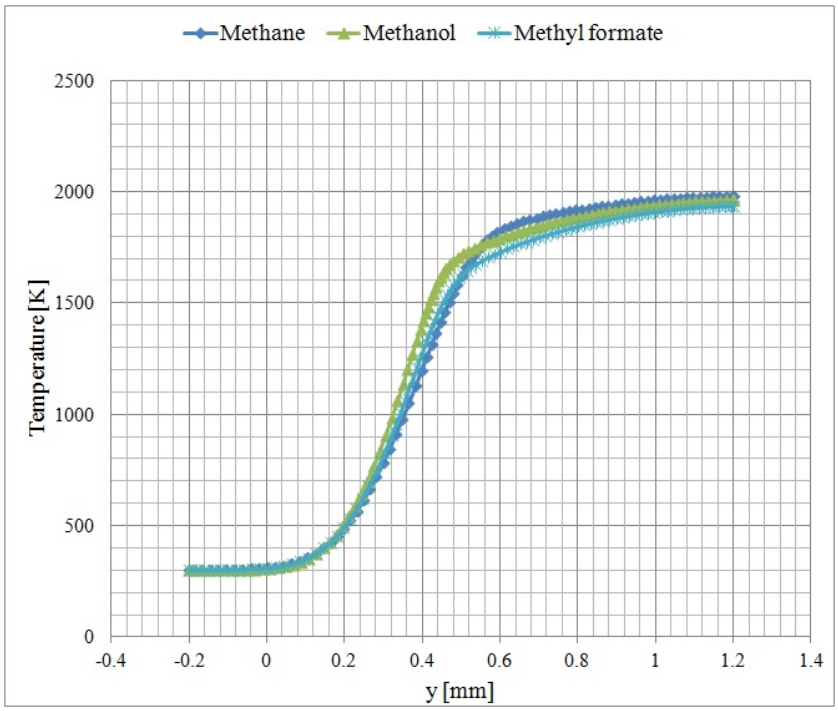

Figure 6.5: Temperature profiles for methane, methanol and methyl formate/air freely propagating flames, $\phi = 1$

the total number of moles for reactants is 8.14, and the products is 8.64 moles. Therefore, the expected mole fraction of N_2 is 0.692875 in the reaction zone and 0.652778 in the product zone. Similarly, the further reduction of N_2 in this flame is through consumption by oxygen and other radicals. The same explanation applies to CH_3OCHO flame, which has 0.7148 mole fraction of N_2 in the reactant side and an expected 0.6528 mole fraction in the product zone for the stoichiometric reaction.

6.3.2 Generation of NO_x

NO concentration profiles for CH_4/air, CH_3OH/air, and CH_3OCHO/air flames are shown in Fig. 6.6a. The minor species concentrations (O, OH, H, H_2, CH, CH_2, CH_3, and N), which are also dominant precursors for NO formation, are presented in Figs. 6.6b- 6.10b. The active radicals in the flame zone-O, OH, H and H_2-for the three flames compares well

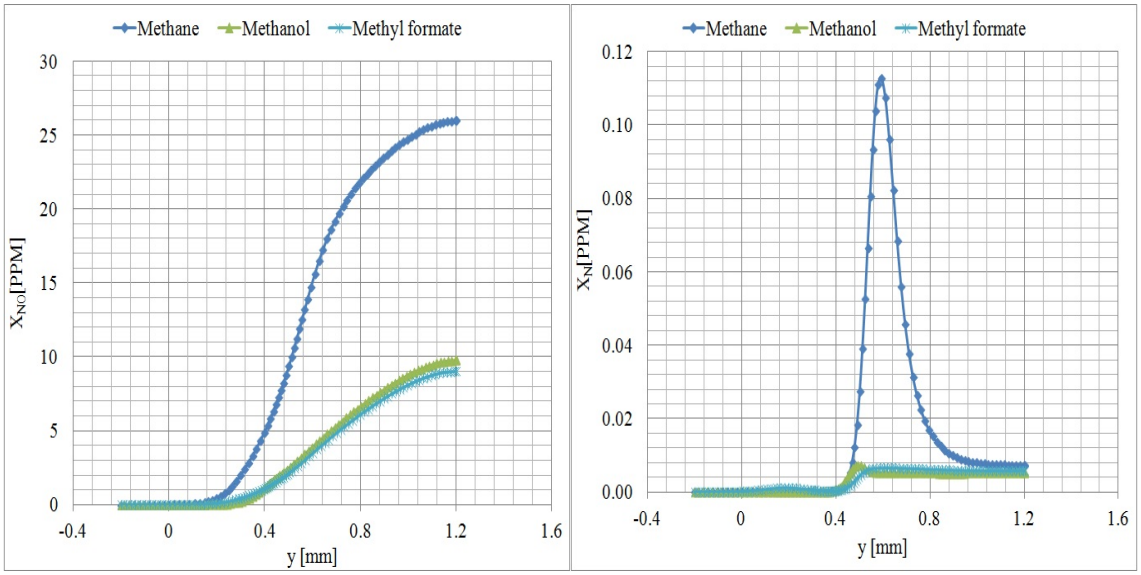

(a) NO mole fraction (b) N mole fraction

Figure 6.6: NO and N concentration profiles for the three flames

within the same order of magnitude. Generally, the occurrence of these species except H_2, starts at point 0.40 mm of the flame. However, H_2 is found far upstream of the reaction zone. For all the flames investigated, the profiles of these species exhibit similar shapes, with only little variation for the maximum concentrations. CH_3OH/air, and CH_3OCHO/air flames exhibit the same behaviour, as far as the combustion intermediates concentration profiles (CH, CH_2, CH_3, and N) preceding NO formation is concerned.

A significantly higher NO concentration profile was observed for CH_4 flame as compared to CH_3OH/air, and CH_3OCHO/air flames. This correlates well with the comparison of the dominant immediate precursor for prompt NO formation, CH. According to Li and William [7], methyl CH_3 radical is the main source of CH radical in methane/air flame. Its combustion path proceeds through C_2 from C_2H_6 through C_2H_5, C_2H_4, C_2H_3, C_2H_2, CH_2 and finally to CH. Assuming the same reaction paths for methanol and methyl formate combustion, then there is low production of CH because of the small quantities of CH_3 produced in these flames. CH radical formed is then consumed by N_2 to form N in the

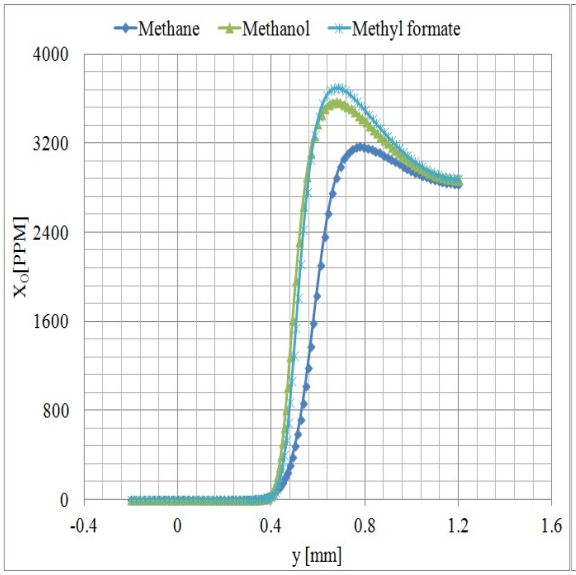

(a) O mole fraction

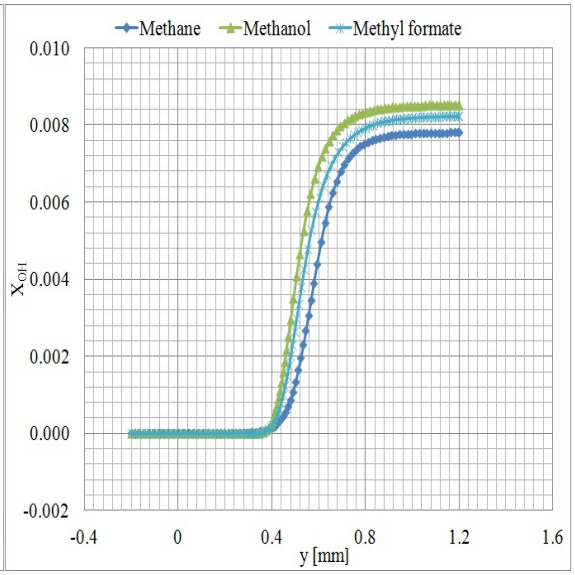

(b) OH mole fraction

Figure 6.7: O and OH concentration profiles for the three flames

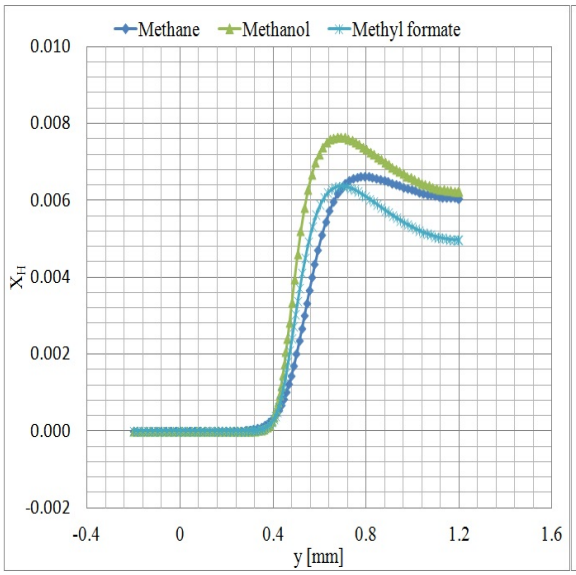

(a) H mole fraction

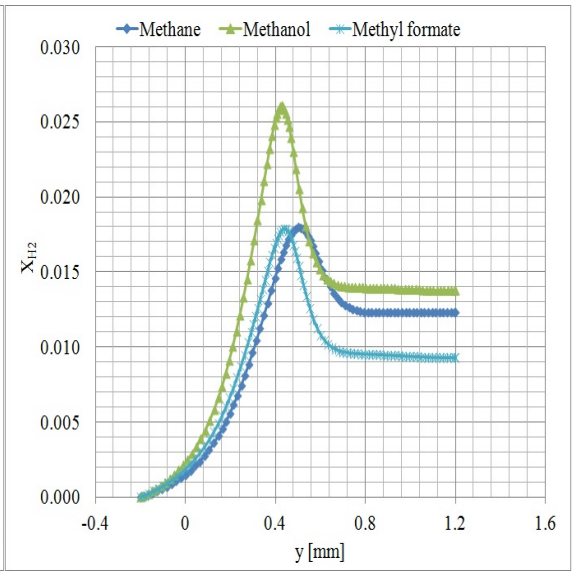

(b) H_2 mole fraction

Figure 6.8: H and H_2 concentration profiles for the three flames

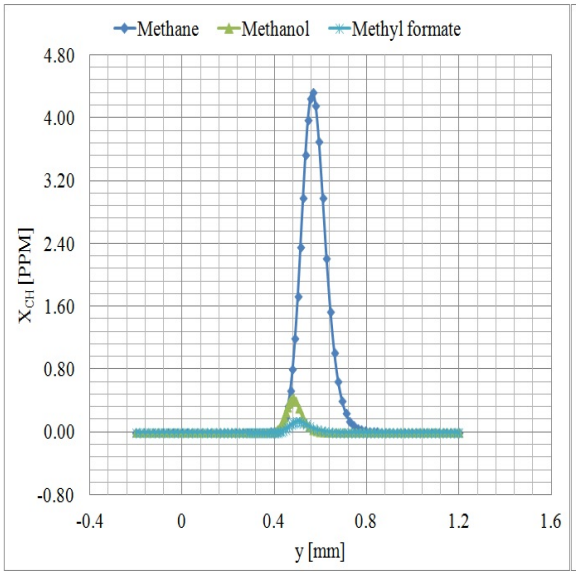

(a) CH mole fraction

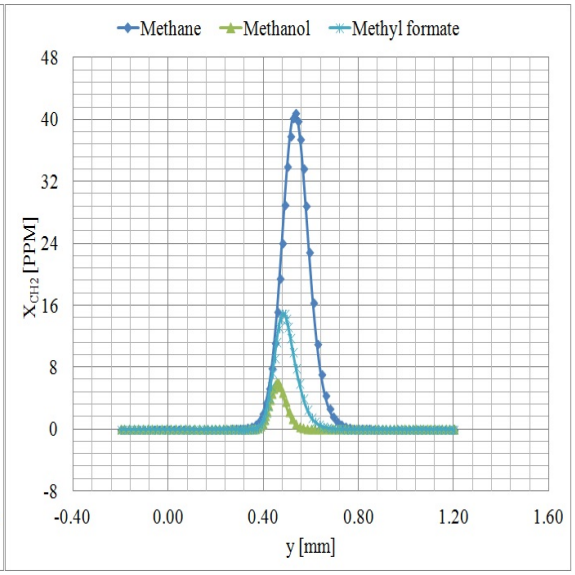

(b) CH_2 mole fraction

Figure 6.9: CH and CH_2 concentration profiles for the three flames

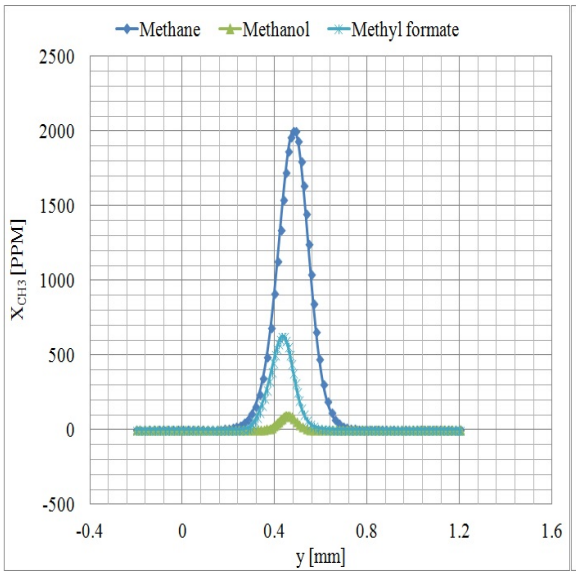

(a) CH_3 mole fraction

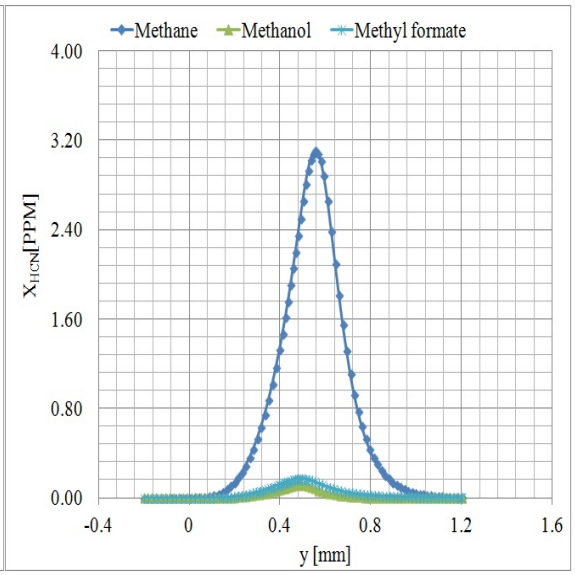

(b) HCN mole fraction

Figure 6.10: CH_3 and HCN concentration profiles for the three flames

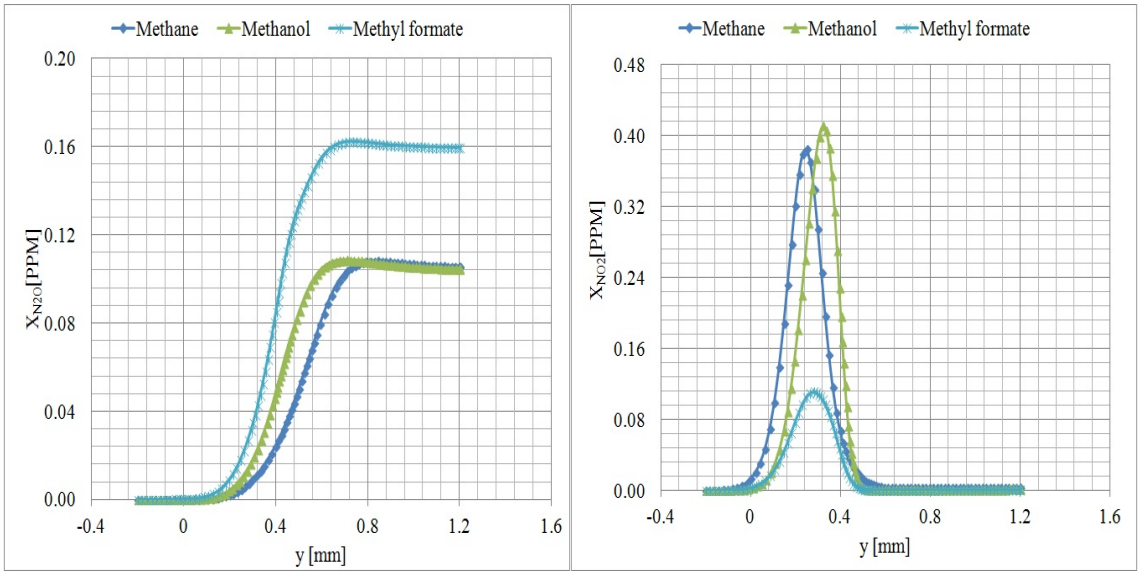

(a) N_2O mole fraction (b) NO_2 mole fraction

Figure 6.11: N_2O and NO_2 concentration profiles for the three flames

reaction;

$$CH_4 + N_2 \rightarrow HCN + N \tag{6.4}$$

N atom resulting from reaction in Eq. (6.4) forms NO through extended Zel'dovich reactions in Eqs (6.5) and (6.6). HCN reacts through various paths to form NCO and NH which subsequently form N atom responsible for NO formation.

$$N + O_2 \rightarrow NO + O \tag{6.5}$$

$$N + OH \rightarrow NO + H \tag{6.6}$$

A comparison of N_2O in the three fuels is shown in Fig. 6.11a. A higher maximum N_2O concentration profile is observed in CH_3OCHO flame. Almost the same amount in the maximum concentration is observed in CH_3OH and CH_4. N_2O is formed through reaction: $N_2 + O + M \longrightarrow N_2O + M$ and consumed through reactions: $N_2O + O \longrightarrow NO + NO$, N_2O

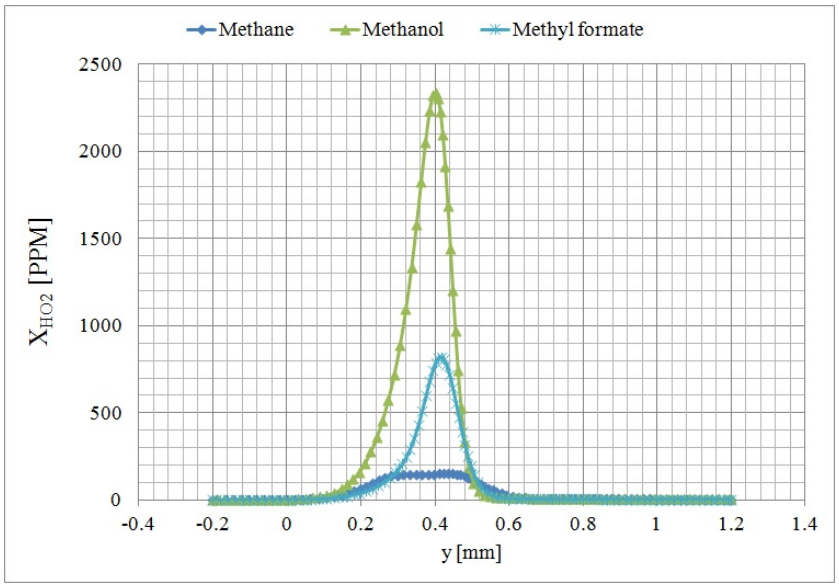

Figure 6.12: HO_2 concentration profiles for the three flames

+ H $\longrightarrow$ N_2 + OH and N_2O + OH $\longrightarrow$ N_2 + HO_2 [49]. The N_2O consumption reactions are sensitive at high temperatures, hence do not have significant impact at relatively low temperatures attained by these flames. The higher amount of N_2O in CH_3OCHO can be linked to a higher peak concentration of O atom observed in its flame, Fig. 6.7a, which reacts with N_2 and a third body to form N_2O. The concentration of O atom is just as high in CH_3OH as in CH_3OCHO, hence the amount of N_2O concentration is expected to be high in its flame. However, a lower concentration of N_2O observed in CH_3OH is attributed to its high amount of OH and H atoms, Figs. 6.7b and 6.8a, respectively, which consume N_2O to form other species.

Shown in Fig.6.11b is a comparison of NO_2 in the three fuels. The axial location of the peak concentration for NO_2 in the three fuels is at low temperature region. Its concentration is higher in CH_3OH followed closely by CH_4, and a significant low value in CH_3OCHO. It is mainly formed from the consumption of NO at low temperature through reaction: HO_2 + NO $\longrightarrow$ NO_2 + OH as shown in sensitivity analysis in section 6.3.4. The concentrations of NO_2 observed in CH_3OH and CH_3OCHO are consistent with HO_2 concentrations profiles

Fig. 6.12. However, a small amount of HO_2 is observed in CH_4. HO_2 is formed in the region where the temperature is approximately between 500 K - 1200 K, in which the reaction: R'OOH $\rightleftharpoons$ Alken + HO_2 is dominant in its formation [33]. R'OOH is easily formed in oxygenated fuels than pure hydrocarbon, thus explaining the low concentration of HO_2 in methane. It is important to note, that the NO atom that react with HO_2 diffuses from the high temperature flame zone [6] to the low temperature zone.

6.3.3 The Effect of Fuel/Air Mixture on NO Formation

The variation of fuel/air mixture in the different fuels investigated, was done to establish its impact on NO formation. Presented in Figs. 6.13-6.15 are results for each of the flames, while Figs. 6.18-6.20 compares NO formation at each equivalence ratio experimented ($\phi =$ 0.7 to $\phi = 1.3$). For methane flame, the NO formation increases with increase in equivalence ratio (shown in Fig 6.17). Methanol and methyl formate flames show a similar behavior, the NO formation increases with increase in equivalence ratio up to $\phi = 1.1$, and starts decreasing with further increase in equivalence ratio. The role of temperature in NO formation is clearly demonstrated in these NO profiles. As depicted in Fig. 6.16, the maximum temperature attained by; methane/air is 2010 K at $\phi = 1.15$, methanol/air is 1973 K at $\phi = 1.1$, and methyl formate/air is 1964 K at $\phi = 1.2$. NO mole fraction profiles have direct correlation with temperature profiles.

A significant dependency on temperature for methane/air NO formation as compared to the other flames is revealed in Figs. 6.18-6.20. This is attributed to the contribution of both prompt NO and thermal NO mechanism to the total NO formed in this particular flame. At low equivalence ratios, temperature profiles decreases. Hence, the contribution by thermal NO become less significant. As the equivalence ratio is increased, temperature

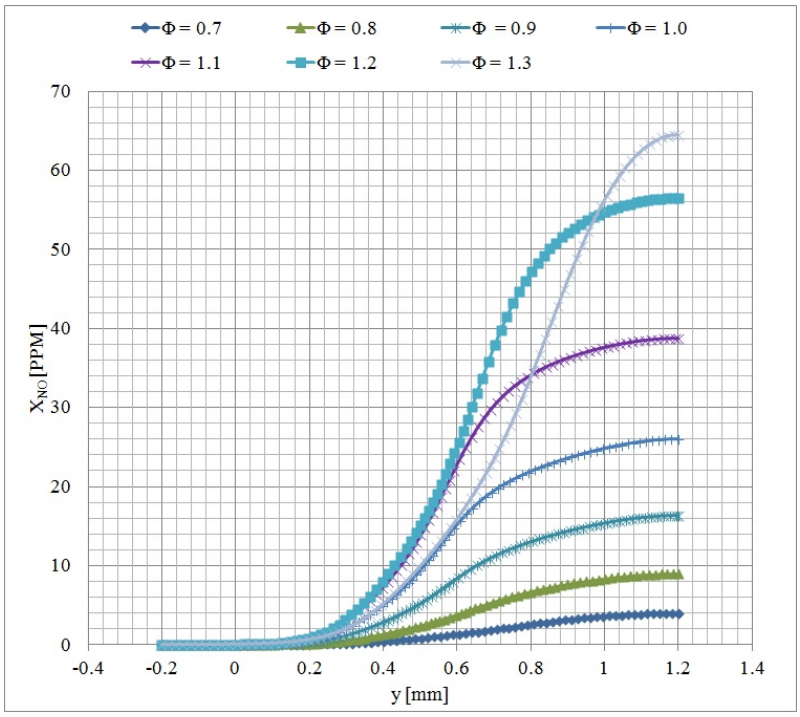

Figure 6.13: NO mole fraction profiles for various equivalence ratios of methane/air freely propagating flame

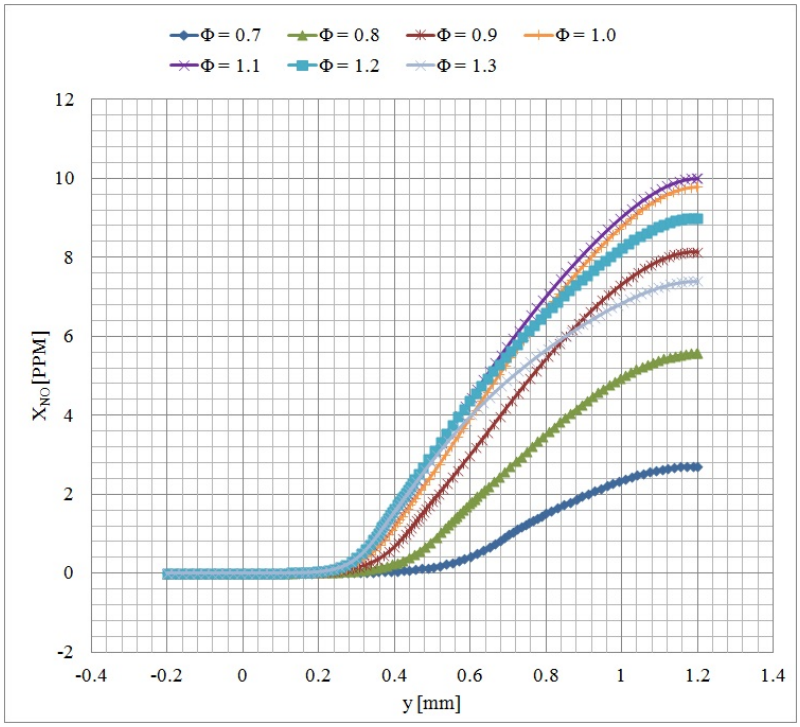

Figure 6.14: NO mole fraction profiles for various equivalence ratios of methanol/air freely propagating flame

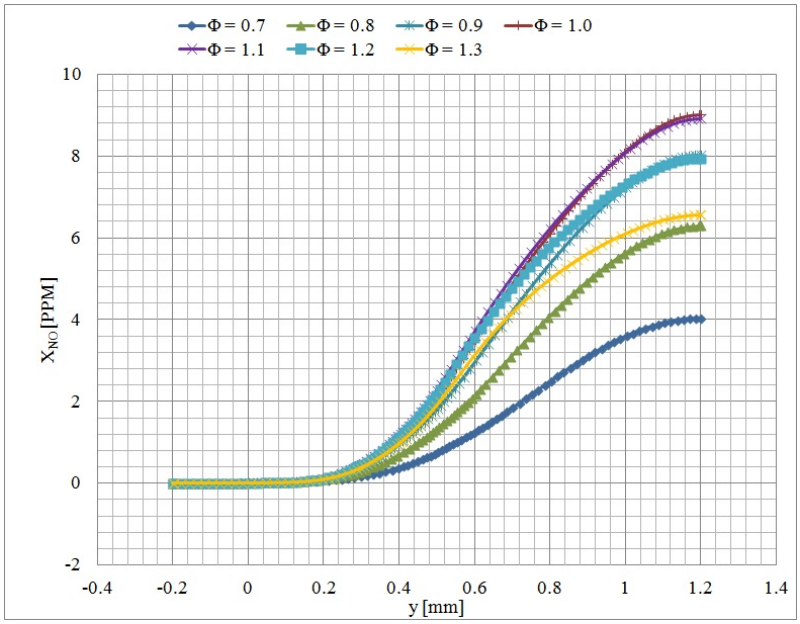

Figure 6.15: NO mole fraction profiles for various equivalence ratios of methyl formate/air freely propagating flame

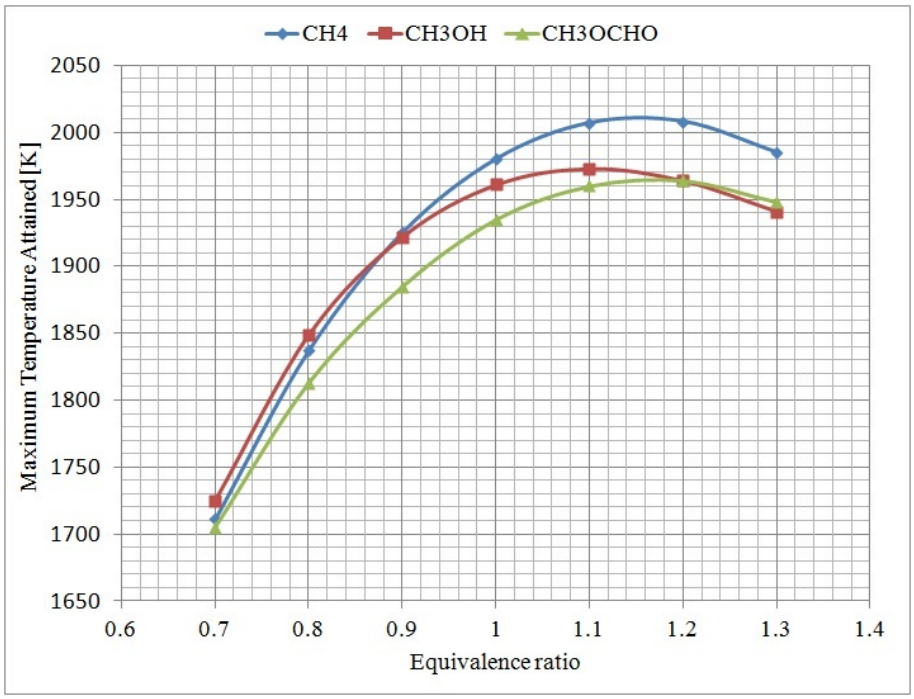

Figure 6.16: Maximum temperature attained by flames at different equivalence ratios

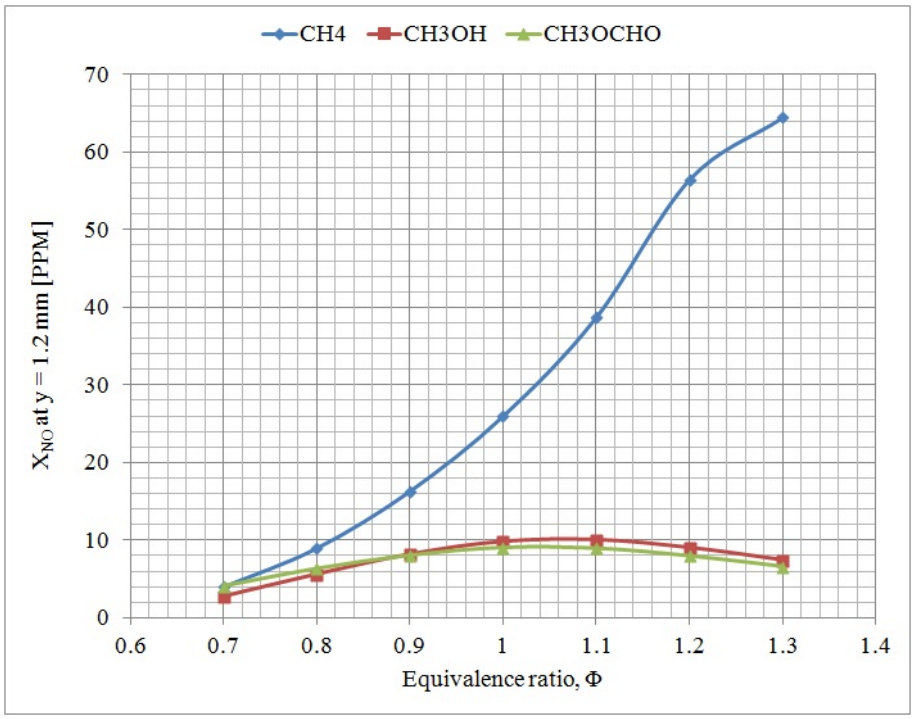

Figure 6.17: NO concentration at y = 1.2 mm for different equivalence ratios

increases and the contribution by thermal NO becomes dominant. It is observed that increase in equivalence ratio does not increase the NO profiles significantly for methanol and methyl formate flames as it does for methane flame. The relevance of reaction; CH + N_2 $\longrightarrow$ HCN + N, as seen in the next section, explains this observation. In methanol and methyl formate flames, there is less production of CH radical as compared to methane flame. This results in less amount of N atom, which is responsible for thermal NO formation through Zel'dovich mechanism (O + N_2 $\longrightarrow$ NO + N, N + OH $\longrightarrow$ NO + H and N + O_2 $\longrightarrow$ NO + O). The Zel'dovich reactions are strongly dependent on temperature. As a result, methane NO profiles are higher at high temperatures. On the contrary, methanol and methyl formate NO mole fraction profiles (whose main source is reaction; NNH + O $\longrightarrow$ NH + NO as identified in the next section) are lower at high temperature.

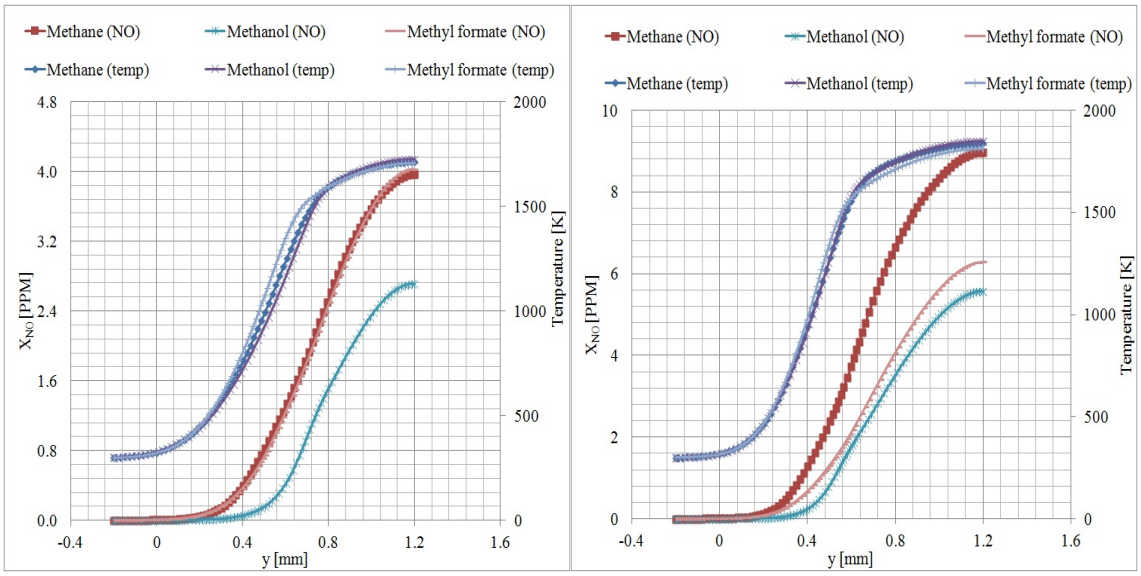

(a) At $\phi = 0.7$ (b) At $\phi = 0.8$

Figure 6.18: Comparison of NO mole fraction profiles for the three flames at $\phi = 0.7$ and $\phi = 0.8$

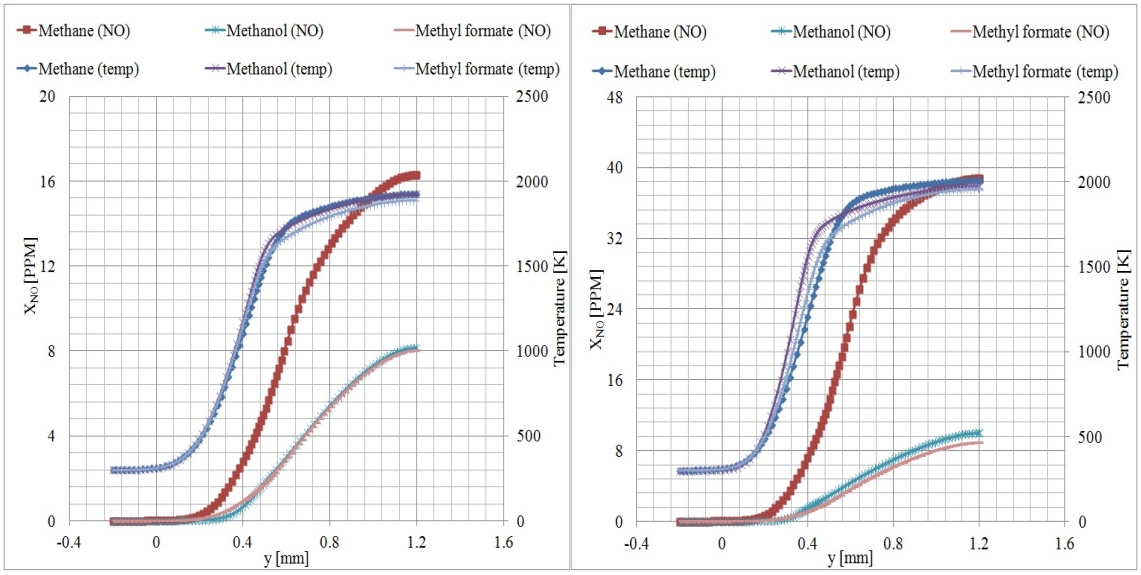

(a) At $\phi = 0.9$ (b) At $\phi = 1.1$

Figure 6.19: Comparison of NO mole fraction profiles for the three flames at $\phi = 0.9$ and $\phi = 1.1$

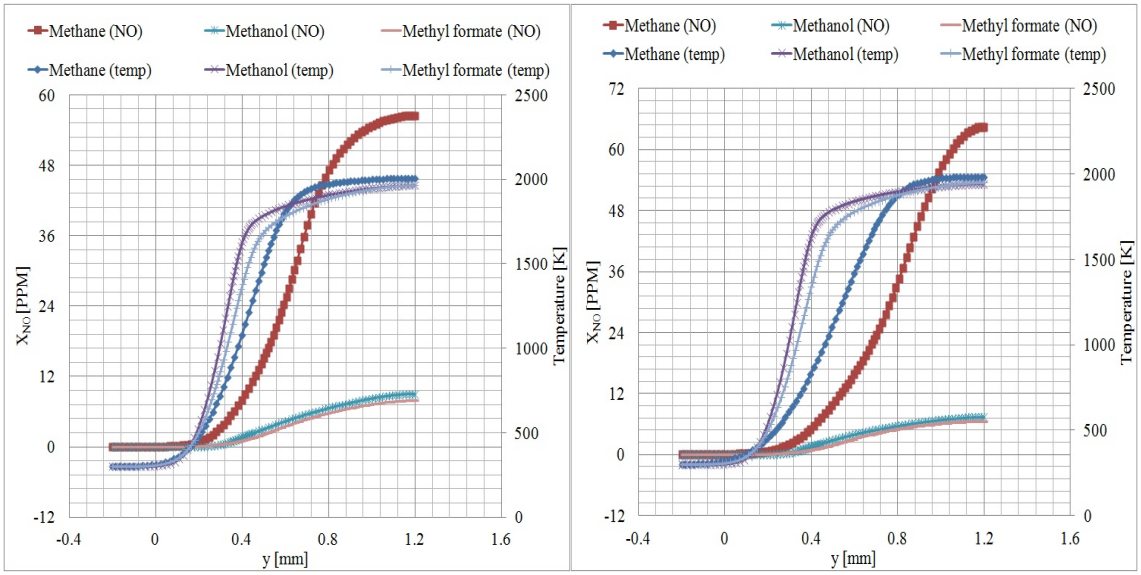

(a) At $\phi = 1.2$ (b) At $\phi = 1.3$

Figure 6.20: Comparison of NO mole fraction profiles for the three flames at $\phi = 1.2$ and $\phi = 1.3$

6.3.4 Sensitivity Analysis

Sensitivity analysis is carried out to predict the effect of variations of the rate constants on the dependent variables. It is obtained by calculating the first-order sensitivity coefficients of the dependent variable, $\partial \mathbf{U}/\partial K_k$, $k = 1, ..., l$. Here $\mathbf{U}$ denotes the vector of the unknown dependent variables, K_k denotes the rate constant for an elementary reaction k, and l denotes the total number of elementary reactions. The first order sensitivities are normalized to get the relative sensitivities or sensitivities coefficients, S^k. In this thesis, the local sensitivities of mole fraction of CH and NO have been performed with respect to the rate constants of elementary reactions.

6.3.4.1 Sensitivity of CH concentration in flames

The sensitivity of CH concentration towards the most important reactions in methane freely propagating flame is shown in Fig. 6.21. The graph shows that the dominant reaction is

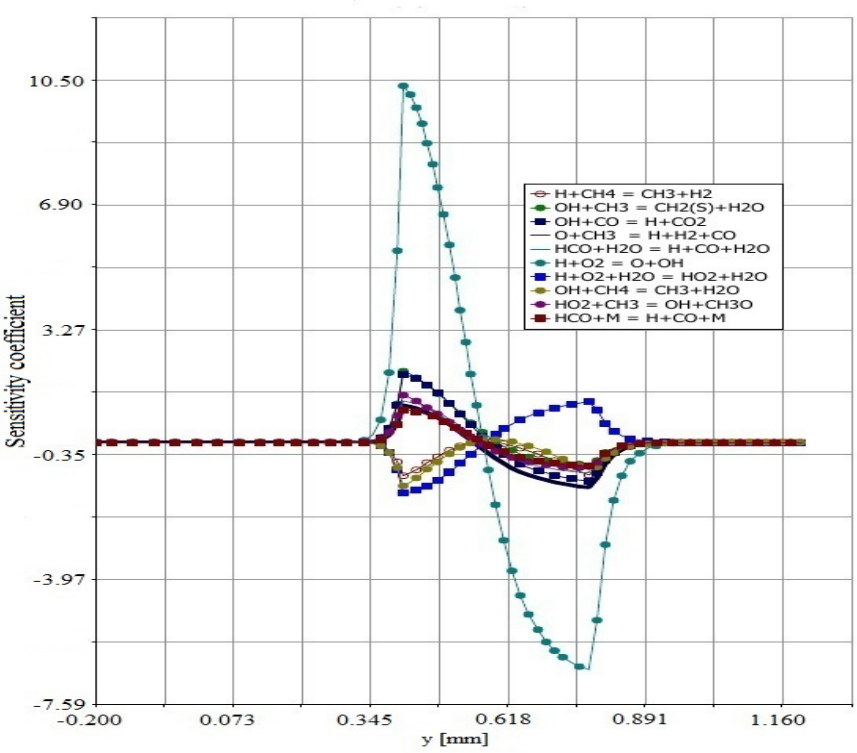

Figure 6.21: The sensitivity of CH concentration for a methane/air freely propagating flame, $\phi = 1$

$H + O_2 \longrightarrow O + OH$. This is a very important chain branching step in every combustion process where H atoms are present [53]. The other reactions which have high positive sensitivity at the production zone of CH (between 0.44 mm to 0.76 mm with peak at 0.57 mm as shown in Fig. 6.9a) are $OH + CH_3 \longrightarrow CH_2(S) + H_2O$ and $OH + CO \longrightarrow H + CO_2$. Therefore, from these reactions it is evident that OH and CH_3 are the most dominant radicals responsible for the CH production. Reactions which have high negative sensitivity at CH production zone are $H + O_2 + H_2O \longrightarrow HO_2 + H_2O$, $OH + CH_4 \longrightarrow CH_3 + H_2O$ and $H + CH_4 \longrightarrow CH_3 + H_2$. Apparently, at the CH consumption zone (0.57 mm to 0.76 mm) the reactions which have positive sensitivity change to negative sensitivity and vice versa with the exception of reactions involving H abstraction in CH_4. These reactions also show that the consumption of CH_3 by OH, HO_2 and O promote the generation of CH. The generation of H radical increases CH production while the H consumption decreases

its production. The plot also reveals that CO, H_2, CH_2(S), HCO, HO_2 and CH_3O are the other radicals which play an active role in the production and consumption of CH radical.

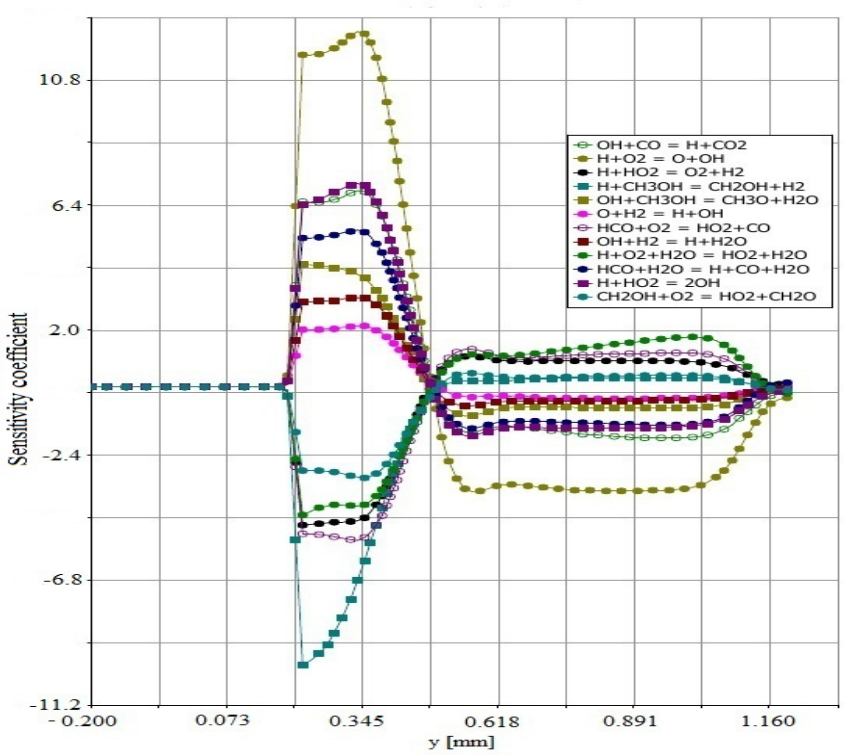

Figure 6.22: The sensitivity of CH concentration for a methanol/air freely propagating flame, $\phi = 1$

Sensitivity analysis of CH concentration in methanol freely propagating flame is presented in Fig. 6.22. Apart from H + O_2 $\longrightarrow$ O + OH reaction, the other reactions which have high positive sensitivity at the CH production zone (0.40 mm to 0.48 mm as shown in Fig. 6.9a) are H + HO_2 $\longrightarrow$ 2OH, OH + CO $\longrightarrow$ H + CO_2 and HCO + H_2O $\longrightarrow$ H + CO + H_2O. Reactions: H + CH_3OH $\longrightarrow$ CH_2OH +H_2 and HCO + O_2 $\longrightarrow$ HO_2 + CO have high negative sensitivity at CH production zone. It is also important to note that the sensitivities of all these reactions change sign at the CH peak concentration position. OH, H and HCO are the dominant radicals which play an active role in the production and consumption of CH radical in this flame. Unlike in methane flame, CH_3 does not play a significant role in CH production in a methanol flame. As shown in Fig. 6.10a,

methanol flame has a low CH_3 production as compared to the other flames. This explain the relatively small amount of CH in a methanol flame.

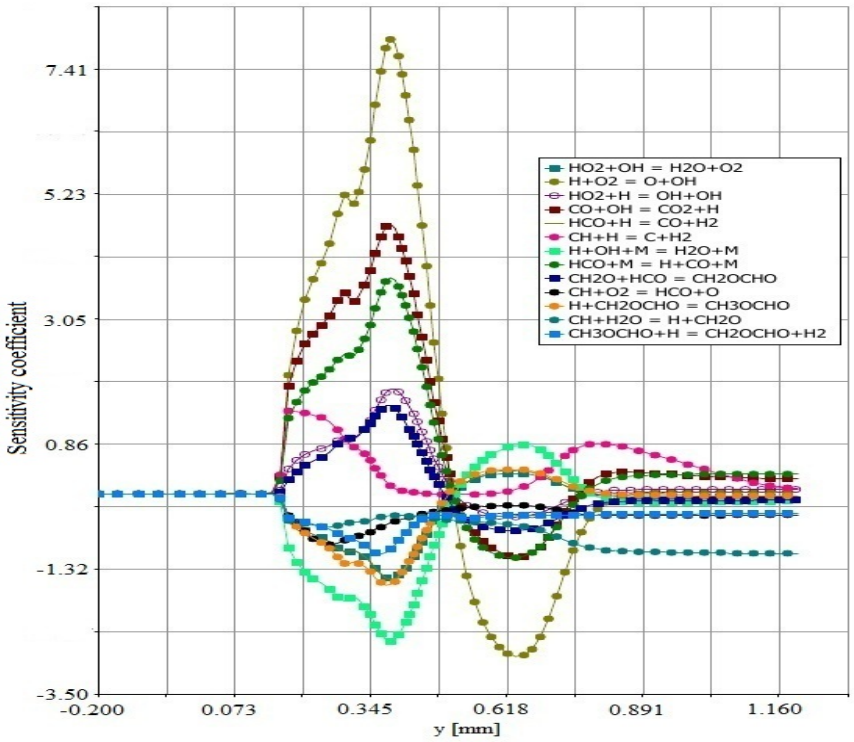

Figure 6.23: The sensitivity of CH concentration for a methyl formate/air freely propagating flame, $\phi = 1$

Sensitivity analysis of CH concentration in methyl formate flame is shown in Fig. 6.23. Just like in the other two flames, H + O_2 $\longrightarrow$ O + OH is the dominant reaction sensitive to the production of CH. Other reactions which have a bigger influence positively at CH production zone (0.42 mm to 0.50 mm as shown in Fig. 6.9a) are CO + OH $\longrightarrow$ CO_2 + H and HCO + M $\longrightarrow$ H + CO + M. Reactions: H + OH +M $\longrightarrow$ H_2O + M and H + CH_2OCHO $\longrightarrow$ CH_3OCHO have high negative sensitivity at CH production zone. Similar to methanol flame, OH, H and HCO are the dominant radicals which play an active role in the production and consumption of CH radical in this flame. In particular, H radical dominates most of these reactions, with its generation promoting CH production and its consumption decreasing CH production. The plot also shows that CH_3 does not play a

significant role in CH production in a methyl formate flame.

6.3.4.2 Sensitivity of NO concentration in flames

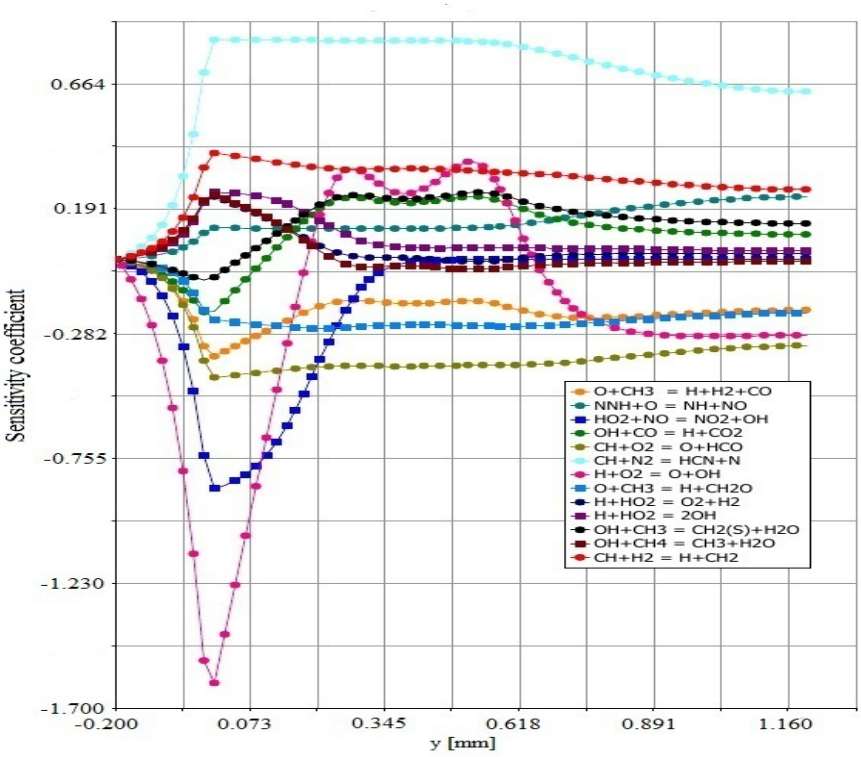

Figure 6.24: The sensitivity of NO concentration for a methane/air freely propagating flame, $\phi = 1$

The sensitivity of NO concentration towards the most important reaction in a methane flame is presented on Fig. 6.24. The most influential reaction with high positive sensitivity in NO production zone (0.16 mm to 1.2 mm as shown in Fig. 6.6a) is CH + N_2 $\longrightarrow$ HCN + N. This reaction is considered to be the dominant initiation reaction responsible for NO formation in flames [7, 14]. The other reactions which have positive sensitivity are CH + H_2 $\longrightarrow$ H +CH_2, H + O_2 $\longrightarrow$ O + OH and OH + CH3 $\longrightarrow$ CH_2(S) + H_2O. On the other hand, the reactions which have greater negative influence are HO_2 + NO $\longrightarrow$ NO_2 + OH, CH + O_2 $\longrightarrow$ O + HCO and O + CH_3 $\longrightarrow$ H + CH_2O. It is interesting to note that all these reactions have dominance effects even in the low temperature part of the flame zone

where NO are produced at slow rate (as early as at -0.064 mm). At this zone, HO_2 + NO $\longrightarrow$ NO_2 + OH is the reaction which has high consumption of NO to form NO_2. This is also seen in Fig. 6.11b, where NO_2 is formed earlier than NO in the flame zone.

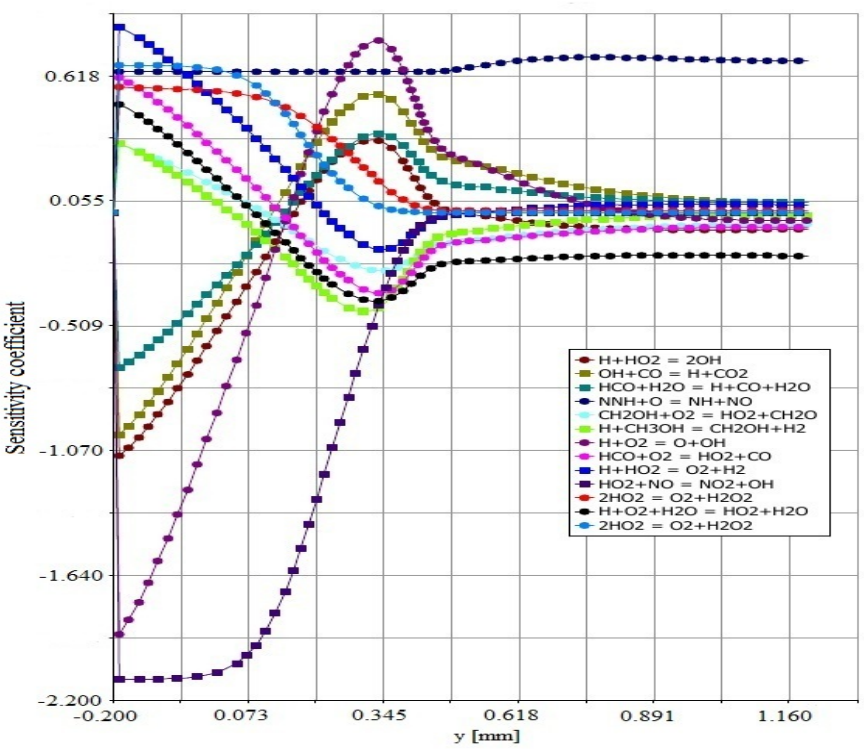

Figure 6.25: The sensitivity of NO concentration for a methanol/air freely propagating flame, $\phi = 1$

The sensitivity of NO concentration in a methanol flame is shown in Fig. 6.25. The plot shows a very interesting behaviour about the sensitivity of the reactions; highly sensitive at very low temperatures. This result in two regions of the flame zone where the rate constants of reactions are very sensitive; first region between -0.2 mm to 0.10 mm and the second region between 0.1 mm to 0.50 mm. Although the formation of NO in this flame starts at 0.30 mm, the first region sensitivity could indicate the formation and consumption of the precursor radicals responsible for NO formation. NNH + O $\longrightarrow$ NH + NO is the only reaction which has positive dominance throughout the flame zone. This reaction has been identified by Hughes *et al.* [6, 49] as the most sensitive in NO formation in H_2/air

flame. The first region is characterized by reactions: $H + HO_2 \longrightarrow O_2 + H_2$, $2OH \longrightarrow O_2 + H_2O_2$, $HCO + O_2 \longrightarrow HO_2 + CO$ and $H + O_2 + H_2O \longrightarrow HO_2 + H_2O$ being most dominant on the positive side. The reactions which have the most positive influence in NO production in the second region are $H + O_2 \longrightarrow O + OH$, $OH + CO \longrightarrow H + CO_2$ and $HCO + H_2O \longrightarrow H + CO + H_2O$. All these reactions have antagonistic effects on both regions. It is also important to note that $HO_2 + NO \longrightarrow NO_2 + OH$ reaction contribute negatively to the production of NO in a methanol flame at low temperatures. Most of these reactions which have great influence in the low temperature region involve HO_2 radical. HO_2 radical is produced at low temperatures $T < 900$ K through hydrogen abstraction from the fuel via relatively slow reaction with oxygen [33].

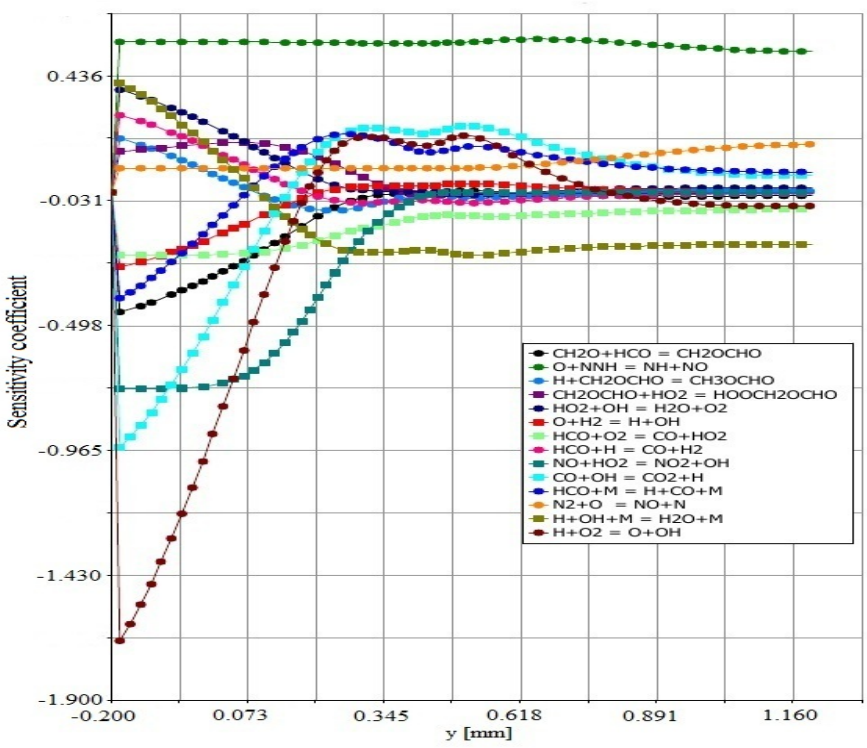

Figure 6.26: The sensitivity of NO concentration for a methyl formate/air freely propagating flame, $\phi = 1$

The sensitivity of NO concentration in a methyl formate flame is presented on Fig. 6.26. Just like NO formation in a methanol flame, the behaviour of the these sensitivity divide

the flame into two regions; first region between -0.2 mm to 0.10 mm and the second region between 0.1 mm to 0.70 mm. Also NNH + O $\longrightarrow$ NH + NO and N_2 + O $\longrightarrow$ NO + N are the only reactions which have positive influence throughout the flame zone. Reactions: H + OH + M $\longrightarrow$ H_2O + M, HO_2 + OH $\longrightarrow$ H_2O + O_2 and HCO + H $\longrightarrow$ CO + H_2 have high positive sensitivity in the first region. While reactions: CO + OH $\longrightarrow$ CO_2 + H, H + O_2 $\longrightarrow$ O + OH and HCO + M $\longrightarrow$ H + CO + M have dominant positive sensitivity in the second region. It is also noted that HO_2 + NO $\longrightarrow$ NO_2 + OH reaction contribute negatively to the production of NO in a methyl formate flame at low temperatures.

6.4 Conclusions

Small amount of NO concentration in the oxygenated fuels (CH_3OH and CH_3OCHO) is observed. The sensitivity analysis of NO concentration reveals that its production in methanol and methyl formate flames is mainly from reaction; NNH + O $\longrightarrow$ NH + NO, as opposed to the well known sources of NO in flames (Zel'dovich mechanism; O + N_2 $\longrightarrow$ NO + N, N + OH $\longrightarrow$ NO + H and N + O_2 $\longrightarrow$ NO + O). This is attributed to the small amount of N radicals present in these flames. This is as a result of prediction of small amount of CH and CH_3 by methyl formate and methanol mechanism, which initiates the reactions responsible for N formation. The Zel'dovich reactions are strongly dependent on temperature. As a result, methane NO profiles, whose formation is contributed by both prompt and thermal NO, are higher at high temperatures. On the contrary, methanol and methyl formate NO mole fraction profiles are lower at high temperature.

CHAPTER SEVEN

DIFFUSION FLAMES

7.1 Introduction

In this chapter, two dimensional planar, laminar, counterflow diffusion flames are considered. A fully infinite computational domain between two opposed nozzles (one ejecting pure fuel and the other pure air) has been used for all diffusion flames studied. For this case, a diffusion flame is assumed to be embedded in a thin boundary layer, which is as a result of stagnating flow between two opposing streams of fuel and air. Major species, temperature, NO and minor species (NO_2, CH, CH_3, O, OH, HCN, N, N_2O and NNH) concentration profiles relating to its formation in methane, methanol and methyl formate flames are presented and discussed. Compared in the last section of this chapter are the formations of NO in the three configuration: homogeneous system, freely propagating and diffusion flames.

7.2 Flow Configuration and Model Details

The flow configuration considered is as shown in Fig. 2.2a in section 2.4, with the fuel and air side positioned at left and right hand side respectively. The temperature of both the fuel and air stream is taken as 300 K. The flames are computed at a constant pressure of 1 bar and a strain rate of 50 s^{-1}. At the fuel nozzle, pure fuel concentration (mole fraction of 1) is specified, while at the air nozzle, the mole fractions concentration of O_2 and N_2 are specified using the air standard composition. The numerical simulations of these flames have been done using the RUN1DL code in the software package COSILAB [45].

7.3 Results and Discussions

7.3.1 Flame Structures

Presented in Figs.7.1, 7.2 and 7.3 are the temperature and major species profiles for methane/air, methanol/air and methyl formate/air diffusion flames respectively. The plot depicts that, the flames are established at the air side; approximately at 2.8 mm, 2.5 mm and 1.8 mm from the stagnation plane (taken as the point where velocity, $V_y = 0$) for methane, methanol and methyl formate flames respectively. This is as expected, since the stoichiometric mixtures of these fuels and air require more air than fuel. Fuel diffuses across the stagnation plane and the flame is established at the point where the mixture fraction is stoichiometric.

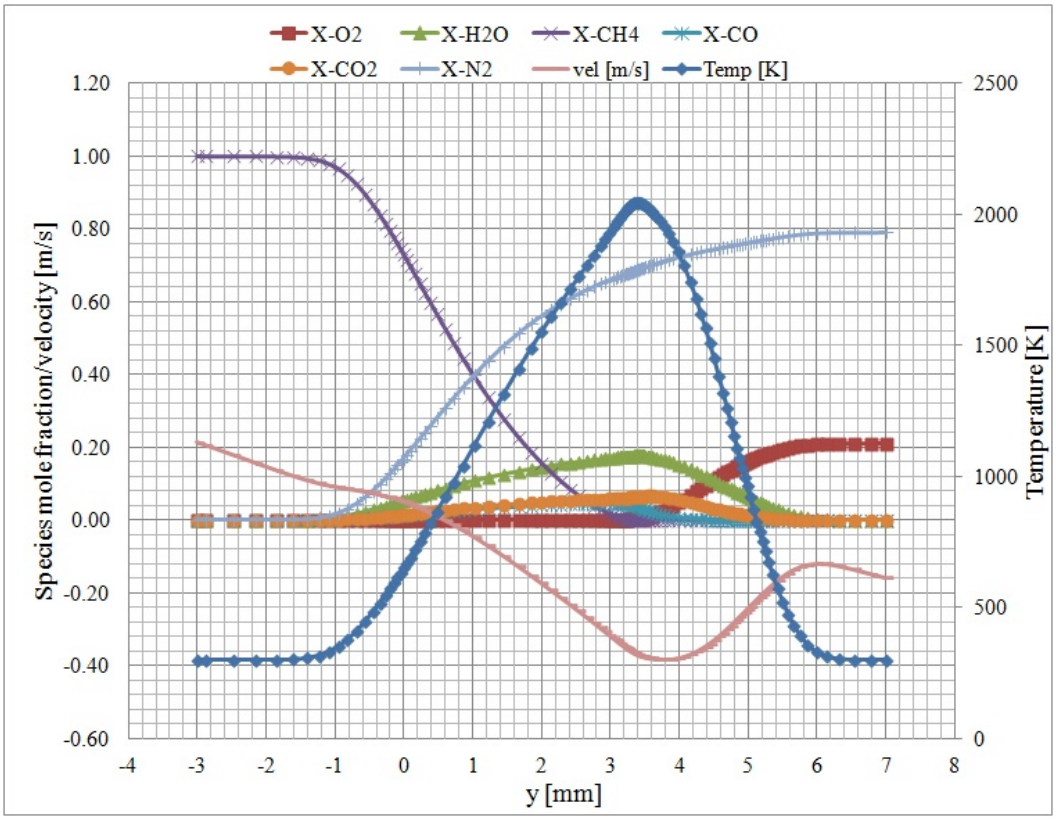

Figure 7.1: Methane/air diffusion flame structure

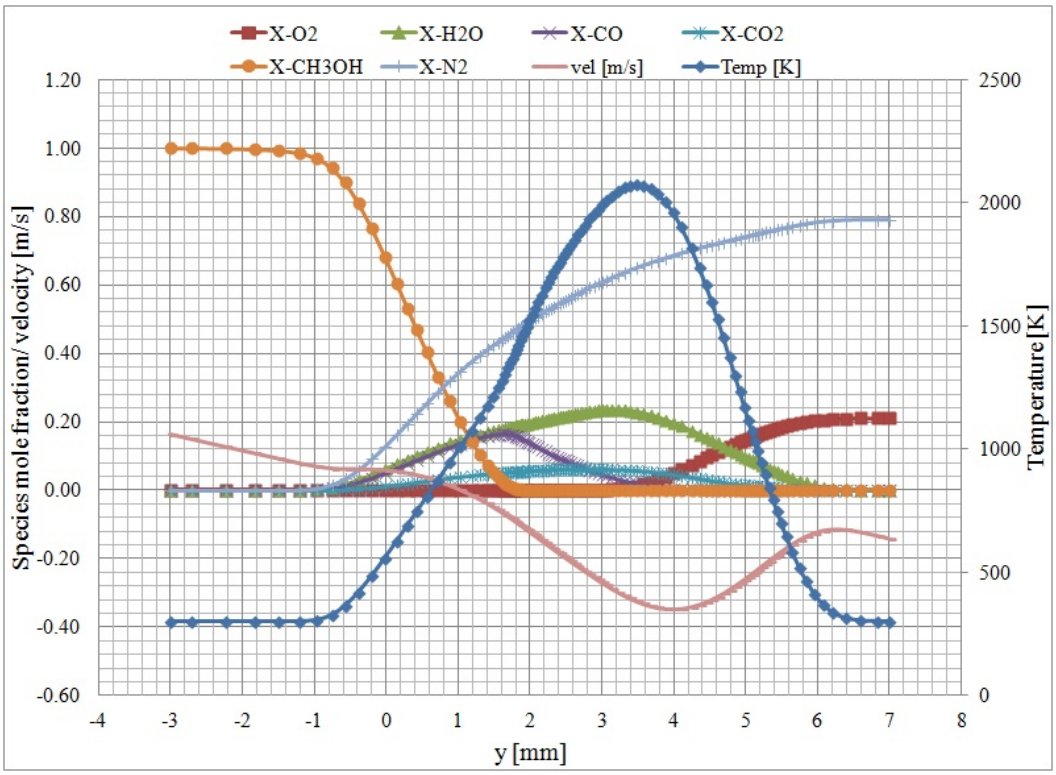

Figure 7.2: Methanol/air diffusion flame structure

Shown in Fig. 7.4 is a comparison of temperature profiles for the three diffusion flames. The diagram shows that, the temperature profiles have similar shapes with a slight difference for peak amount and position. Methanol is observed to have a slightly higher peak temperature, followed by the peaks of methane and methyl formate. In methane flame, the mole fractions of reactants (CH_4 and O_2) fall to near zero values at the axial location corresponding to the position of peak temperature occurrence. In methanol and methyl formate flames, the mole fraction of O_2 fall to near zero values at the axial position corresponding to peak temperature position, while the mole fractions of fuels fall to near zero values at position different from that of O_2 (1.8 mm and 1.5 mm from temperature peak position for CH_3OH and CH_3OCHO respectively). It is interesting to note, that these positions correspond to the positions where CO peaks in these particular fuels. Also a significant difference (approximately 3 times higher) is observed in the maximum concentration of

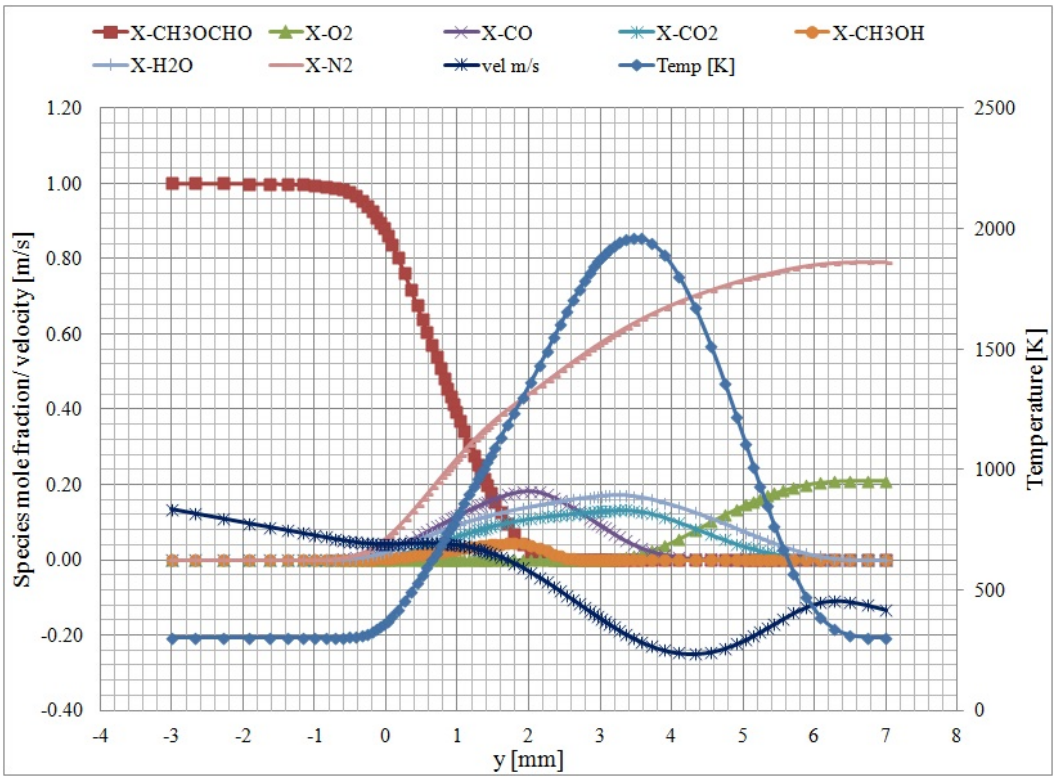

Figure 7.3: Methyl formate/air diffusion flame structure

CO in CH_3OH and CH_3OCHO flames compared to that of CH_4 flame. At the point where fuel falls to zero, it has been consumed to radical and other products; CO amongst them. For instance, Dooley *et al.* [17] identified reactions: $CH_3OCHO \longrightarrow CH_3OH + CO$ and $CH_3OCHO \longrightarrow CH_4 + CO_2$ to account for 38% and 3% of fuel consumption respectively. The CO is then converted to CO_2 at this region due to presence of oxygen. The presence of N_2 deep on the fuel side for all flames studied is as a result of its diffusion across the stagnation plane.

7.3.2 Generation of NO_x

Shown in Figs. 7.5-7.9 are the species concentration profiles for NO and other minor species related to its formation. A comparison of NO production in the three flames is shown in Fig. 7.5a. The plot reveals a significantly high NO mole fraction concentration in CH_4

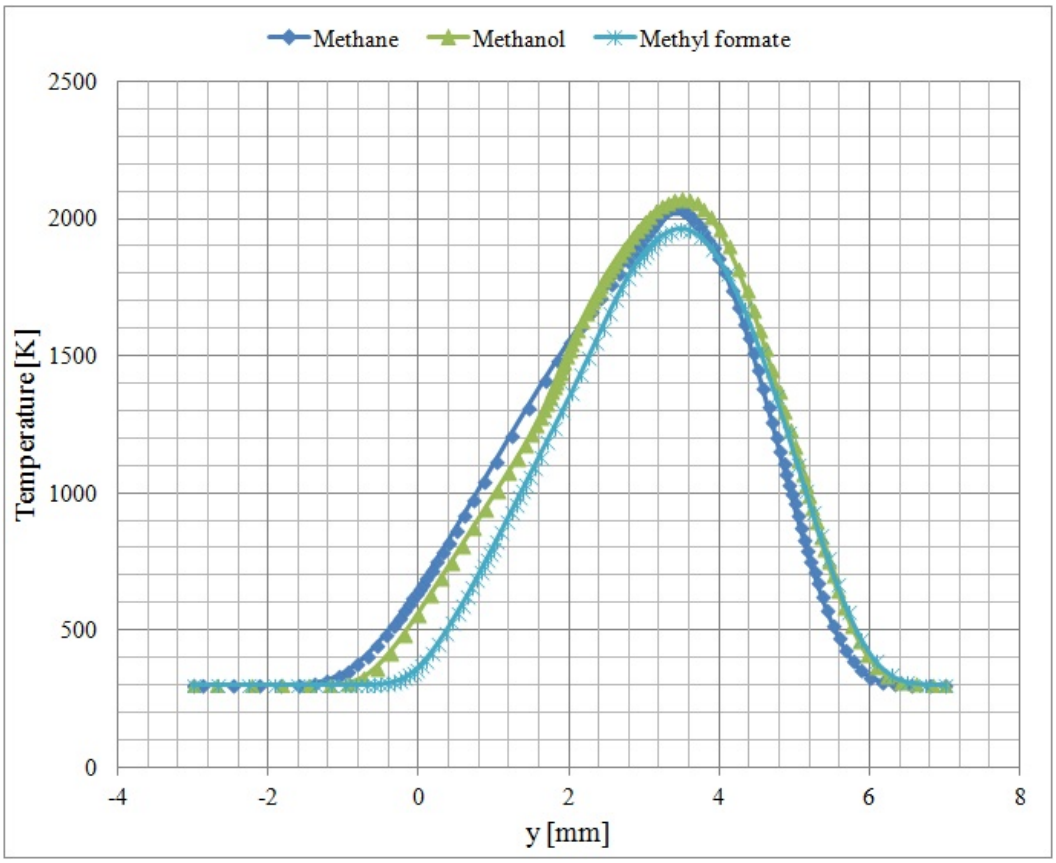

Figure 7.4: Temperature profiles for methane, methanol and methyl formate/air diffusion flames

flame as compared to those for CH_3OH and CH_3OCHO flames. The difference is explained in the next paragraph by looking at the concentration profiles of the dominant species responsible for prompt and thermal NO formation in each of the flames.

A comparison of O and OH atoms for the three flames is shown in Fig. 7.6. The graph shows similar curves for both O and OH in the different fuels with slight difference in the peak amount and position. These radicals play a significant role in both prompt and thermal NO formation through Zel'dovich mechanism [7, 14]. Therefore, a small difference in the NO production is expected from these fuels. However, the big difference observed is attributed to a small amount of prompt NO predicted for CH_3OH and CH_3OCHO flames due to low values of CH produced in their flame zones (Fig. 7.7a). This is also consistent

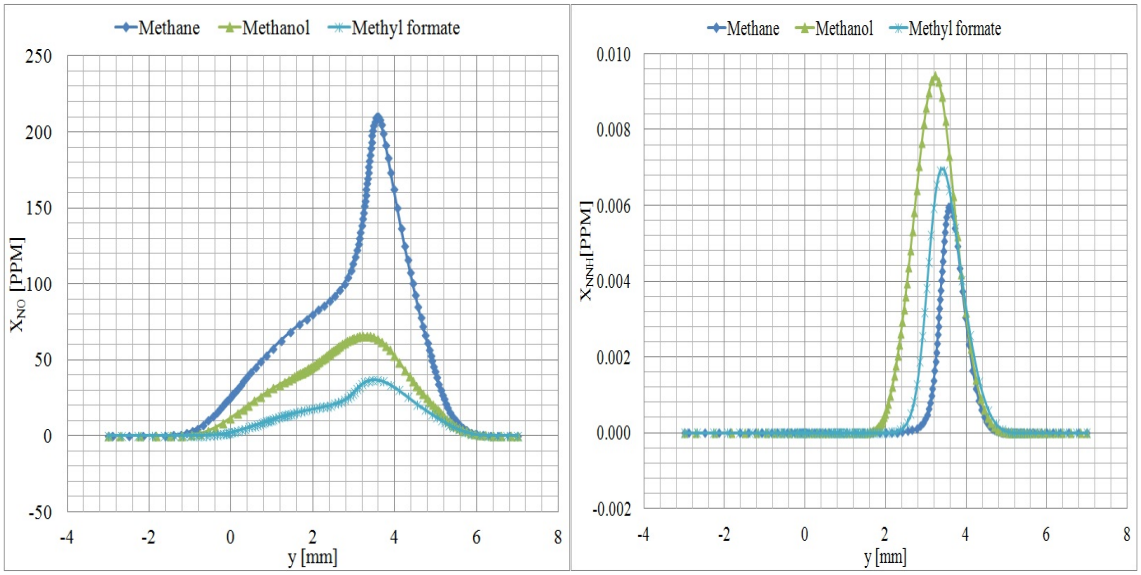

(a) NO mole fraction (b) NNH mole fraction

Figure 7.5: NO and NNH concentration profiles for the three diffusion flames

with the low values of HCN and N atoms observed in these flames, CH_3OH and CH_3OCHO, as depicted in Fig. 7.8. The source of these radicals is through reaction: CH + N_2 $\longrightarrow$ HCN + N and the other subsequent reactions.

NO concentration profiles in CH_3OH and CH_3OCHO flames are sensitive to reaction: NNH + O $\longrightarrow$ NH + NO (see section 6.3.4). This reaction favours the production of NO in these flames because its activation energy is zero, hence at low temperatures it proceeds fast. Also the production of NNH in CH_3OH and CH_3OCHO flames, Fig. 7.5b, are within the same range as that for CH_4.

N_2O concentration profile comparison is presented in Fig. 7.9a. The plot shows that CH_3OH and CH_3OCHO flames have almost the same quantities of N_2O in terms of mole fraction, which are slightly higher than that of CH_4. N_2O is formed through reaction: N_2 + O + M $\longrightarrow$ N_2O + M. This reaction take place with collision with a third body M which lowers its activation energy as compared to Zel'dovich rate limiting step: N_2 + O $\longrightarrow$ NO + N [33]. Hence, it proceeds at low temperatures and high pressures. This is the

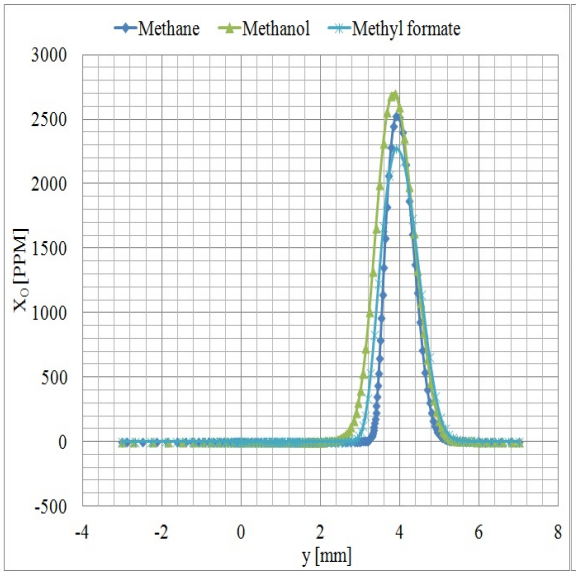

(a) O mole fraction

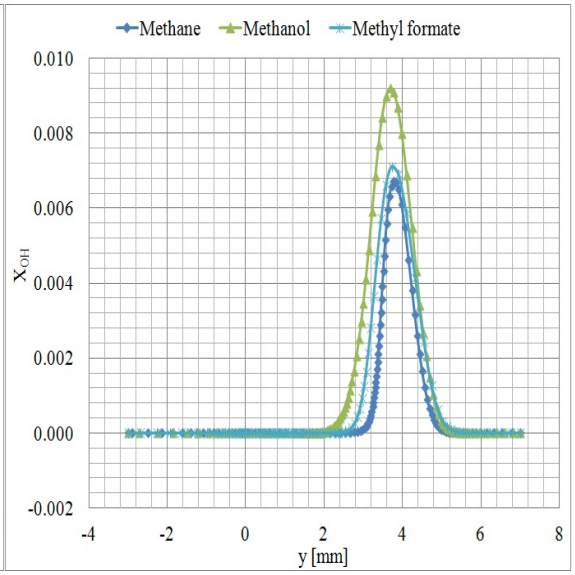

(b) OH mole fraction

Figure 7.6: O and OH concentration profiles for the three diffusion flames

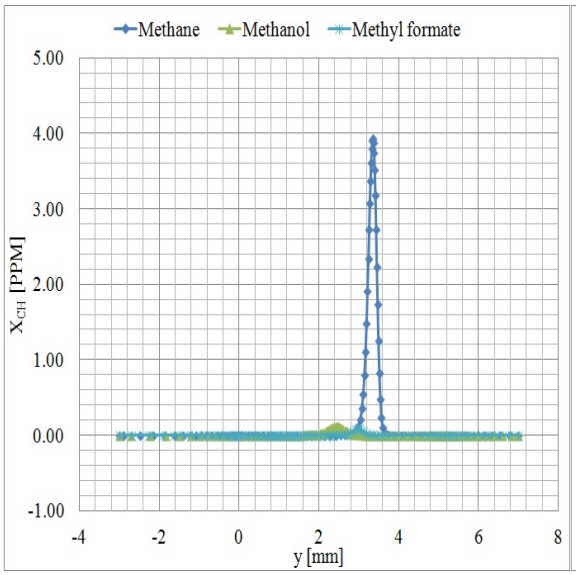

(a) CH mole fraction

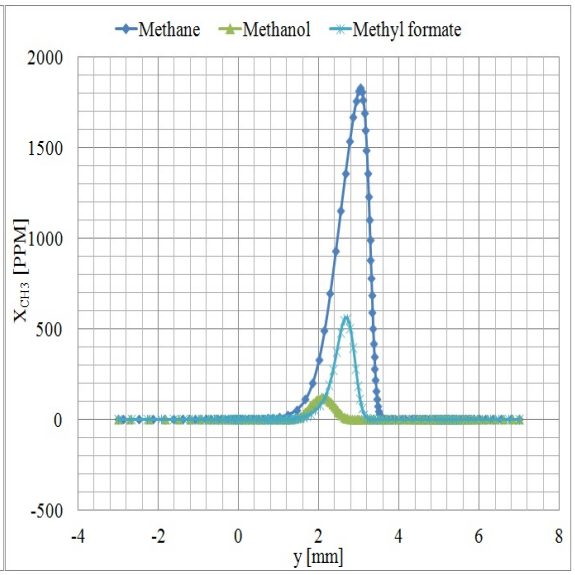

(b) CH_3 mole fraction

Figure 7.7: CH and CH_3 concentration profiles for the three diffusion flames

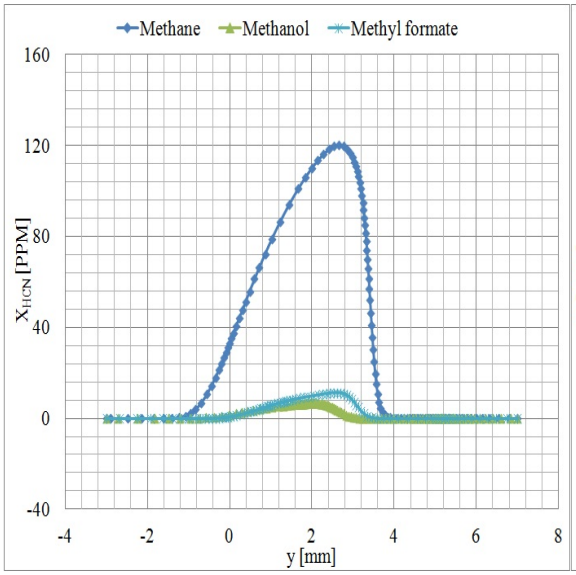

(a) HCN mole fraction

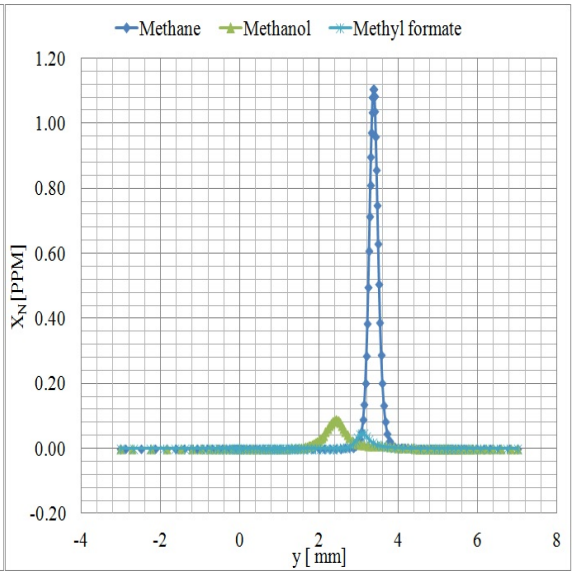

(b) N mole fraction

Figure 7.8: HCN and N concentration profiles for the three diffusion flames

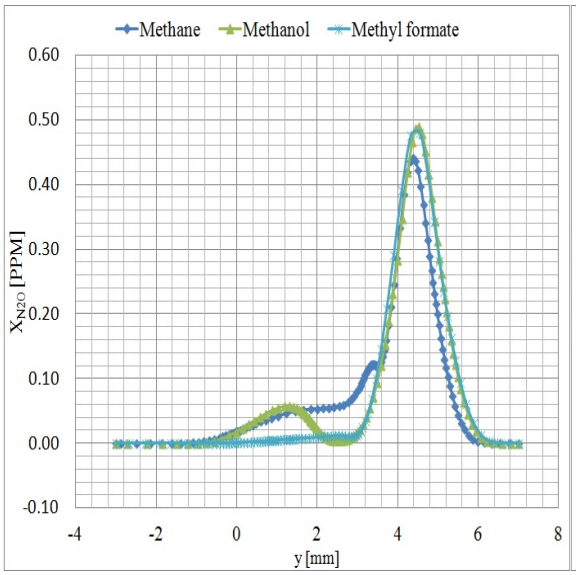

(a) N_2O mole fraction

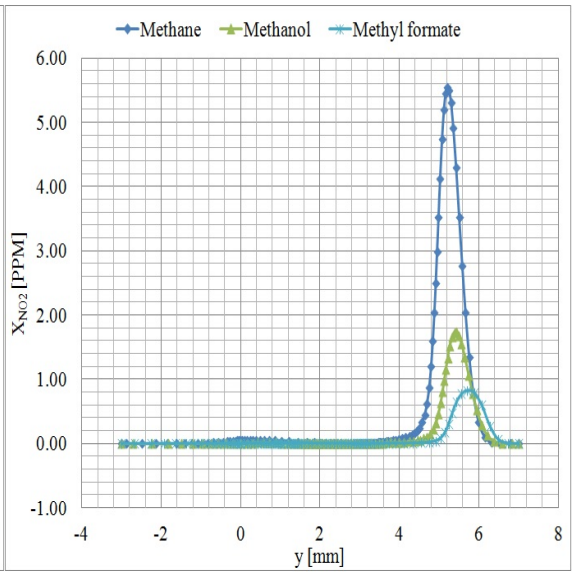

(b) NO_2 mole fraction

Figure 7.9: N_2O and NO_2 concentration profiles for the three diffusion flames

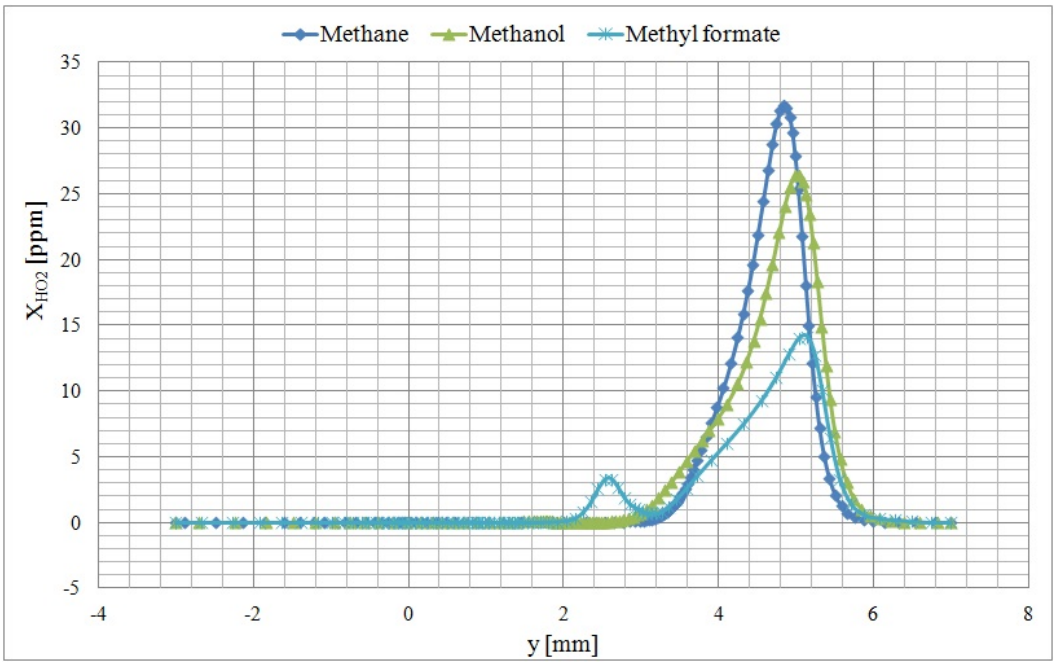

Figure 7.10: HO_2 concentration profiles for the three diffusion flames

main source of NO in lean combustion after reacting with O [33], which is analogous to the slightly higher concentration observed in oxygenated fuels.

Shown in Fig. 7.9b is a comparison of NO_2 in the flames. NO_2 is mainly formed from the consumption of NO at low temperature through reaction: $HO_2 + NO \longrightarrow NO_2 + OH$ as shown in sensitivity analysis in section 6.3.4. At high temperature it is formed through reaction $OH + NO \longrightarrow NO_2 + H$. The peak concentration value for NO_2 is higher in CH_4 flame, followed by CH_3OH flame and is lowest in CH_3OCHO flame. The peak concentration is on the air side for all flames (1.8 mm, 1.9 mm and 2.2 mm from temperature peak position for CH_4, CH_3OH and CH_3OCHO respectively). These correspond to the location of the peak position of HO_2 (Fig. 7.10), dominant species responsible for their formations. The amount of HO_2 for each of the flames is also consistent with NO_2 produced.

7.4 Comparison of NO Formation in Different Flow Configurations

Table 7.1 compares NO production in homogeneous system, freely propagating and diffusion flames. A significantly higher NO formation in homogeneous system is observed compared to those in diffusion and freely propagating flames. Homogenous system attained high temperatures due to high initial temperatures. Hence, NO is formed mostly through temperature dependent thermal NO mechanism. A temperature difference of 66, 111 and 26 K between the diffusion and freely propagating flames result in an increase of 7.69, 6.63 and 3.89 times in NO production for CH_4, CH_3OH and CH_3OCHO respectively. Similarly, a temperature difference of 950, 949 and 965 K between the homogeneous system and freely propagating flames result in an increase of 446, 1163 and 1144 times in NO production for CH_4, CH_3OH and CH_3OCHO respectively. Generally, it can be seen that a small increase in temperature bring a significant increase in NO production.

Table 7.1: A comparison of maximum NO formed in different flow configurations

Fuel	Homogeneous system		Freely propagating		Diffusion flame	
	Maximum X_{NO} (10^{-2})	Maximum temperature[K]	Maximum X_{NO} [PPM]	Maximum temperature[K]	Maximum X_{NO} [PPM]	Maximum temperature[K]
CH_4	1.16	2930	26.0	1980	200	2046
CH_3OH	1.14	2910	9.8	1961	65	2072
CH_3OCHO	1.03	2900	9.0	1935	35	1961

7.5 Conclusions

NO formations in methane/air, methanol/air, and methyl formate/air diffusion flames have been discussed in this chapter. A significantly higher peak amount of NO is formed in CH_4 flame; approximately 3.23 and 6 times higher than those of CH_3OH and CH_3OCHO flames

respectively. This is mainly attributed to the fact that, the temperatures attained by diffusion flames (approximately 2000 K for initial temperature of 300 K) favours the formation of prompt NO. The dominant immediate precursor species for prompt NO formation, i.e, CH, HCN and N, are predicted in significantly small quantities in CH_3OH and CH_3OCHO flames compared to that in CH_4. Therefore, the observation of small quantities of NO formed in CH_3OH and CH_3OCHO is justified.

CHAPTER EIGHT

CONCLUSIONS

Numerical simulations of NO_x production in CH_4, CH_3OH and CH_3OCHO under three different flame configurations: homogenous system; freely propagating flame; and diffusion flame; have been investigated.

It has been established that, under the different flow configurations considered, CH_4 has high amount of total NO present in the flame region as compared to the oxygenated fuels (CH_3OH and CH_3OCHO). The difference in the amount of NO produced by each fuel differ under different configurations. A significant difference (one order of magnitude higher) is observed in CH_4 under freely propagating and diffusion flames as compared to oxygenated fuels. In homogenous system the difference in the amount of NO produced by the three fuels is within the same order of magnitude.

NO production in combustion system is mainly controlled by temperature. Maximum flame temperatures of approximately (1930 K - 1980 K) are observed for the three fuels in freely propagating flames. Under these temperatures, NO is produced mainly through prompt-NO. The maximum total NO produced in this flame type is to the order of 10^{-5} for CH_4 and 10^{-6} for CH_3OH and CH_3OCHO. In prompt NO, reaction: $CH + N_2 \longrightarrow HCN + N$ is the determining step. A small amount of dominant immediate precursor species CH and subsequently N atoms in CH_3OH and CH_3OCHO explain the low values of NO concentration as compared to that for CH_4. In addition, NO concentration showed a high sensitivity to reaction: $NNH + O \longrightarrow NH + NO$ in oxygenated fuels (CH_3OH and CH_3OCHO) as opposed to high sensitivity of reaction: $CH + N_2 \longrightarrow HCN + N$ seen in CH_4 flames. The low concentration of N atoms in oxygenated fuels makes the contribution through the reaction path that results in NNH being significant.

Maximum flame temperatures of approximately (1960 K - 2050 K) are observed for the three fuels in diffusion flames. The maximum total NO produced in this flame type is to the order of 10^{-4} for CH_4 and 10^{-5} for CH_3OH and CH_3OCHO. Just like in the freely propagating flames, the temperatures attained by diffusion flames favour the production of NO mainly through prompt-NO. Therefore, the same argument applies.

In homogenous system, maximum flame temperatures of approximately (2900 K - 2930 K) are observed for the three fuels. The maximum total NO produced in this flame type is to the order of 10^{-2} for all fuels. Under these temperatures, thermal NO reaction by Zel'dovich mechanism is the dominating source of NO. The rate-limiting step in the Zel'dovich mechanism: $N_2 + O \longrightarrow NO + N$ is the decisive reaction for NO formation at high temperature. The availability of the O atoms and nitrogen molecules in all three fuels considered result in a similar amount of NO formed. The small difference in the production of NO is attributed to the different maximum temperatures attained by these mixtures and the prompt NO formation.

CHAPTER NINE

RECOMMENDATIONS

The low values of total NO predicted for oxygenated fuels in freely propagating and diffusion flames could still be investigated further. The maximum temperatures attained by these flames favours the production of NO mainly through prompt-NO. Though the chemical kinetics model for methyl formate developed by Dooley et al. [16] (used in this thesis) have been widely validated for the intermediates species (CH_3OH, CH_2O, CH_4, CH_3, C_2H_4, C_2H_2 and CH_3CHO), there is need to quantitatively measure the immediate prompt-NO precursor species CH and N. In addition, the contribution to the total NO through other species apart from N atom such as NNH could be studied.

In our analysis we have used Leeds NO mechanism, in which the initiation route for prompt-NO is $CH + N_2 \rightleftharpoons HCN + N$, to predict NO formation. The alternative initiation route for prompt-NO formation: $CH + N_2 \rightleftharpoons NCN + H$, which have been proposed [10,11], can also be implemented on a methyl formate mechanism. This could improve the NO prediction.

Though a sensitivity analysis was performed to ascertain the accuracy of predicted NO production, a quantitative measurement of NO in a methyl formate flame is desired to further validate the results.

REFERENCES

[1] R. Kiplimo, P.N. Kioni, and G.T. Thiongo, "Compression engine performance on croton megalocarpus methyl esters," in *Proceedings of 2006 JKUAT Scientific Technological and Industrialisation Conference*, 2006.

[2] P. Pepiot-Desjardins, H. Pitsch, R. Malhotra, S. R. Kirby, and A. L. Boehman, "Structural group analysis for soot reduction tendency of oxygenated fuels," *Combustion and Flame*, vol. 154, pp. 191–195, 2008.

[3] A. Schonborn, N. Ladommatos, J. Williams, R. Allan, and J. Rogerson, "The influence of molecular of fatty acid monoalkyl esters on diesel combustion," *Combustion and Flame*, vol. 156, pp. 1396–1412, 2009.

[4] Gerhard Knothe, C. A. Sharp, and T. W. Ryan, "Exhaust emissions of biodiesel, petrodiesel, neat methyl esters, and alkanes in a new technology engine," *Energy and Fuel*, 2006.

[5] P. V. Rao, "Effect of properties of karanja methyl ester on combustion and NO_x emissions of a diesel engine," *Journal of Petroleum Technology and Alternative Fuels*, vol. 2(5), pp. 63–75, 2011.

[6] I. Glassman and R. A. Yetter, *Combustion.* Elsevier, 2008.

[7] S. C. Li and F. A. Williams, "NO_x formation in two-stage methane-air flames," *Combustion and Flame*, vol. 118, pp. 399–414, 1999.

[8] K. J. Hughes, T. Turanyi, M. J. Pilling, and A. S. Tomlin, "Leeds NO_x mechanism," *http://garfield.chem.elte.hu/Combustion.*, 1999.

[9] G. P. Smith, D. M. Golden, M. Frenklach, N. W. Moriarty, B. Eiteneer, M. Goldenberg, C. T. Bowman, R. K. Hanson, S. Song, W. C. Gardener Jr., V. V. Lissianski, and Z. Qin, "GRI Mech Version 3.0," *http://www.me.berkeley.edu/grimech/ or*.

[10] A. El bakali, L. Pillier, P. Desgroux, B. Lefort, L. Gasnot, J.F. Pauwels, and I. Da Costa, "NO prediction in natural gas flames using gfd-kin® 3.0 mechanism NCN and HCN contribution to prompt-NO formation," *Fuel*, vol. 85, pp. 896–909, 2006.

[11] A. A. Konnov, "Implementation of the NCN pathway of prompt-NO formation in the detailed reaction mechanism," *Combustion and Flame*, vol. 156, pp. 2093–2105, 2009.

[12] N. Lamoureux, P. Desgroux, A. El Bakali, and J.F. Pauwels, "Experimental and numerical study of the role of NCN in prompt-NO formation in low-pressure CH_4-O_2-N_2 and C_2H_2-O_2-N_2 flames," *Combustion and Flame*, vol. 157, pp. 1929–1941, 2010.

[13] H. Guo, F. Liu, and G. J. Smallwood, "A numerical study of NO_x formation in laminar counterflow CH_4/air flames," *Combustion and Flame*, vol. 143, pp. 282–298, 2005.

[14] S. Naha and S. K. Aggarwal, "Fuel effects on NO_x emmisions in partially premixed flames," *Combustion and Flame*, vol. 139, pp. 90–105, 2004.

[15] E. C. Zabetta and M. Hupa, "A detailed chemical kinetic mechanism including methanol and nitrogen pollutants relevant to the gas-phase combustion and pyrolysis of biomass-derived fuels," *Combustion and Flame*, vol. 152, pp. 14–27, 2008.

[16] S. Dooley, M. Chaos, M.P. Burke, Y. Stein, F.L. Dryer, C.A. Daly, V.P. Zhukov, and O. Finch, "An experimental and kinetic modeling study of methyl formate oxidation," *Proceedings of the European Combustion Meeting*, 2009.

[17] S. Dooley, F.L. Dryer, B. Yang, T.A. Cool, T. Kasper, and N. Hansen, "An experimental and kinetic modeling study of methyl formate oxidation at low pressure flames," *Combustion and Flame*, vol. 158, 2011.

[18] W. J. Pitz, C. K. Westbrook, O. Herbinet, and E. J. Silke, "Progress in chemical kinetic modeling for surrogate fuels," *The 7th COMODIA International Conference on Modeling and Diagnostics for Advanced Engine Systems*, 2008.

[19] C. V. Naik and C. K. Westbrook, "Kinetic modeling of combustion characteristics of real biodiesel fuels," *Proceedings of the 6^{th} U.S. National Combustion Meeting*, 2009.

[20] S. Dooley, H. W. Sang, M. Chaos, J. Heyne, J. Yiguang, F. L. Dryer, K. Kumar, C. J. Sung, H. Wang, M. A. Oehlschlaeger, R. J. Santoro, and T. A. Litzinger, "A jet fuel surrogate formulated by real fuel properties," *Combustion and Flame*, vol. 157, 2010.

[21] E. M. Fisher, W. J. Pitz, H. J. Curran, and C. K. Westbrook, "Detailed chemical kinetic mechanisms for combustion of oxygenated fuels," *Proceedings of the Combustion Institute*, 2000.

[22] C. K. Westbrook, W. J. Pitz, P. R. Westmoreland, F.L. Dryer, M. Chaos, P. Osswald, K. Kohse-Hoinghaus, T. A. Cool, J. Wang, B. Yang, N. Hansen, and T. Kasper, "A detailed chemical kinetic reaction mechanism for oxidation of four small a detailed chemical kinetic reaction mechanism for oxidation of four small alkyl esters in laminar premixed flames," *32nd International Symposium on Combustion Montreal, Canada*, 2008.

[23] P. A. Glaude, O. Herbinet, S. Bax, J. Biet, B. Valerie, and F. B. Lederc, "Modeling of the oxidation of methyl esters validation for methyl hexanoate, methyl heptanoate and

methyl decanoate in a jet stirred reactor," *Combustion and Flame*, vol. 157, pp. 2035–2050, 2010.

[24] O. Herbinet, W. J. Pitz, and C. K. Westbrook, "Detailed chemical kinetic mechanism for the oxidation of biodiesel fuels blend surrogate," *Combustion and Flame*, 2009.

[25] C. V. Naik , C. K. Westbrook, O. Herbinet, W. J. Pitz, and M. Mehl, "Detailed chemical kinetic reaction mechanism for biodiesel components methyl stearate and methyl oleate," *The 33rd International Symposium on Combustion Beijing, China*, 2010.

[26] C. K. Westbrook, C. K. Naik, O. Herbinet, W. J. Pitz , M. Mehl, S. M. Sarathy, and H. J. Curran, "Detailed chemical kinetic reaction mechanisms for soy and rapeseed biodiesel fuels," *Combustion and Flame*, vol. 158, pp. 742–755, 2011.

[27] S. M. Sarathy, M. J. Thomson, W. J. Pitz, and T. Lu, "An experimental and kinetic modeling study of methyl decanoate combustion," *33rd International Symposium on Combustion Beijing, China*, 2010.

[28] V. I. Golovitchev and J. Yang, "The construction of combustion models for rme biodiesel fuel for ice application," *Department of Applied Mechanics, Chalmers University of Technology, S-4 12 96, Gtebo rg, Sweden.*

[29] S. Gail, M.J. Thomson, S.M. Sarathy, S.A. Syed, P. Dagaut, P. Dievart, A.J. Marchese, and F.L. Dryer, "A wide-ranging kinetic modeling study of methyl butanoate combustion," *Proceedings of the Combustion Institute*, 2007.

[30] K. Seshadri, T. Lu, O. Herbinet, S. Humer, U. Niemann, W. J. Pitz, and K. L. Chung, "Experimental and kinetic modeling study of extinction and ignition of methyl

decanoate in laminar nonpremixed flows," *Thirty-Second International Symposium on Combustion Montreal, Canada*, 2008.

[31] S. Bax, H. H. Mohammed, P. A. Glaude, and O. Herbinet, "Experimental study of the oxidation of methyl oleate in a jet stirred reactor," *Combustion and Flame*, vol. 157, pp. 120–1229, 2010.

[32] Y. L. Wang, Q. Feng, F. N. Egolfopoulos, and T. T. Tsotsis, "Studies of c_4 and c_{10} methyl ester flames," *Combustion and Flame*, 2011.

[33] G. P. Merker, C. Schwarz, and R. Teichmann, *Combustion Engines Development*. Springer, 2009.

[34] Fawzy El-Mahallawy and Saad El-Din Habik, *Fundamentals and Technology of Combustion*. Elsevier, 2002.

[35] S. R. Turns, *An Introduction to Combustion: Concept and Application*. McGraw Hill Publisher, 2000.

[36] K. Terao, *Irreversible Phenomena: Ignitions, Combustion and Detonation Waves*. Springer, 2007.

[37] C. K. Westbrook, "Chemical kinetics of hydrocarbon ignition in practical combustion systems," *Proceedings of the Combustion Institute*, vol. 28, pp. 1563–1577, 2000.

[38] S. S. Vasu , D.F. Davidson, and R.K. Hanson , "OH time-histories during oxidation of n-heptane and methylcyclohexane at high pressures and temperatures," *Combustion and Flame*, vol. 156, pp. 736–749, 2009.

[39] *COSILAB Manual: Thermodynamics & Transport: Fundamental & Practical Aspects, and User Guide*.

[40] A. Burcat and B. Ruscic, "Third millennium ideal gas and condensed phase thermochemical database for combustion with updates from active thermochemical tables," *Argonne National Laboratory Report No. ANL-05/20 TAE 960*, 2005.

[41] "Chemical kinetics models database," *http://www.princeton.edu/mae/people/faculty /dryer/homepage/kineticmodels/methylformate/.*

[42] K. K. Kuo, *Principles of Combustion.* John Wiley & Sons, 1986.

[43] F. A. William, *Combustion Theory.* The Benjamin Cummings Publishing company, Inc., 1985.

[44] B. Rogg, "Numerical modelling and computation of reactive stagnation-point flows," *Computers and Experiments in Fluid Flow*, 1989.

[45] "COSILAB software package," *www.rotexo.com/cms/index.php.*

[46] B. Rogg, "Adaptive methods in computational fluid dynamics of chemically reacting flows," *Computer-Methods in Applied Mechanics and Engineering*, 1991.

[47] P. Deuflhard, "A modified newton method for the solution of ill-conditioned systems of nonlinear equations with application to multiple shooting," *Numer. Math.*, 1974.

[48] R. S. Barlow, A. N. Karpetis, J. H. Frank, and J. Y. Chen, "Scalar profiles and NO formation in laminar opposed-flow partially premixed methane/air flames," *Combustion and Flame*, vol. 127, pp. 2102–2118, 2001.

[49] K. J. Hughes, A.S. Tomlin, E. Hamparsounmian, W. Nimmo, I. G. Zsely, M. Ujvari, T. Turanyi, A. R. Clague, and M. J. Pilling, "An investigation of important gas-phase reactions of nitrogeneous species from simulation of experimental measurements in combustion systems," *combustion and Flame*, vol. 124, pp. 573–589, 2001.

[50] D. J. Seery and C. T. Bowman , "An experimental and analytical study of methane oxidation behind shock waves," *Combustion and Flame*, vol. 14, 1970.

[51] J. Huang, P.G. Hill, W.K. Bushe, and S.R. Munshi, "Shock-tube study of methane ignition under engine-relevant conditions: Experiments and modeling," *Combustion and Flame*, vol. 136, pp. 25–42, 2004.

[52] R. Seiser, K. Seshadri, and F. A. Williams, "Detailed and reduced chemistry for methanol ignition," *Combustion and Flame*, vol. 158, pp. 1667–1672, 2011.

[53] T. Turanyi, "Applications of sensitivity analysis to combustion chemistry," *Reliability Engineering and System Safety*, vol. 57, pp. 41–48, 1997.

APPENDIX A

Methyl Formate Oxidation Chemistry

The mechanism of the first 76 elementary reactions for methyl formate oxidation developed by Dooley *et al.* [16] is given in table A.1. The full mechanism has 269 species taking part in 1583 homogeneous reactions. The rate of production of the chemical species i, w_i, involved in the mechanism is given as

$$w_i = W_i \sum_{k=1}^{l} (v''_{i,k} - v'_{i,k}) K_k \prod_{j=1}^{N} \left(\frac{\rho Y_j}{W_j} \right)^{v'_{j,k}} \quad i = 1, ..., N; \tag{A.1}$$

where the rate constant is defined by Arrhenius equation:

$$K = AT^{\alpha} exp(-E/RT); \tag{A.2}$$

and l is the number of elementary reactions in the mechanism, $v'_{i,k}$ and $v''_{i,k}$ are the stoichiometric coefficients of species i in reaction k, $k = 1, ..., l$, for reactants and products respectively, K_k is the specific rate constant for reaction k, AT^{α} and E is pre-exponential factor and activation energy in the specific rate constant respectively, W_i and W_j is molecular weight of species i and j respectively, Y_j is mass fraction for species j, ρ is mixture density, and R is universal gas constant. The forward and backward reactions are treated separately.

Table A.1: Methyl formate oxidation chemistry developed by Dooley *et al.* 2009

	Reactions	**A(cm^3/mol s)**	**Exponent**	**E (cal/mol)**
1	H+O2 <=> O+OH	3.547E+015	-4.06E-001	1.6599E+004
2	O+H2 <=> H+OH	5.080E+004	2.67E+000	6.2900E+003
3	H2+OH <=> H2O+H	2.160E+008	1.51E+000	3.4300E+003
4	O+H2O <=> OH+OH	2.970E+006	2.02E+000	1.3400E+004
5	H2+M <=> H+H+M	4.577E+019	-1.40E+000	1.0438E+005
6	H2+AR <=> H+H+AR	5.840E+018	-1.10E+000	1.0438E+005
7	H2+HE <=> H+H+HE	5.840E+018	-1.10E+000	1.0438E+005
8	O+O+M <=> O2+M	6.165E+015	-5.00E-001	0.0000E+000
9	O+O+AR <=> O2+AR	1.886E+013	0.00E+000	-1.7880E+003
10	O+O+HE <=> O2+HE	1.886E+013	0.00E+000	-1.7880E+003
11	O+H+M <=> OH+M	4.714E+018	-1.00E+000	0.0000E+000
12	H+OH+M <=> H2O+M	3.800E+022	-2.00E+000	0.0000E+000
13	H+O2(+M) <=> HO2(+M)	1.475E+012	6.00E-001	0.0000E+000
14	HO2+H <=> H2+O2	1.660E+013	0.00E+000	8.2300E+002
15	HO2+H <=> OH+OH	7.079E+013	0.00E+000	2.9500E+002
16	HO2+O <=> O2+OH	3.250E+013	0.00E+000	0.0000E+000
17	HO2+OH <=> H2O+O2	2.890E+013	0.00E+000	-4.9700E+002
18	HO2+HO2 <=> H2O2+O2	4.200E+014	0.00E+000	1.1982E+004
19	HO2+HO2 <=> H2O2+O2	1.300E+011	0.00E+000	-1.6293E+003
20	H2O2(+M) <=> OH+OH(+M)	2.951E+014	0.00E+000	4.8430E+004
21	H2O2+H <=> H2O+OH	2.410E+013	0.00E+000	3.9700E+003
22	H2O2+H <=> HO2+H2	4.820E+013	0.00E+000	7.9500E+003
23	H2O2+O <=> OH+HO2	9.550E+006	2.00E+000	3.9700E+003
24	H2O2+OH <=> HO2+H2O	1.000E+012	0.00E+000	0.0000E+000
25	H2O2+OH <=> HO2+H2O	5.800E+014	0.00E+000	9.5570E+003
26	CO+O(+M) <=> CO2(+M)	1.800E+010	0.00E+000	2.3840E+003
27	CO+O2 <=> CO2+O	2.530E+012	0.00E+000	4.7700E+004
28	CO+HO2 <=> CO2+OH	3.010E+013	0.00E+000	2.3000E+004
29	CO+OH <=> CO2+H	2.229E+005	1.89E+000	-1.1587E+003
30	HCO+M <=> H+CO+M	4.748E+011	6.59E-001	1.4874E+004
31	HCO+O2 <=> CO+HO2	7.580E+012	0.00E+000	4.1000E+002
32	HCO+H <=> CO+H2	7.230E+013	0.00E+000	0.0000E+000
33	HCO+O <=> CO+OH	3.020E+013	0.00E+000	0.0000E+000
34	HCO+OH <=> CO+H2O	3.020E+013	0.00E+000	0.0000E+000
35	HCO+O <=> CO2+H	3.000E+013	0.00E+000	0.0000E+000
36	HCO+HO2 <=> CO2+OH+H	3.000E+013	0.00E+000	0.0000E+000
37	HCO+CH3 <=> CO+CH4	2.650E+013	0.00E+000	0.0000E+000

	Reactions	A(cm^3/mol s)	Exponent	E (cal/mol)
38	HCO+HCO <=> H2+CO+CO	3.000E+012	0.00E+000	0.0000E+000
39	HCO+HCO <=> CH2O+CO	3.000E+013	0.00E+000	0.0000E+000
40	HCO+O2 <=> O2CHO	1.200E+011	0.00E+000	-1.1000E+003
41	CH2O+O2CHO <=> HCO+HO2CHO	1.990E+012	0.00E+000	1.1660E+004
42	HO2CHO <=> OCHO+OH	5.010E+014	0.00E+000	4.0150E+004
43	H+CO2+M <=> OCHO+M	7.500E+013	0.00E+000	2.9000E+004
44	CH2O+M <=> HCO+H+M	3.300E+039	-6.30E+000	9.9900E+004
45	CH2O+M <=> CO+H2+M	3.100E+045	-8.00E+000	9.7510E+004
46	CH2O+H <=> HCO+H2	5.740E+007	1.90E+000	2.7486E+003
47	CH2O+O <=> HCO+OH	1.810E+013	0.00E+000	3.0800E+003
48	CH2O+OH <=> HCO+H2O	3.430E+009	1.18E+000	-4.4700E+002
49	CH2O+O2 <=> HCO+HO2	1.230E+006	3.00E+000	5.2000E+004
50	CH2O+HO2 <=> HCO+H2O2	4.110E+004	2.50E+000	1.0210E+004
51	CH2O+CH3 <=> HCO+CH4	3.636E-006	5.42E+000	9.9800E+002
52	CH2O+HO2 <=> OCH2O2H	1.500E+011	0.00E+000	1.1900E+004
53	OCH2O2H <=> HOCH2O2	3.000E+011	0.00E+000	8.6000E+003
54	HOCH2O2+HO2 <=> HOCH2O2H+O2	3.500E+010	0.00E+000	-3.2750E+003
55	HOCH2O+OH <=> HOCH2O2H	1.000E+013	0.00E+000	0.0000E+000
56	CH3+O <=> CH2O+H	8.430E+013	0.00E+000	0.0000E+000
57	CH3+O2 <=> CH3O+O	1.990E+018	-1.57E+000	2.9230E+004
58	CH3+O2 <=> CH2O+OH	3.510E-001	3.52E+000	7.3800E+003
59	CH3+HO2 <=> CH3O+OH	2.410E+010	7.60E-001	-2.3250E+003
60	CH3+CH3(+M) <=> C2H6(+M)	2.277E+015	-6.90E-001	1.7486E+002
61	CH3+H(+M) <=> CH4(+M)	1.270E+016	-6.30E-001	3.8300E+002
62	CH4+H <=> CH3+H2	5.470E+007	1.97E+000	1.1210E+004
63	CH4+O <=> CH3+OH	3.150E+012	5.00E-001	1.0290E+004
64	CH4+OH <=> CH3+H2O	5.720E+006	1.96E+000	2.6390E+003
65	CH3+HO2 <=> CH4+O2	3.160E+012	0.00E+000	0.0000E+000
66	CH4+HO2 <=> CH3+H2O2	1.810E+011	0.00E+000	1.8580E+004
67	CH3+CH3OH <=> CH4+CH3O	1.440E+001	3.10E+000	6.9350E+003
68	CH3O+CH3 <=> CH2O+CH4	1.200E+013	0.00E+000	0.0000E+000
69	CH3O+H <=> CH2O+H2	2.000E+013	0.00E+000	0.0000E+000
70	CH3+O2(+M) <=> CH3O2(+M)	1.006E+008	1.63E+000	0.0000E+000
71	CH3O2+CH2O <=> CH3O2H+HCO	1.990E+012	0.00E+000	1.1660E+004
72	CH4+CH3O2 <=> CH3+CH3O2H	1.810E+011	0.00E+000	1.8480E+004
73	CH3OH+CH3O2 <=> CH2OH+CH3O2H	1.810E+012	0.00E+000	1.3710E+004
74	CH3O2+CH3 <=> CH3O+CH3O	5.080E+012	0.00E+000	-1.4110E+003
75	CH3O2+HO2 <=> CH3O2H+O2	2.470E+011	0.00E+000	-1.5700E+003
76	CH3O2+CH3O2 <=> CH2O+CH3OH+O2	3.110E+014	-1.61E+000	-1.0510E+003

.....Continue to 1583^{rd} reaction

APPENDIX B

Nitrogen Oxidation Chemistry

The mechanism of the first 63 elementary reactions for nitrogen oxidation developed by Hughes *et al.* [8] is given in table B.1. The full mechanism has 43 species taking part in 164 homogeneous reactions. The rate of production of the chemical species i is given by Eq. A.1, whereby the rate constant is defined by Eq. A.2.

Table B.1: The Leeds Nitrogen Chemistry Mechanism 2.0

	Reactions	**A(cm^3/mol s)**	**Exponent**	**E (cal/mol)**
1	H2+CN <=> HCN+H	1.930E+004	2.87E+000	1.6292E+003
2	CH4+N <=> NH+CH3	1.000E+013	0.00E+000	2.3991E+004
3	CH4+CN <=> HCN+CH3	9.030E+004	2.64E+000	-2.9797E+002
4	O2+N <=> NO+O	9.030E+009	1.00E+000	6.4968E+003
5	O2+NH <=> HNO+O	3.910E+013	0.00E+000	1.7880E+004
6	O2+NH <=> NO+OH	7.589E+010	0.00E+000	1.5293E+003
7	O2+NH2 <=> HNO+OH	1.510E+012	-3.90E-001	3.6091E+004
8	O2+NH2 <=> H2NO+O	1.100E+018	-1.34E+000	3.3592E+004
9	O2+CN <=> NCO+O	7.230E+012	0.00E+000	-4.1721E+002
10	O2+NCO <=> NO+CO2	1.720E+007	0.00E+000	-7.3358E+002
11	CO+N2O <=> CO2+N2	9.770E+010	0.00E+000	1.7443E+004
12	CO2+N <=> NO+CO	1.900E+011	0.00E+000	3.3972E+003
13	N2+CH <=> HCN+N	1.570E+012	0.00E+000	1.7940E+004
14	N2+CH2 <=> HCN+NH	1.000E+013	0.00E+000	7.3984E+004
15	NO+N2O <=> N2+NO2	1.000E+014	0.00E+000	4.9666E+004
16	NO+N2H2 <=> N2O+NH2	3.000E+012	0.00E+000	0.0000E+000
17	NO+C <=> CN+O	1.930E+013	0.00E+000	0.0000E+000
18	NO+C <=> CO+N	2.890E+013	0.00E+000	0.0000E+000
19	NO+H <=> N+OH	2.170E+014	0.00E+000	4.9487E+004
20	N+OH <=> NO+H	2.830E+013	0.00E+000	0.0000E+000
21	NO+CH <=> CO+NH	1.200E+013	0.00E+000	0.0000E+000
22	NO+CH <=> CN+OH	1.200E+013	0.00E+000	0.0000E+000
23	NO+CH <=> HCN+O	9.600E+013	0.00E+000	0.0000E+000
24	NO+CH2 <=> HOCN+H	1.390E+012	0.00E+000	-1.0992E+003
25	NO+CH2(S) <=> HCN+OH	9.640E+013	0.00E+000	0.0000E+000

	Reactions	A(cm^3/mol s)	Exponent	E (cal/mol)
26	NO+CH3 <=> HCN+H2O	9.275E+011	0.00E+000	1.6706E+004
27	NO+CH3 <=> H2CN+OH	9.275E+011	0.00E+000	1.6706E+004
28	NO+HO2 <=> NO2+OH	2.090E+012	0.00E+000	-4.7790E+002
29	NO+HO2 <=> HNO+O2	2.000E+011	0.00E+000	1.9857E+003
30	NO+HCCO <=> HOCN+CO	2.000E+013	0.00E+000	0.0000E+000
31	NO+N <=> N2+O	4.280E+013	0.00E+000	1.5699E+003
32	N2+O <=> NO+N	1.810E+014	0.00E+000	7.6089E+004
33	NO+NH <=> N2+OH	3.200E+013	0.00E+000	1.2715E+004
34	NO+NH <=> N2O+H	4.162E+014	-4.50E-001	0.0000E+000
35	NO+NH2 <=> NNH+OH	2.410E+015	-1.17E+000	0.0000E+000
36	NO+NH2 <=> N2+H2O	5.480E+015	-1.17E+000	0.0000E+000
37	NO+NNH <=> N2+HNO	5.000E+013	0.00E+000	0.0000E+000
38	NO+HNO <=> N2O+OH	2.951E+005	0.00E+000	0.0000E+000
39	NO+NCO <=> N2O+CO	1.390E+018	-1.73E+000	7.5508E+002
40	NO+M <=> N+O+M	3.625E+015	0.00E+000	1.4830E+005
41	NO2+NO2 <=> NO+NO+O2	2.000E+012	0.00E+000	2.6820E+004
42	NO2+H <=> NO+OH	3.470E+014	0.00E+000	1.4695E+003
43	NO2+O <=> NO+O2	1.000E+013	0.00E+000	5.9976E+002
44	NO2+N <=> NO+NO	8.070E+011	0.00E+000	0.0000E+000
45	NO2+N <=> N2O+O	1.000E+012	0.00E+000	0.0000E+000
46	NO2+NH <=> HNO+NO	1.000E+011	5.00E-001	3.9737E+003
47	NO2+NH <=> N2O+OH	9.710E+012	0.00E+000	0.0000E+000
48	NO2+NH2 <=> N2O+H2O	2.030E+017	-1.70E+000	0.0000E+000
49	NO2+CN <=> NCO+NO	3.000E+013	0.00E+000	0.0000E+000
50	NO2+M <=> NO+O+M	3.133E+016	0.00E+000	6.5558E+004
51	N2O+C <=> CN+NO	5.120E+012	0.00E+000	0.0000E+000
52	N2O+H <=> N2+OH	4.370E+014	0.00E+000	1.8872E+004
53	N2O+O <=> N2+O2	1.000E+014	0.00E+000	2.8012E+004
54	N2O+O <=> NO+NO	6.920E+013	0.00E+000	2.6621E+004
55	N2O+OH <=> N2+HO2	6.310E+011	0.00E+000	9.9332E+003
56	N2O+N <=> N2+NO	1.000E+013	0.00E+000	1.9866E+004
57	N2O+NH <=> HNO+N2	2.000E+012	0.00E+000	5.9594E+003
58	N2O+CN <=> NCO+N2	1.000E+013	0.00E+000	0.0000E+000
59	N2O+M <=> N2+O+M	2.857E+015	0.00E+000	5.9976E+004
60	NH3+H <=> NH2+H2	5.420E+005	2.40E+000	9.9140E+003
61	NH3+O <=> NH2+OH	9.640E+012	0.00E+000	7.2904E+003
62	NH3+OH <=> NH2+H2O	3.160E+012	0.00E+000	2.0072E+003
63	NH3+HO2 <=> NH2+H2O2	2.510E+012	0.00E+000	2.3840E+004

.....Continueto 164^{th} reaction

APPENDIX C

Small Chain Hydrocarbon Oxidation Chemistry

The mechanism of the first 57 elementary reactions for oxidation of small hydrocarbons developed by Smith *et al.* [9] is given in table C.1. The full mechanism has 53 species taking part in 325 homogeneous reactions. The rate of production of the chemical species i is given by Eq. A.1, whereby the rate constant is defined by Eq. A.2.

Table C.1: GRI-Mech Version 3.0 7/30/99 in CHEMKIN-II format

	Reactions	**A(cm^3/mol s)**	**Exponent**	**E (cal/mol)**
1	2O+M <=> O2+M	1.200E+017	-1.00E+000	0.0000E+000
2	O+H+M <=> OH+M	5.000E+017	-1.00E+000	0.0000E+000
3	O+H2 <=> H+OH	3.870E+004	2.70E+000	6.2600E+003
4	O+HO2 <=> OH+O2	2.000E+013	0.00E+000	0.0000E+000
5	O+H2O2 <=> OH+HO2	9.630E+006	2.00E+000	4.0000E+003
6	O+CH <=> H+CO	5.700E+013	0.00E+000	0.0000E+000
7	O+CH2 <=> H+HCO	8.000E+013	0.00E+000	0.0000E+000
8	O+CH2(S) <=> H2+CO	1.500E+013	0.00E+000	0.0000E+000
9	O+CH2(S) <=> H+HCO	1.500E+013	0.00E+000	0.0000E+000
10	O+CH3 <=> H+CH2O	5.060E+013	0.00E+000	0.0000E+000
11	O+CH4 <=> OH+CH3	1.020E+009	1.50E+000	8.6000E+003
12	O+CO(+M) <=> CO2(+M)	1.800E+010	0.00E+000	2.3850E+003
13	O+HCO <=> OH+CO	3.000E+013	0.00E+000	0.0000E+000
14	O+HCO <=> H+CO2	3.000E+013	0.00E+000	0.0000E+000
15	O+CH2O <=> OH+HCO	3.900E+013	0.00E+000	3.5400E+003
16	O+CH2OH <=> OH+CH2O	1.000E+013	0.00E+000	0.0000E+000
17	O+CH3O <=> OH+CH2O	1.000E+013	0.00E+000	0.0000E+000
18	O+CH3OH <=> OH+CH2OH	3.880E+005	2.50E+000	3.1000E+003
19	O+CH3OH <=> OH+CH3O	1.300E+005	2.50E+000	5.0000E+003
20	O+C2H <=> CH+CO	5.000E+013	0.00E+000	0.0000E+000
21	O+C2H2 <=> H+HCCO	1.350E+007	2.00E+000	1.9000E+003
22	O+C2H2 <=> OH+C2H	4.600E+019	-1.41E+000	2.8950E+004
23	O+C2H2 <=> CO+CH2	6.940E+006	2.00E+000	1.9000E+003
24	O+C2H3 <=> H+CH2CO	3.000E+013	0.00E+000	0.0000E+000
25	O+C2H4 <=> CH3+HCO	1.250E+007	1.83E+000	2.2000E+002

	Reactions	A(cm^3/mol s)	Exponent	E (cal/mol)
26	O+C2H5 <=> CH3+CH2O	2.240E+013	0.00E+000	0.0000E+000
27	O+C2H6 <=> OH+C2H5	8.980E+007	1.92E+000	5.6900E+003
28	O+HCCO <=> H+2CO	1.000E+014	0.00E+000	0.0000E+000
29	O+CH2CO <=> OH+HCCO	1.000E+013	0.00E+000	8.0000E+003
30	O+CH2CO <=> CH2+CO2	1.750E+012	0.00E+000	1.3500E+003
31	O2+CO <=> O+CO2	2.500E+012	0.00E+000	4.7800E+004
32	O2+CH2O <=> HO2+HCO	1.000E+014	0.00E+000	4.0000E+004
33	H+O2+M <=> HO2+M	2.800E+018	-8.60E-001	0.0000E+000
34	H+2O2 <=> HO2+O2	2.080E+019	-1.24E+000	0.0000E+000
35	H+O2+H2O <=> HO2+H2O	1.126E+019	-7.60E-001	0.0000E+000
36	H+O2+N2 <=> HO2+N2	2.600E+019	-1.24E+000	0.0000E+000
37	H+O2+AR <=> HO2+AR	7.000E+017	-8.00E-001	0.0000E+000
38	H+O2 <=> O+OH	2.650E+016	-6.70E-001	1.7041E+004
39	2H+M <=> H2+M	1.000E+018	-1.00E+000	0.0000E+000
40	2H+H2 <=> 2H2	9.000E+016	-6.00E-001	0.0000E+000
41	2H+H2O <=> H2+H2O	6.000E+019	-1.25E+000	0.0000E+000
42	2H+CO2 <=> H2+CO2	5.500E+020	-2.00E+000	0.0000E+000
43	H+OH+M <=> H2O+M	2.200E+022	-2.00E+000	0.0000E+000
44	H+HO2 <=> O+H2O	3.970E+012	0.00E+000	6.7100E+002
45	H+HO2 <=> O2+H2	4.480E+013	0.00E+000	1.0680E+003
46	H+HO2 <=> 2OH	8.400E+013	0.00E+000	6.3500E+002
47	H+H2O2 <=> HO2+H2	1.210E+007	2.00E+000	5.2000E+003
48	H+H2O2 <=> OH+H2O	1.000E+013	0.00E+000	3.6000E+003
49	H+CH <=> C+H2	1.650E+014	0.00E+000	0.0000E+000
50	H+CH2(+M) <=> CH3(+M)	6.000E+014	0.00E+000	0.0000E+000
51	H+CH2(S) <=> CH+H2	3.000E+013	0.00E+000	0.0000E+000
52	H+CH3(+M) <=> CH4(+M)	1.390E+016	-5.34E-001	5.3600E+002
53	H+CH4 <=> CH3+H2	6.600E+008	1.62E+000	1.0840E+004
54	H+HCO(+M) <=> CH2O(+M)	1.090E+012	4.80E-001	-2.6000E+002
55	H+HCO <=> H2+CO	7.340E+013	0.00E+000	0.0000E+000
56	H+CH2O(+M) <=> CH2OH(+M)	5.400E+011	4.54E-001	3.6000E+003
57	H+CH2O(+M) <=> CH3O(+M)	5.400E+011	4.54E-001	2.6000E+003

.....continue to 325^{th} reaction